

Sustainable Melting:

The Role of Recycled Low Alloy Aluminum

Marcelo Mejía & Wesley Episcopo

2024



LTH
FACULTY OF
ENGINEERING

CODEN: LUTMDN/(TMMV-5363)/1-98/2024

Master Thesis
Division of Production and Materials Engineering
Lund University

Supervisor: Christina Windmark
Examiner: Volodymyr Bushlya

CODEN: LUTMDN/(TMMV-5363)/1-98/2024

Authors: Marcelo Mejía & Wesley Episcopo
Lund, Sweden 2024

Avdelningen för Industriell Produktion
Lunds Tekniska Högskola
Lunds universitet
Box 118
221 00 Lund
Sverige

Division of Production and Materials Engineering
LTH, Faculty of Engineering
Lund University
Box 118
SE-221 00 LUND
Sweden

Printed in Sweden
Media-Tryck
Lund 2024

Foreword

This thesis project would not have been possible without the support of Tomas Liljenfors at BRYNE AB. His generosity, patience, and friendly demeanor greatly aided us throughout our research. We also extend our gratitude to our supervisor and master's program coordinator, Christina Windmark. Her encouragement and guidance helped us navigate our academic path and find our voice. Our development is a testament to her passion as an educator and her motivation to push the envelope of materials engineering. Special thanks go to Robin Thuresson, a coworker at BRYNE AB and fellow student, whose companionship eased our journey through orientation and beyond.

Wesley would like to personally thank his father, mother, and sister for standing by his side.

Marcelo would like to extend gratitude to his mother and brother for being fundamental pillars of support throughout the entire process. Their words of encouragement were instrumental for achieving the goals proposed throughout the project.

Finally, this publication is part of research conducted at Lund University, funded by a Swedish Institute Scholarship and a Lund University Global Scholarship. This support provided an invaluable journey filled with experiences over the past two years, culminating in this significant milestone.

Lund 23-05-2024
Marcelo Mejía & Wesley Episcopo

Sammanfattning

Denna avhandling undersöker smältningsprocessen för återvunna kraftigt oxiderade bilky-lare och fokuserar på den ekonomiska livskraften och miljöpåverkan av återcirkulering av sekundära låglegerade aluminiumprodukter i produktionen. Genom att använda praktiska insikter från företaget BRYNE AB och deras LOOP-teknologi, behandlar studien utmaning-arna med att mäta oxider och föroreningar samt spårelement under smältningsprocessen. De viktigaste resultaten betonar svårigheterna med att bibehålla legeringsrenhet och kvantifiera förluster som är förknippade med smältningsprocessen. De föreslagna produktionskostnads- och utsläppsmodellerna är utformade för att fånga dessa förluster och relaterade utsläpp, vil-ket ger en omfattande ram för att bättre förstå och optimera smältningsprocessen i linje med initiativet för vetenskapsbaserade mål, vilket slutligen främjar hållbarhet och cirkulära eko-nomiska metoder.

Nyckelord: Återvinning av aluminium, Sekundärt aluminium, Låglegering, Materialkompo-sition, Oxidation, Miljöpåverkan, Ekonomisk livskraft, Utsläppsmodellering, Slagg.

Abstract

This thesis investigates the melting process of recycled heavily oxidized car chillers, focusing on the economic viability and environmental impact of recirculating secondary low alloy aluminum products into production. Utilizing practical insights from Company BRYNE AB and their LOOP technology, the study addresses the challenges in measuring oxides and impurities and trace elements during the melting process. Key findings emphasize the difficulties in maintaining alloy purity and quantifying losses associated with the melting process. The proposed production cost and emissions models are designed to capture these losses and associated emissions, providing a comprehensive framework to better understand and optimize the melting process in alignment with the Science Based Targets initiative, ultimately promoting sustainability and circular economy practices.

Keywords: Aluminum Recycling, Secondary Aluminum, Low Alloy, Material Composition, Oxidation, Environmental Impact, Economic Viability, Emissions Modeling, Dross.

Abbreviations and Definitions

CRM - Critical Raw Material
CSRD - Corporate Sustainability Reporting Directive
DI - Density Index
ERP - Enterprise Resource Planning
GHG - Greenhouse Gas
ITEs - Impurities and Trace Elements
KPI - Key Performance Indicator
LCA - Life Cycle Assessment
OES - Optical Emission Spectroscopy
PPM - Product Performance Matrix
SBT - Scientific Based Targets
SPA - Statistical Production Analysis
WFD - Waste Framework Directive

Charging or Charged: refers to the process of introducing raw materials, such as ores, fluxes, and fuels, into a furnace.

Comminution: the process of reducing the size of solid materials into smaller particles.

Dross: is created when oxidation occurs between molten aluminum and moisture in the air. It consists of metallic and non-metallic (slag) material.

Greenwashing: when a company or product is inaccurately portrayed as environmentally friendly or sustainable. This misleading practice involves presenting data in a way that suggests eco-friendliness, despite little to no actual effort being made to reduce the company's environmental impact.

Melt or Bath: refers to aluminum in a liquid state, also commonly known as molten metal.

Primary: denotes nearly pure or virgin aluminum combined with refined ore. Scrap sourced from post-industrial products, where the lifecycle is shorter, and the material often stays within the production site or undergoes minimal handling before being remelted as new primary aluminum.

Salt Flux: the dictionary defines flux as the rate of flow of fluid, particles, or energy through a given surface. Salt flux, in particular, aids in directing reactions within the melt, ultimately enhancing yield.

Scrap: refers to discarded or leftover metal materials that are no longer needed for their original purpose.

Secondary: also known as recycled, dirty, or used, is derived from post-consumer products. After passing through multiple hands, it undergoes remelting at specialized sites equipped to purify the alloy.

Slag: refers to the byproduct that forms during the melting or refining process. It is part of the dross and consists mainly of ITEs and non-metallic materials.

Contents

1	Introduction	1
1.1	Circular Economy and the Classification of Waste	1
1.2	Economic Challenges and Opportunities of Recycling	3
1.3	Aim	5
1.4	Structure of Thesis	5
2	Theoretical Background	7
2.1	Classification of Aluminum Alloys	7
2.2	Sorting and Scrap Preparation	8
2.3	Melting Process and Oxidation	9
2.4	Dross, Slag, and Salt Slag	11
2.5	Measurement Techniques & Equipment	14
2.6	Environmental Load and Carbon Emission Cost Models	19
2.7	Production Cost Model	22
2.8	Sustainable Eye	27
3	Methodology	29
3.1	Material Preparation	29
3.2	Heating the Furnace	29
3.3	Equipment Setup and Safety	29
3.4	Density Index and First Bubble Methods	30
3.5	Optical Emission Spectroscopy	33
3.6	LOOP Procedure	33
3.7	Adding Salt Flux as a Refining Agent	35
3.8	Documentation	36
3.9	Constructing the Models	36
4	Experimental Results	39
4.1	Optical Electron Spectroscopy	39
4.2	Density Index Estimation and First Bubble Experimentation	51
4.3	Loop Measurements	56
4.4	Production Cost Model Proposal	61
4.5	Carbon Emission Model Proposal	66
5	Discussion	71
5.1	Production Cost Model	71
5.2	Carbon Emissions Model	74
5.3	Remarks about Material Composition and OES Data	76
5.4	Material Degradation and Quality	77
6	Conclusion	79
	Bibliography	81
A	Appendix	89

1 Introduction

Extensive research over the years has clearly documented the substantial economic benefits and emission reductions associated with recycling metals. This recognition has spurred proactive efforts from both the metals industry and governmental bodies, directing their focus towards prioritizing resource allocation towards the optimization of recycling efficiencies.

This thesis explores the challenges and opportunities inherent in the melting phase of secondary low alloy aluminum, particularly focusing on its viability within a circular economy framework. The aim is to open a dialogue concerning the modeling of costs and emissions associated with the remelting process, ultimately striving to reintroduce wrought aluminum in a cleaner form than current practices allow. Company BRYNE will provide invaluable practical insights and support. Drawing upon their expertise and resources, the thesis will delve into the methodologies employed with their innovative LOOP technology, sparking a discussion on insights gained into measuring oxides during the remelting process.

1.1 Circular Economy and the Classification of Waste

The ongoing climate debate strategizes on implementing policy to realize the long-term objectives outlined in the Paris Agreement, specifically, the transition towards an economy with net zero emissions [1]. Proposed “roadmaps” signal the start of a global race for energy efficiencies along with mounting pressure on the industrial sector to embrace or shift towards clean energy sources. While both targets are crucial for advancing industrial production processes and mitigating greenhouse gasses (GHG) emissions, there is still much to explore regarding the utilization of secondary materials already in circulation and reducing our dependency on primary materials.

The circular economy, in a production concept, advocates for strategies that reduce natural resource consumption and address pollution. These strategies heavily rely on an efficient recycling infrastructure and encompasses several levels of the Waste Hierarchy (Figure 1.1). To achieve this objective, effective recycling strategies must be implemented, material flows in production processes optimized, clear labeling practices established, and international regulations governing material usage and recycling developed [2].

1.1.1 *Rebranding Waste*

The European Union addresses the concept of recycling through its Waste Framework Directive (WFD), which outlines the criteria for categorizing waste as secondary raw material or as a by-product, particularly noting hazardous substances [2]. The classification of waste holds significant sway in determining the practicality and economic viability of collection methods, recycling strategies, and consumer choices between recycling and disposal. It is crucial for waste classification to advance alongside scientific progress and remain aligned with developments in chemicals legislation. Discrepancies in classification not only affect the adoption of secondary raw materials but also raise concerns about citizen safety. For ex-

ample, in Rachel Carson’s influential work *Silent Spring* which catalyzed an environmental movement culminating in the establishment of the United States Environmental Protection Agency, lobbying endeavors by chemical manufacturers of dichlorodiphenyltrichloroethane (DDT) in the USA resulted in public officials disregarding the unregulated use of pesticides in agriculture [3]. This illustrates the significant impact humans wield over the environment and underscores the importance of responsible waste management practices.

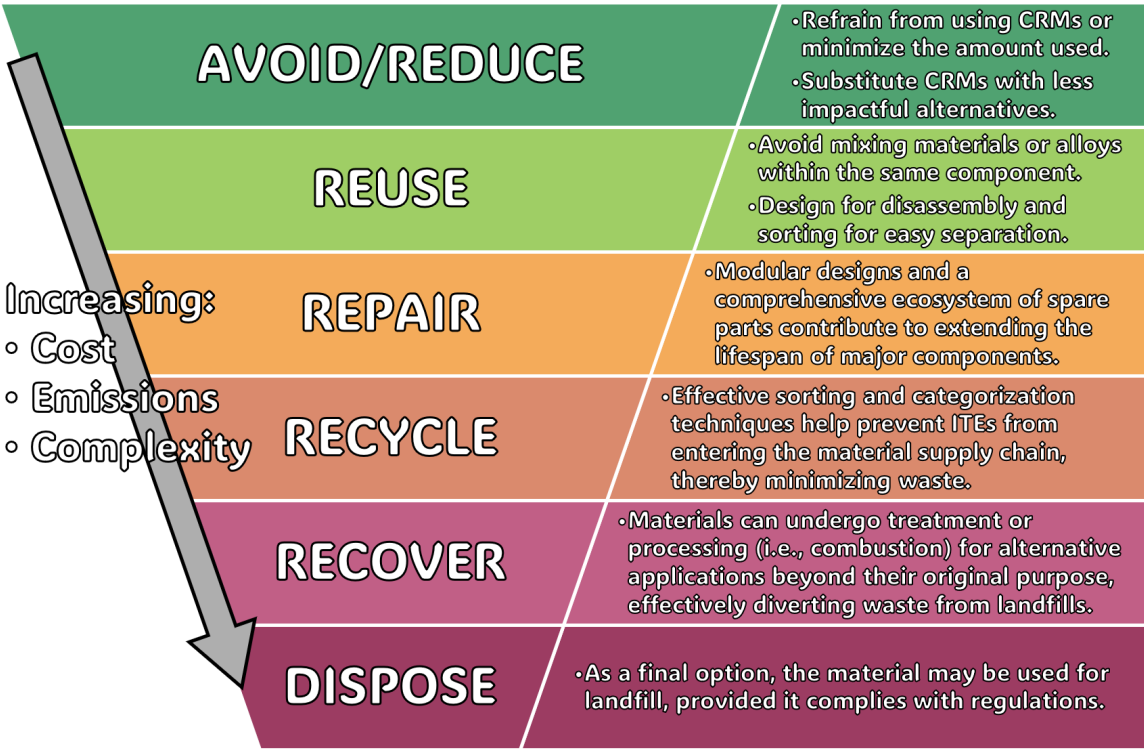


Figure 1.1: An industrial perspective on waste management using a six-step waste hierarchy, influenced by the five-step structure outlined in the Waste Framework Directive which excludes the repair step [2].

1.1.2 Clarifying the Emission Framework

The amount of public emissions data is staggering [4]. Not all, but some companies organize this information to disguise themselves as environmentally friendly [5]. Similar to how the Texas farmer circles bullet holes on the side of their barn and declares themselves a sharpshooter [6], major companies each year face fines for Greenwashing [7].

Building upon the foundations of organized waste management and clear recycling strategies, the sustainability initiative must incorporate GHG emissions within the framework. Gaining prominence among this framework is the Science Based Targets (SBT) initiative [8]. Within the SBT framework, emissions are categorized—whether direct or indirect—into three distinct scopes, delineating the responsibility and accountability of companies in mitigating climate change impacts. Scope 1 pertains to emissions directly produced by a company’s activities, scope 2 includes indirect emissions from purchased energy, and scope 3 encompasses a broader range of indirect emissions throughout the entire value chain, including material extraction, transportation, and waste management.

While the EU itself does not directly sponsor the SBT framework, numerous European-based companies are actively engaged in it [8]. In line with the objectives outlined by the SBT network, the EU took significant steps in early 2023 by enforcing the Corporate Sustainability Reporting Directive (CSRD). This directive introduces new regulations mandating companies to disclose social and environmental information. These regulations extend not only to EU-based companies but also to non-EU entities with substantial involvement in the EU market [9].

Of particular relevance to this thesis is the CSRD requirement for a materiality assessment in sustainability reporting. This mandate ensures that stakeholders receive essential information concerning the material impact and long-term sustainability related to climate change, labor practices, responsible sourcing, life cycle assessment (LCA), and local community development [9]. This transparent reporting approach aligns with the path that secondary low alloy aluminum must follow within the broader context of the SBT framework to enhance its viability in today's economy [10].

1.2 Economic Challenges and Opportunities of Recycling

1.2.1 *Energy Demands*

Effective management of aluminum presents a significant opportunity to advance sustainability initiatives. With its low mass density, remarkable corrosion resistance, and high strength, aluminum emerges as a desirable material across various industries. However, despite its widespread applications, extracting primary aluminum from bauxite ore is notably energy-intensive compared to other industrial metals like Mg, Cu, Zn, and steel [11, 12, 13]. In contrast, remelting aluminum from secondary sources offers a remarkable energy savings compared to ore refinement [12, 13, 14]. While it is theoretically possible for all metals, not just aluminum, to undergo infinite recycling without property degradation, this principle is limited to metals in their purest state. In practice, this concept only holds true for a minority of metals within circularity loops [15].

1.2.2 *Sorting*

Sorting utilizes methods grounded in chemical, physical, and mechanical principles. As components are broken down through various processes, contamination among the different alloy types involved inevitably occurs. The degree of contamination is contingent upon factors such as: 1) insufficient identification and sorting, 2) mixing of similar alloys with distinct compositions, 3) mechanical contamination stemming from processes like cutting, and 4) continuous degradation as the alloy is repeatedly recycled and introduced into an ever-expanding pool of recycled material [15, 16, 17].

1.2.3 *Future Production*

As electrifying vehicles becomes more widespread, there's a corresponding surge in the need for aluminum. European Aluminium, the prominent representative body for the aluminum sector in Europe, foresees a rise in the proportion of secondary aluminum in use within the EU. The current estimate suggests an increase from 37% of 14,000 kilotons in

2024 (5180 kilotons) to 49% of 18,000 kilotons in 2050 (8820 kilotons) [18].

As of 2020, global GHG emissions from the transportation sector accounted for approximately 15% of Earth's GHG emissions [4]. Progress in light alloy research as a substitute for heavier alloys holds promise for enhancing fuel economy to reach a "breakeven distance" where the fuel economy savings outweigh the GHG burden of primary aluminum production [19]. However, a significant limitation in the adoption of light alloys, among other factors, is the inexperience of the associated manufacturing technology compared to conventional steel materials [16]. Furthermore, realizing this "breakeven distance" hinges on efforts to simultaneously reduce the energy demands of increased primary aluminum production. Further complications arise when considering scenarios that anticipate reduced on-shore primary production, aimed at lowering GHG emissions. In such cases, there is a heightened reliance on precise and transparent GHG reporting from suppliers operating off-shore [20].

1.2.4 Recycling as a Solution

A seemingly straightforward and localized approach to meeting demand while adhering to GHG regulatory limits is to increase the quantity of aluminum re-entering the recycling loop. However, in the existing recycling infrastructure, the introduction of impurities and trace elements (ITEs) into secondary low alloy wrought aluminum is widespread, leading to the necessity of degrading the alloy to a cast alloy with less stringent ITE restrictions. Consequently, the resultant blend of various metals and oxides presents challenges for separation. Current recycling techniques possess limited separation capabilities, likening the recycling process to purifying contaminated water by diluting it with clean water (primary aluminum) until the pollution levels reach an acceptable standard for use [10, 15, 16].

1.2.5 Quality Techniques to Monitor Molten Aluminum

When recovering aluminum, the losses are often seen as mass lost during the remelting process. However, material degradation can occur within the retained mass due to excessive oxidation and effects the material performance after casting. Oxide content in molten metal is a common issue in secondary aluminum melting, affecting production yield in both casting and wrought alloys. The LOOP technique developed by BRYNE offers an industrial solution for measuring oxide content during the melting phase. By combining this with hydrogen content measurement techniques like the Density Index and the First Bubble Method, it becomes possible to assess the effectiveness of salt flux refinement in cleaning secondary low alloy aluminum [21].

1.3 Aim

This thesis is conducted from an industry perspective and proposes both a cost and an emissions model regarding the mass losses and material degradation incurred from melting car chillers as the low alloy aluminum is reintegrated into the production cycle. The following research questions will be addressed:

- RQ1:** What costs and emissions might accompany the remelting process of heavily oxidized car chillers or other sources of secondary low alloy aluminum?
- RQ2:** How does the oxide content, as identified by BRYNE’s quality techniques, challenge the purification of secondary low alloy aluminum during remelting?
- RQ3:** What do the combined results of the LOOP, Density Index, and First Bubble Method indicate about the quality of the melt?

1.4 Structure of Thesis

Chapter	Summary
Chapter 2: Theoretical Background	This section contains background definitions related to aluminum alloy classification, metallurgical processing, dross and slag, salts, measurement techniques, and equipment used throughout the experiments. This includes the LOOP technology, as well as environmental loads and cost models.
Chapter 3: Methodology	Outlined here is the procedure used for conducting experiments utilizing the LOOP technology at BRYNE facilities, as well as the methods employed to estimate density index, hydrogen content, and optical emission spectroscopy.
Chapter 4: Results	Presented are the measurement distances utilized in the LOOP to determine fluidity, changes in material composition via optical emission spectroscopy, density index, and nucleating technique (“first bubble”) both before and after cleaning treatment. Additionally, proposals for cost and carbon emission models for the setup used in the experiments are provided.
Chapter 5: Discussion	Identification of changes during the cleaning treatment of the aluminum alloys regarding composition, fluidity, and quality, along with assumptions and potential improvements to the proposed equations, and how these changes may impact the scientific based targets used within the industry.
Chapter 6: Conclusion	Addresses the research questions and proposes avenues for future research in the field.

2 Theoretical Background

2.1 Classification of Aluminum Alloys

The wide and complex field of aluminum alloys includes various alloying elements, heat treatments, and mechanical processes. For uniformity and clear expectations regarding the properties of each aluminum alloy composition, standardization is crucial.

The initial classification of aluminum alloys hinges on whether they belong to the wrought or cast alloy category. Wrought alloys maintain a lower element percentage to preserve aluminum's ductile traits, crucial for products subjected to mechanical processes like rolling, forging, pressing, or extrusion. In contrast, cast alloys are intended to be shaped through casting and subsequently finished via machining. While similar alloying elements are used, they are often present in higher percentages to achieve desired properties for cast products [22].

As per the American National Standard Alloy And Temper Designation Systems For Aluminum (ANSI H35.1), wrought aluminum alloys are categorized into families based on their composition. This nomenclature system consists of a four-digit code. The first digit signifies the primary alloy, often referred to as the "series" or "grades." The second digit indicates if there is a modification of the original alloy; for instance, 6160 is the first modification of 6060. Lastly, the third and fourth digits are assigned arbitrarily to distinguish the alloy, except for the 1xxx series, which denote the purity level. Table 2.1 lists the alloy series/grades and their primary alloying elements [22].

Table 2.1: Wrought aluminum alloy classification [22].

Alloy Series	Primary alloying elements
1xxx	Unalloyed, aluminum > 99%
2xxx	Copper
3xxx	Manganese
4xxx	Silicon
5xxx	Magnesium
6xxx	Magnesium and Silicon
7xxx	Zinc
8xxx	Other elements

For the consistency of this thesis, the nomenclature approved by ANSI and established by The Aluminum Association (AA) will be employed. It is important to note that other commonly used nomenclature systems exist in both academic and industrial communities:

- **ANSI/AA (The Aluminium Association):** AA is the most widely accepted system. It designates the prefix "AA" and is followed by four digits.
- **UNS (Unified Numbering System):** UNS is predominantly used in North America. UNS designates a one letter prefix "A" and is followed by five digits. The system does not ensure precise composition and often refers to other nomenclature systems, such as the

conversion of aluminum 6061 (AA6061) into UNS A96061.

- **EN (European Norm):** EN was created by the European Union to unify the already existing designations within each of its member states. EN designates the prefix “EN,” followed by “AC” or “AW” depending on if the alloy is wrought (AW) or cast (AC), and ends with a four digit numbering sequence that is identical to AA.
- **ISO (International Organization for Standardization):** ISO designates the prefix “AL” followed by the complete chemical composition of the alloy. ISO is often found in academia and research communities, while the industry sector has yet to fully embrace this format.

A comparison of these four prominent systems is presented in Table 2.2.

Table 2.2: Aluminum alloys across different nomenclature systems [23].

ANSI/AA	UNS	EN	ISO
AA6061	A96061	EN AW-6061	Al-Mg1SiCu
AA6063	A96063	EN AW-6063	Al-Mg0.5Si
AA2024	A92024	EN AW-2024	Al-Cu4Mg1
AA7075	A97075	EN AW-7075	Al-Zn6MgCu

2.2 Sorting and Scrap Preparation

Greater cost savings, cleaner material preservation, and reduced emissions are clear benefits of sorting alloys before purifying them through melting, according to the Waste Hierarchy concept [2]. Recurring losses during melting and the inevitable accumulation of ITEs as alloys are recycled limit the number of times the material can be circulated before requiring dilution using primary resources [15, 17].

Sorting based on composition offers the chance to either reuse the alloy as it is or adjust its composition with minimal resource investment. Wrought aluminum, containing a small percentage of alloying elements [22], is highly prone to contamination [13, 15, 24]. The stringent limit of ITEs in wrought alloys, in contrast to cast alloys, presents a significant challenge to existing recycling facilities [13, 24, 25]. Various sorting techniques, whether used alone or in combination, provide multiple solutions for handling different types of scrap. Table 2.3 summarizes the techniques used in sorting and comminution methods in regards to secondary aluminum.

Table 2.3: Common techniques used in comminution and sorting methods [13, 25].

Method	Technique	Definition
Comminution	Impact Crusher	Utilizes high-speed rotating hammers smash hard materials like rocks and concrete into smaller pieces.
	Shredder	Similar to crushers, but optimizes parameters for different materials to achieve desired sizes or forms.
	Jaw Crusher	Material is compressed between two spring or hydraulic-loaded plates until it shatters.
Sorting	Hand Sorting	Operators distinguish aluminum from other materials, often collaborating with cameras and other sensors.
	Magnetic Separator	Strong magnets are used along a conveyor belt to deflect magnetic materials, such as iron.
	Eddy Current Separator	Induces a magnetic field that attracts metallic particles of a certain size. It is often used after a screen.
	Air Separator	Material weight is utilized, and air jets sit underneath the conveyor belt to float lighter materials away.
	Cyclone	Based on the inertia of different materials. Heavier objects spin to the outside while lighter objects remain central. It is particularly useful for separating dust.
	Sink Float	Material is submerged in a bath whose density is between the desired components to be separated.
	Hot Crush	Cast alloys have a lower solidus temperature than wrought ones. Both alloys are heated; cast is crushed whereas wrought is deformed.

2.3 Melting Process and Oxidation

Because of its strong affinity for oxygen, aluminum readily reacts with the surrounding air, leading to the formation of aluminum oxide. Drawing from research and insights found in Christoph Schmitz's textbook *Handbook of Aluminium Recycling* (2014), the reaction follows the equation [25]:



The resulting mass balance is:

$$2 \cdot 27 + \frac{3}{2} \cdot 32 = 104 \quad (2.2)$$

While in its solid state, this reaction benefits aluminum alloys as it generates a protective layer on exposed surfaces, effectively halting further oxidation and corrosion. However, in its liquid state, the oxide layer continues to form but is constantly disrupted by thermal or mechanical forces, resulting in continuous oxidation of the melt (Figure 2.1c).

Schmitz (2014) explains that a positive energy value (ΔH) in Equation 2.1 indicates an

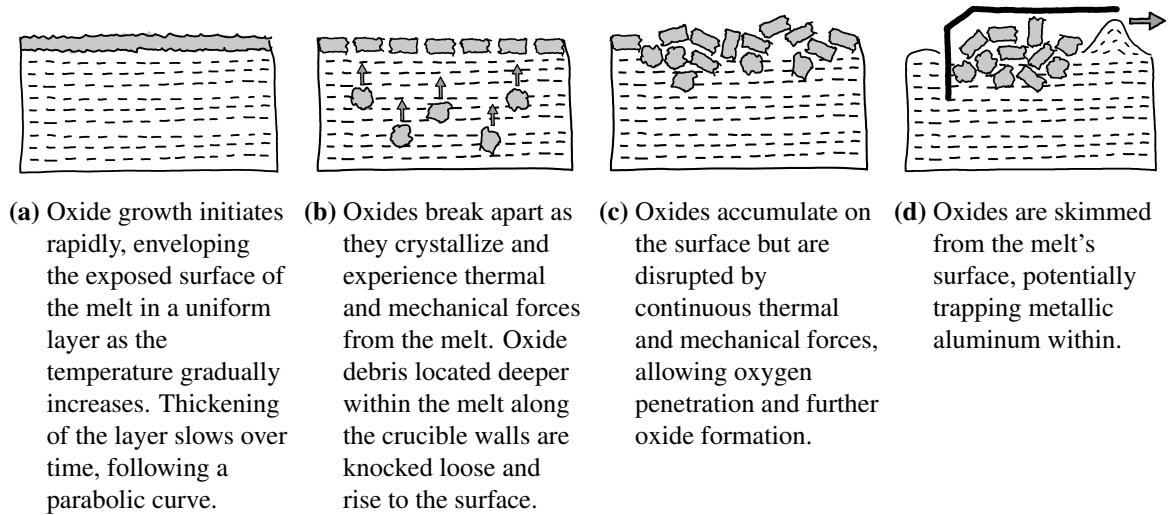


Figure 2.1: Depiction of oxide formation on the surface of the aluminum melt [25].

exothermic reaction. As mentioned earlier, oxidation occurs rapidly, and being exothermic means the reaction does not require additional energy to proceed. When examining the crucible's shape within the furnace and the resulting exposed surface area of the melt, we can derive the ratio between oxidation velocity (\dot{m}) and surface area (a_{spec}):

$$a_{spec} = \frac{m}{A} \quad (2.3)$$

$$\frac{\dot{m}}{m} = k_s \cdot a_{spec} \cdot \exp\left(-\frac{E}{R \cdot T}\right) \quad (2.4)$$

with m = mass, A = area, \dot{m} = velocity of oxidation, k_s = velocity factor, E = activation energy of reaction, R = gas constant, and T = absolute temperature.

By multiplying Equation 2.4 by time, one can determine the quantity of oxides generated. And, referencing Equation 2.2, the specific density of the aluminum oxide (104) is roughly twice that of the aluminum (54). Meaning the theoretical weight of oxides can be derived.

However, it's worth noting that while this calculation is helpful, the final weight estimation may not precisely reflect real-world test data. This is due to several other factors influencing oxidation during the melting process of primary alloys, and additional variables introduced during the melting of secondary alloys. According to Schmitz (2014), the oxidation velocity factor (k_s) does not remain constant with temperature. Oxide growth spikes between 760°C and 780°C, contingent upon the composition of the melt. Virtually all alloying elements exert an influence on oxide growth at higher temperatures [25].

For example as secondary material is melted down from a solid state to a liquid state, heat is initially applied to the exterior of the solid ingot and must gradually penetrate inward until the bulk of the ingot reaches the melting temperature. The heat transfer process from the furnace environment through the solid ingot is inefficient due to the presence of various alloying elements and cavities scattered throughout the microstructure of the secondary al-

loy. As a result, the secondary alloy undergoes multiple instances of melting and cooling at a microscopic level as different elements are heated and subsequently solidified upon contact with other elements that have yet to attain their respective melting temperatures. The resulting temperature fluctuations produce additional oxides within the bulk of the ingot. Figure 2.2 illustrates a possible example of the intricate path heat must navigate as it penetrates the ingot.

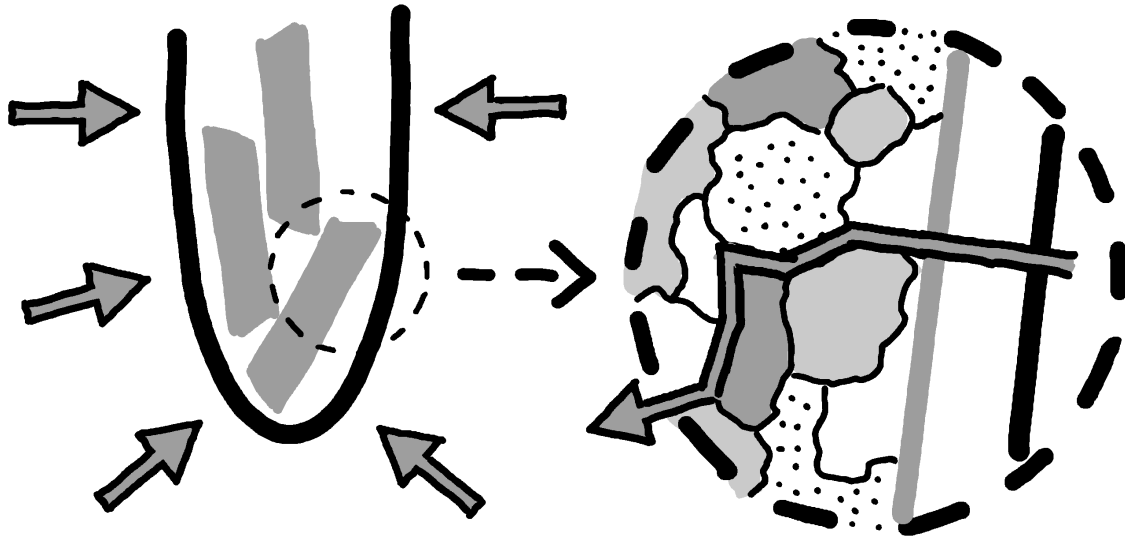


Figure 2.2: Heat from the crucible radiates into the ingots. The rate and uniformity of heat penetration vary based on the composition of the scrap material [25].

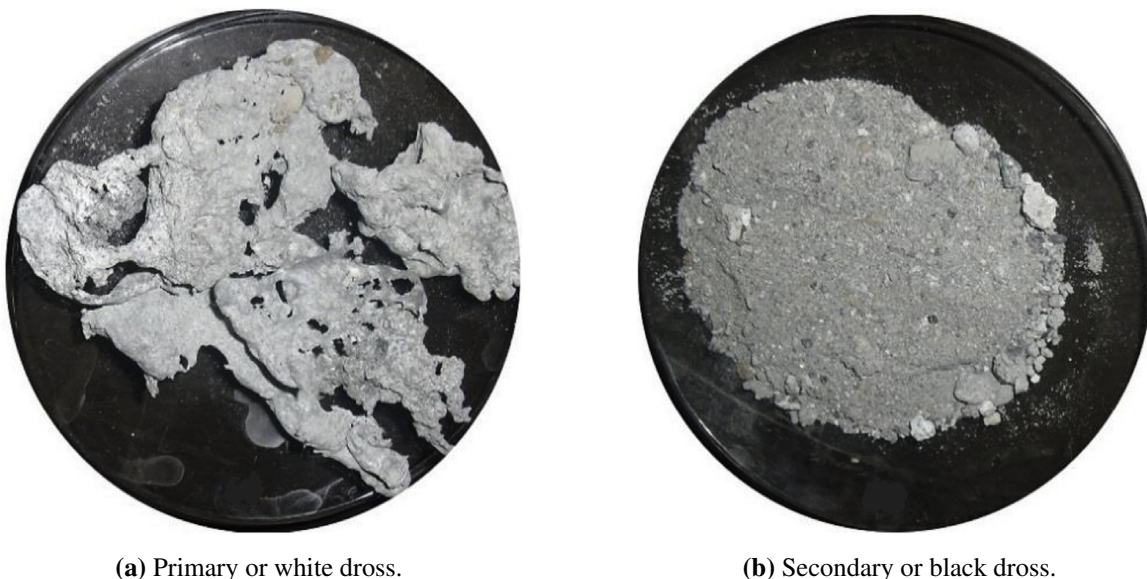
2.4 Dross, Slag, and Salt Slag

The waste, residue, or loss generated from oxidation is known as “dross.” Depending on the charged material, dross may contain varying percentages of metallic aluminum and non-metallic substances referred to as “slag.” When salt is used in the purification process, the slag takes on the term “salt,” transforming into salt slag. Slag and/or salt slag consist of oxides, which may include, among others, aluminum oxides, oxides of alloying elements (Si, Cu, Fe, Zn, etc.), spinels, chlorides, fluorides, carbides, nitrides, sulfides, and phosphides [13, 15, 24, 25, 26].

Importantly, especially concerning secondary scrap, without precise knowledge of the composition of the charged materials, establishing the correlation between charged material and resulting oxide formations is nearly impossible using existing quality measuring techniques. While understanding the complete composition of material throughout the melting process is highly beneficial to plant operators, the resources and expertise required for rigorous quality checks are often not economically feasible. Such limitations do not imply that the industry operates without insight; instead, it depends on recycling infrastructure, supplier transparency, and clever yet straightforward techniques to ascertain the composition of secondary alloys. This involves careful consideration of the risks associated with certain impurities finding their way past quality control measures [21, 25].

According to research [13, 26, 27], the aluminum industry simplifies the categoriza-

tion of dross as either black or white, based on whether salt is added to the melting process or not, respectively. White dross forms within primary industry melting furnaces and typically contains metallic aluminum ranging from 15% to 70% of its composition, which is easily remelted. Recovery is feasible because the primary aluminum is nearly pure, and the resulting white dross has minimal ITEs, contamination, or slag, allowing it to be safely reintroduced into the melting process. Black dross forms within secondary industry melting furnaces when salts are involved. The dark color is due to ITEs reacting with the salt. The typical metallic aluminum content is 10-20% of its composition. Hence, reclaiming the entrapped aluminum within black dross requires specialized equipment to separate the salt slag.



(a) Primary or white dross.

(b) Secondary or black dross.

Figure 2.3: Image comparison of primary/white and secondary/black dross [26].

2.4.1 *Thermitting*

Within the furnace, dross encounters some of the highest temperatures, primarily due to its direct contact with the melt and the exothermic reaction previously expressed in Equation 2.1. Even after the dross is removed from the furnace (Figure 2.1d), this reaction persists and consumes any residual metallic aluminum trapped within the dross. This phenomenon is commonly referred to as “thermitting” in the industry, attributed to the brief bursts of heat and localized temperature rise observed [21, 26].

If not managed properly, a sufficiently large pile of dross will continue to react for many hours. The heat emitted from the pile poses a safety risk, and plant regulations mandate that the dross must cool before handling. Unfortunately, at this stage, most of the entrapped metallic aluminum will have burnt away, resulting in material and cost losses, as well as additional emissions. Solutions to limit thermitting include quenching the dross in water, depositing it in another furnace for recovery, or simply spreading it on the floor [24, 25, 27].

2.4.2 Salt Flux

Salt flux boasts numerous applications during the melting phase of aluminum [24, 25, 26]. Essentially, it is added to the melt to capture ITEs and enhance the efficiency of the melting process. Common applications include:

- Thickening and repair of the oxide layer to prevent further oxidation (Figure 2.4a and 2.4b).
- Forming a matrix with the oxide layer that allows metallic aluminum droplets to descend through and redeposit into the melt (Figure 2.4c).
- Mixed and stirred into the melt as a refining agent, the salt flux adheres to ITEs and oxides within secondary melting furnaces, causing the particles to rise to the surface. This process aids in purifying post-consumer scrap, leading to the formation of black dross.

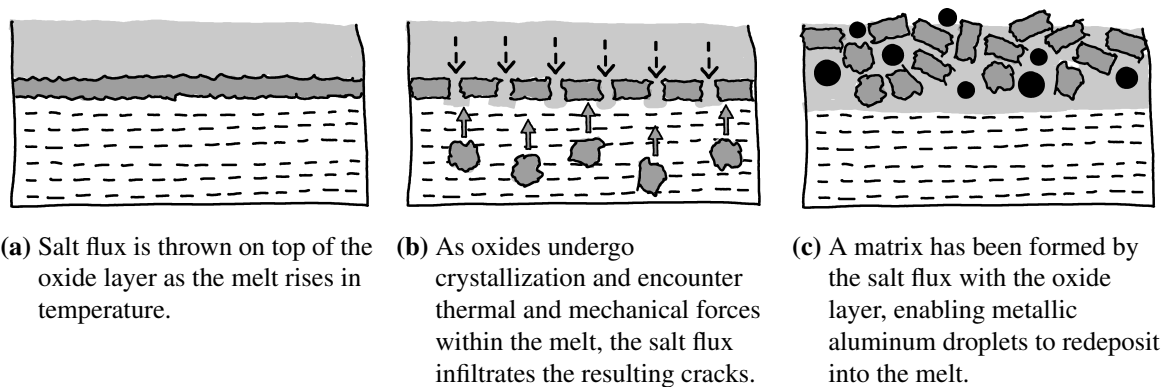


Figure 2.4: Depiction of oxide formation with the addition of salt flux on the surface of the aluminum melt [26].

Despite its advantages, salt flux is employed sparingly due to the classification of the resulting salt slag as a toxic and hazardous waste product according to the European Waste Catalogue and Hazardous Waste List [28]. Capuzzi and Timelli (2018) elaborate upon each code within the catalog identifying the hazardous properties of salt slag. Their findings and the definitions listed in the catalog are summarized in Table 2.4.

Within salt slag lies the potential to reclaim its salt content through additional processing. Otherwise, appropriate disposal methods are imperative, directing salt slag to specialized landfills designed for hazardous materials. Predominantly comprised of sodium chloride (NaCl) and potassium chloride (KCl), salt slag poses risks of chloride leaching and GHG emissions upon contact with water. Legislative restrictions in the US, Canada, and Europe forbid the disposal of salt slag into landfills, compelling companies in these regions to innovate treatment techniques. As a result, they have developed the expertise to retrieve both the salt and the entrapped metallic aluminum droplets [13, 24, 25, 26, 28].

Table 2.4: Codes identifying the hazardous properties of salt slag found within the European Waste Catalogue and Hazardous Waste List [13, 28].

Code	Title	Definition
H3-A	Highly flammable	Substances and preparations that have the potential to become hot and spontaneously ignite upon contact with air at ambient temperature, without any external application of energy.
H4	Irritant	Non-corrosive substances and preparations that, through immediate, prolonged, or repeated contact with the skin or mucous membrane, have the potential to cause inflammation.
H5	Harmful	Substances and preparations that, if inhaled, ingested, or absorbed through the skin, may pose limited health risks.
H13	Leachable	Substances and preparations that, after disposal, can produce another substance, such as a leachate, which exhibits any of the characteristics listed above.

2.4.2.1 Aرسال 2125

The salt flux chosen for the tests conducted within this thesis, is Aرسال 2125. This particular salt flux serves as a refining agent intended for mixing within the melt. It is marketed to be effective for for all hypoeutectic and eutectic aluminum, both wrought and casting alloys, boasting the following attributes:

- Removes oxides from the melt by flotation and reduces the hydrogen content.
- Yields a fine, powdery dross with low metallic content.
- Works in all furnace and crucible types.
- Facilitates the easy removal of adherences.
- Exhibits minimal smoke and odor emissions.

2.5 Measurement Techniques & Equipment

2.5.1 Optical Emissions Spectroscopy

Optical emission spectroscopy (OES) is the scrutiny of light that is emitted from a medium without any external optical stimulation [29]. Emission spectroscopy has its early starts in 1834 with Fox Talbot's experiments with a spectroscope using strontium and lithium. It is through this technique that several elements of the periodic were discovered such as rubidium, caesium, and thallium in 1861, indium in 1864, and gallium in 1875 [30]. With the development of atomic physics, an area capable of providing explanations of the origin of the observed phenomena, emissions spectroscopy started to become more reliable and progress as a technique for chemical analysis.

The basic principle behind OES is the use of energized samples through energy, leading to a state of excitation of the atoms. These atoms transition back to lower energy states, emission rays or spectrum rays are emitted, which are then used for measurements according to their corresponding photon wavelengths. The identification of the elemental composition

relies on the positions of these emission rays, while the intensity of the rays determines the concentration of each element [31].

Optical emission spectroscopy involves collecting, dispersing spectrally, and detecting light. Due to the typically strong OES signals from plasmas, optimization of light collection and detection efficiencies may not always be necessary. However, efficient detection becomes crucial when swift analysis is paramount, especially when only a small portion of the surface is under scrutiny, such as in endpoint detection during plasma etching of patterned films [31].



Figure 2.5: Example of apparatus used for optical electron spectroscopy, in image an iSpark 8820 OES Metal Analyzer from Thermo Fischer Scientific [32].

Figure 2.5 illustrates an apparatus use for OES. The emission originating from a specific volume within the plasma chamber is focused onto the entrance slit of a spectrometer using a sequence of lenses. As emission within the 200-900 nm range is commonly collected, it is advisable to utilize UV-grade fused-silica lenses. The position of the imaged volume can be laterally adjusted by relocating the collection lenses or, exclusively in research reactors, by translating the plasma reactor itself. The collected light can be projected directly onto the spectrometer slits or conveyed to it via optical fibers. The results of experiments using OES provides with chemical composition detected within the tested sample, useful to determine what elements from the periodic table constitutes it [29].

2.5.2 *Reduced Pressure Test*

In the manufacturing of high-quality aluminum alloy castings, porosity stands out as a crucial factor affecting quality. Although some level of porosity is unavoidable in any casting process, its presence can greatly compromise surface quality and lead to a decline in mechanical properties and resistance to corrosion. Hydrogen, a gas capable of dissolving extensively in molten aluminum while showing minimal solubility in its solid state, primarily contributes to “gas porosity” in castings, in contrast to “shrinkage porosity”, which arises from volume reduction during solidification [33]. Various elements can also impact the formation of gas porosity, including the pressure occurring during solidification material, the chemical configuration and solidification capability of the alloy and the rate at which cool-

ing occurs. The cleanliness of the melts, especially with regard to the existence of oxides and inclusions, is also gaining recognition as a significant factor, as it affects the nucleation of hydrogen gas [34]. Hence, it is crucial to regulate the hydrogen levels of the melt to manage the quality of the casting output.

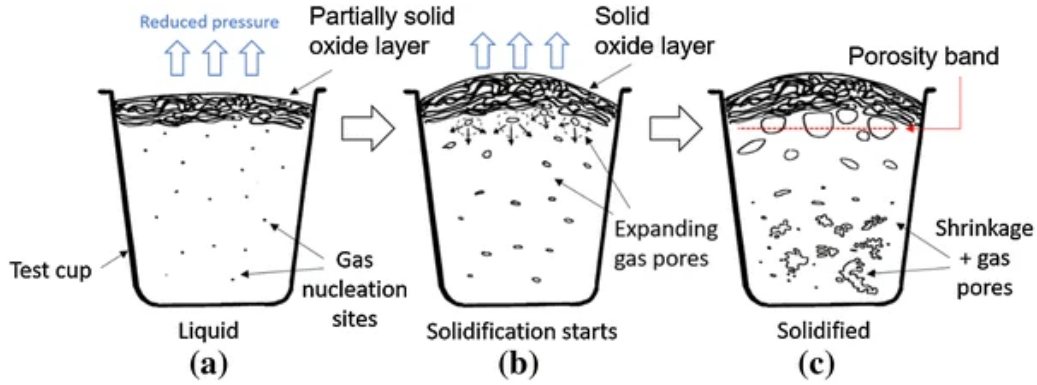


Figure 2.6: Solidifying mechanism for the RPT for a melt with a high oxide content (a) Sample material before solidification starts, (b) start of solidification, and (c) sample after solidification [35].

Techniques had been developed to understand and measure meticulously the hydrogen levels in metal melt before casting it. Among such techniques is the reduced pressure test (RPT), also known as Straube-Pfeiffer test or vacuum gas test, popularly adopted in foundries [36]. The procedure commonly followed in foundries will be further describe in the methodology section and employs general procedure establish in literature as well as mentoring from BRYNE [21, 37, 38].

The visual evaluation consists of making a section of the samples, making observations of the pores found within the sections, and comparing the results with a gas sample chart. The chart is usually composed of different photos of various photos of distinct cuts of RPT samples. The photos will reference a definite density, DI, and/or percentage of porosity number. The downside of this technique is that it relies on the visual evaluation of the operator, meaning that each operator will report different results according to their own expertise. Furthermore, the sample requires preparation for visual evaluation, which includes cutting in half (creation of sections), grinding and polishing, which requires work and tools [37].

The Density Index method is the traditionally used method used in most foundries around the world for its simplicity and easy to estimate parameters [38]. DI can be used a key performance indicator for metal purity [39]. DI can be calculated using the following Equation 2.5:

$$DI = \left(\frac{\sigma_A - \sigma_B}{\sigma_A} \right) \cdot 100 \quad (2.5)$$

where:

- σ_A - represents the density the sample solidified under atmospheric pressure
- σ_B - represents the value of density solidified under vacuum

2.5.3 First Bubble Method

This test was proposed by Y. Dardel, principle that serves as basis for hydrogen measuring devices used in the industry [40]. The method uses Sievert's Law for partial vapor pressure [41]. This law states the amount of gas dissolved in a liquid is determined by both the partial pressure of the gas within the liquid a constant associated with the liquid's temperature and the gas's solubility [39].

$$H = k\sqrt{P_{H_2}} \quad (2.6)$$

where:

- H - represents the concentration of hydrogen that has dissolved in the aluminum melt
- P_{H_2} - represents the partial pressure of hydrogen in the atmosphere
- k - represents a temperature-dependent constant

Alternative equation to the one above is:

$$\log(C_H) = 0.5 \cdot \log(p_{H_2}) - \frac{A}{T} + B \quad (2.7)$$

where:

- C_H - represents the concentration of hydrogen that has dissolved in the melt or in this thesis, aluminum melt
- P_{H_2} - represents the partial pressure of hydrogen in the atmosphere
- T - represents a temperature
- A, B - represents Sievert's constants, which depends on the alloy composition used in the experiments

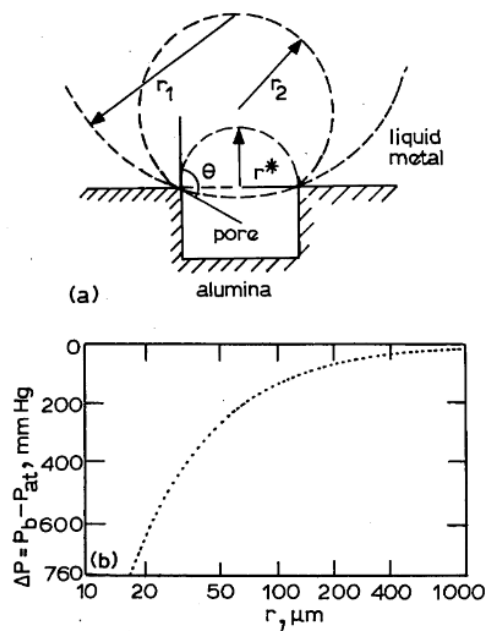


Figure 2.7: (a) Diagram of how of a bubble of hydrogen or nucleation occurs within the alumina pore and (b) graph illustrating the effect of pressure and the radii of a pore [42].

In general, the test occurs using a small sample of molten metal being placed in a closed chamber and under the effects of vacuum affecting progressively until a first bubble appears in the molten metal surface [41]. Looking at Figure 2.7, as the pressure of vacuum decreases, the radius of the pore or bubble form in the alumina increases in volume forming and increasing hydrogen will diffuse into it [42]. This phenomenon is important because the method is based on operator knowledge and experience using the apparatus, so understanding of the material composition, the effects of melting temperature, and alloying.

2.5.4 Fluidity using LOOP

The definition of fluidity varies according to the area of study and application. The “fluidity” used in foundry is utilized to demonstrate the distance a molten metal can circulate in a mould of consistent cross-sectional area before solidification occurs [43].

Fluidity research and technology is not a recent development. One of the first documented scientific research of the variables affecting fluidity are from Portevin and Bastien in the 1900s [44]. Their research consisted the construction of an early version of a fluidity spiral test, permitting the quantification of essential parameters affecting the fluidity of cast iron. Around the 1950’s, fluidity studies regarding aluminum alloys began at the Massachusetts Institute of Technology (MIT) and later reviewed in the 30th World Foundry Congress [45].

Fluidity is an important quality of molten material. It can determine whether a mold cavity can completely fill or have an early halt, thus resulting in an incomplete fill. Various variables determine the fluidity of a molten material [46]:

1. Metallurgical factors, including composition (alloying effect), superheat, latent heat, surface tension, viscosity, and mode of solidification and,
2. Mold/casting factors, which includes cooling rate, degree of super heat, mold material, and superficial characteristics.

Considering the advancements in the comprehension of fluidity and its variables affecting it, there is no dependable theoretical models that are capable of predicting fluidity phenomena in aluminum alloys [46], hence mechanisms to achieve a thorough understanding of fluidity are developed, an example being the “LOOP” system. The LOOP is a tool use for measuring metal quality through its fluidity. It is designed for a one-time use and elaborated with compressed Alkaline Earth Silicate (AES) wool for safety reasons. Its chemical composition, physical composition, thermal conductivity, and dimensions is layout in Table 2.5a, Table 2.5b, Table 2.5c, and Table 2.5d respectively.

The LOOP test is a combination of the LOOP, a filler cup (made of AES wool as well), and plug (allows the accumulated metal in the cup to flow inside the spiral and is made of the same material as the LOOP and filler cup) that conforms to a system capable of measuring fluidity. The LOOP consists of two major components:

1. Drag: component on which a spiral is embedded.
2. Cope: component that contains an opening for the molten metal to flow through the spiral and a vent that lets gases escape during experimentation. It is glued over the drag with a

special kind of glue known as water glass (it is a binder metasilicate).

The molten metal is poured into the filler cup and after unplugging the stopper, the metal pours into a channel of five millimeters thick. The spiral embedded is marked with distance points, allowing a user to determine the fluidity. The distance a material flows will depend on its properties such as chemical composition and the experimental setup being used, for instance, temperature of furnace and cleaning treatment applied.

2.6 Environmental Load and Carbon Emission Cost Models

The manufacturing sector is gradually acknowledging the importance of environmental sustainability [47, 48]. Yet, it confronts notable hurdles, such as escalating pollution and carbon emissions, notably from emerging economies [49]. Although environmental regulations play a crucial role in protecting public health, they can also impede productivity and competitiveness [50]. Thus, there exists an urgent demand for the industry to alleviate its environmental burdens by embracing cleaner technologies and promoting more sustainable approaches. An approach for industries and organizations is to employ mathematical models to monitor, adjust to new inputs, and outputs of environmental loads and carbon emissions for a thorough understanding of their processes. One way to help with the development of such models is the creation of the carbon emission factors (CEFs), which are standard coefficients used to estimate carbon emission activities in terms of how much carbon dioxide is used [51]. These factors are then employed in mathematical modeling equations, fitting to where they are most needed for proper estimations of carbon emissions.

Recent progress in mathematical modeling of environmental loads has been propelled by the increasing utilization of computational fluid dynamics (CFD) and finite element analysis (FEA). Norton [52] underscores the increased realism achieved through CFD simulations in designing ventilation systems for agricultural production, while Stopford [53] delves into the increasing sophistication and application of CFD within the power generation and combustion sectors. These advances have also been complemented by the evolution of economic input-output models for environmental life-cycle assessment [54] and the examination of load modeling techniques [55]. However, more research is warranted to address the constraints of existing load models and integrate emerging load factors. In the following subsections, carbon emissions models and cost models are discussed in the context of manufacturing, how they are used, and what calculations can they be performed.

2.6.1 Carbon Emissions Models Overview

Developing a robust quantitative model of carbon emissions is imperative to curb carbon emissions within the mechanical manufacturing sector. Carbon emissions during mechanical manufacturing processes exhibit characteristics such as diverse sources, unclear evaluation boundaries, and challenges in accurate quantification. The establishment of a carbon emission quantitative model serves as a foundation for low-carbon manufacturing and carbon emission reduction technologies. By implementing such a model, professionals can effectively identify areas of intensive carbon emissions and derive theoretical guidance and foundations for emission reduction efforts. Currently, research on carbon emission mod-

Table 2.5: Various properties of LOOP technology [21].

(a) LOOP chemical composition in %.

Chemical Compound	%
SiO ₂	60 - 67
CaO	27 - 33
MgO	3 - 7
Al ₂ O ₃	< 1
Fe ₂ O ₃	3 - 7

(b) LOOP physical properties.

Physical	Value
Color	White/beige
Melting Point	< 1330
Density	270 kg/m
Modulus of rupture	> 700 kPa
Highest recommended user temperature	1100°C

(c) LOOP thermal conductivity in W/mK.

Average temperature	Conductivity
400°C	0.07
600°C	0.10
800°C	0.14

(d) LOOP dimensions.

External Dimensions	Measurements
Lower part	196mm x 196mm x 14mm
Filler	∅ 65mm x 50mm x ∅ 80mm
Stopper	≈ 80mm pull-wire height
Total Weight	≈ 150g

els within the mechanical manufacturing industry is mainly focused on layers that include part design, processing technology, processing equipment, and processing systems [56].

In manufacturing systems, the design features of parts influence successive manufacturing processes; therefore, acceptable and practical design features can reduce the production of carbon emissions for subsequent processes [57]. Multiple research efforts are ongoing in this area. Studies revolving around the effects of microdesign features in the production of carbon emissions [58]. A proposed model to predict an estimated theoretical energy consumption using study cases of milling parts with prism shapes [59]. The development of an empirical model for carbon emissions for three cylindrical parts with different work processes was proposed by Pawanr et al. [60], while Zheng [61] proposes a model of evaluation of carbon emissions that can be used in sand casting processes.

Processing technology of parts represents a high sources of carbon emissions in a manufacturing process [62]. Research at this level has been conducted in a variety of areas. Evaluation of material testing including Ti-Al-4V titanium alloys through different turning scenarios such as wet and dry turning variations showing 22% less carbon emissions in dry turning over its wet counterpart [63]. In the case of a manufacturing process that employs stamping procedures in the chain value, a carbon emission assessment model have been created, with results impacting an overall 20% reduction in CO₂ [64]. There are relevant technologies that have progressively been research, like grinding, laser welding, and drilling [65, 66, 67].

There are many different types of machining processes in the manufacturing industry, affecting energy consumption and carbon emissions in each processing stage, therefore, constructing an accurate carbon emission model for parts manufacturing has proven to be a difficult research [56]. Based on a elaborated research on CNC based machining systems, Li et al. (2013) proposes a quantitative model for measuring carbon emissions within such systems:

$$CE_{ms} = CE_{elec} + CE_{tool} + CE_{coolant} + CE_m + CE_{chip} \quad (2.8)$$

where:

- CE_{ms} stands for the total CO₂ emissions generated in a given system
- CE_{elec} stands for the CO₂ emissions generated by electricity required for machining operations
- CE_{tool} stands for the CO₂ emissions generated by production of cutting tools
- $CE_{coolant}$ stands for the CO₂ emissions generated by the use of cutting fluids
- CE_m stands for the CO₂ emissions generated by the dissipation of raw materials using a CNC machine
- CE_{chip} stands for the CO₂ emissions generated by the chip removal phenomenon occurring during CNC machining operations.

Parameters such as this are establish with the purpose to be reuse in different manufacturing scenarios as they deem applicable. For instance, Jiang et al. (2019) employs the carbon emission for electricity in a customized version for turning machines:

$$C_{energy} = CF_{ene} + EC_{ene} \quad (2.9)$$

In this equation, CF_{ene} stands for the carbon emission of electricity which will depend on the electrical grid of the territory, zone, and country, and EC_{ene} corresponds to the power employ by machinery, which the authors broke down into:

$$EC_{ene} = P_{basic}t_{stand-by} + P_{idle}t_{idle} + \int_0^{t_{cut}} P dx \quad (2.10)$$

Equation 2.10 exemplifies parameterization of the electrical power require for a machinery to work on standby, idle state, and actual running time in the manufacturing case of turning machining operations [69].

Development of denominated “carbon emission assessment index” has been research and formulated for machine tools, assessing three main perspectives: social, environmental, and economical [70]. Inclusion of carbon emissions generated by the operator is another variation of a model that have been developed in addition to the processing energy consumption caused by machining tools [71]. An almost real-time energy consumption predictor model used for machining tools is being constructed utilizing real time data collection combine with an adaptive Gaussian Process regression model, retrieving data from a milling machine’s tool and sensors and transform the data into compatible inputs for the model while optimizing its computational capabilities to near real time calculations [72]. The article written by Lv et al. [73] describes a “green” model of CO₂ emissions for five different machining tools and evaluating them in three “green” categories including energy efficiency, carbon efficiency and green degree (ability to impact the environment resources and comply with the requirements of sustainable development).

The mechanical processing layer in manufacturing is normally utilized for batch productions with various CNC machine tools working in parallel and sequentially [74]. Similarly to processing equipment, the operations happening inside a machining system can become complex and aleatory, thus, emission models can become difficult to produce. In the literature, a model to quantify sustainability levels in a mechanical processing system was structured and an entire carbon emission analysis framework was designed and tested using CNC machining system scenarios [68, 75].

The research of the layers for mechanical manufacturing explained above have demonstrated limitations to certain aspects of the process. Areas including logistics systems and scheduling often result in overlooked, or even include only energy considerations for emissions calculations. As a standard, emission models tend to generalize their aim to specific processes or the generation of parts. Theoretical model proposed by He et al. [56] includes a framework that includes aspects for all layers in general terms and areas of transportation and logistics, which may proved useful for companies that desire to measure their entire system.

2.7 Production Cost Model

2.7.1 *Confiding in the Model*

The power of a model lies in how well it matches reality. A solid model takes in feedback from different sources, allowing for flexibility and continuous improvement. En-

gineers, in charge of production, use investigative tools to gather cost data and plug it into the model for fine-tuning. Moreover, these investigations should lead to broader decision-making options to set up meaningful key performance indicators (KPIs), guiding future production goals.

Based on Olsson (1976, 1985), the cost model for integrated product development needs collaboration across the company's departments. It should account for costs related to market demands, construction, manufacturing, finances, and research. The model's calculations, aided by tools such as Statistical Production Analysis (SPA), should offer data for conducting a value analysis, evaluating the extra value derived from the suggested alterations [76, 77].

2.7.2 Reference Model

Ståhl et al. (2007) has devised an economic model (Equation 2.11) for judging production development within discrete part manufacturing [78] based on concepts from Olsson's work. This model will serve as the basis for all proposed models derived from relationships observed during the aluminum melting process.

$$\begin{aligned}
k = & \frac{k_A}{N_0 \cdot n_b \cdot n_{part}} \Big|_a + \frac{k_B}{N_0} \left[\frac{N_0}{(1 - q_Q)(1 - q_B)} \right]_b \\
& + \frac{k_{CP}}{60N_0} \left[\frac{t_0 \cdot N_0}{(1 - q_Q)(1 - q_P)} \right]_{c1} \\
& + \frac{k_{CS}}{60N_0} \left[\frac{t_0 \cdot N_0}{(1 - q_Q)(1 - q_P)} \cdot \frac{q_s}{(1 - q_S)} + T_{su} + \frac{1 - U_{RP}}{U_{RP}} \cdot T_{pb} \right]_{c2} \\
& + \frac{n_{op} \cdot k_D}{60N_0} \left[\frac{t_0 \cdot N_0}{(1 - q_Q)(1 - q_P)(1 - q_S)} + T_{su} + \frac{1 - U_{RP}}{U_{RP}} \cdot T_{pb} \right]_d
\end{aligned} \tag{2.11}$$

Ståhl's model is divided into four sections (a-d), each pertaining to a distinct aspect of the production system.

- a:** Tooling costs.
- b:** Raw material costs.
- c1:** Equipment cost during production.
- c2:** Equipment cost at standstill.
- d:** Labor costs.

In each section, Ståhl utilizes loss parameters concerning quality rejections (q), downtime (s), and production rate losses (p). Each loss parameter consists of relationships detailing the production system under consideration. Within the context of discrete part production, these loss parameters interact with each other according to the diagram illustrated in Figure 2.8 [78].

Ståhl and Windmark further explain the cost in their textbook *Sustainable Production Systems: The link between technology and economy with a global perspective* (2022), that the loss parameters are selected by a type of investigative technique called Statistical Production Analysis (SPA). SPA utilizes a Production Performance Matrix (PPM) that sorts

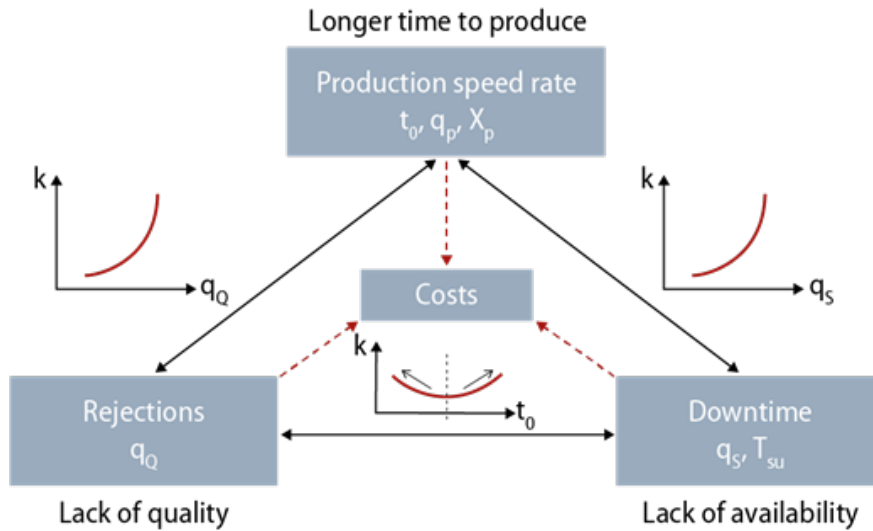


Figure 2.8: Relationship between loss parameters Q, S, and P and their influence on part cost (k) [16].

loss parameters into Factor Groups. This breakdown of production data provides a detailed snapshot of the equipment under review. The categorized raw data can be inputted into the cost equation to troubleshoot issues, calculate KPIs, or investigate improvements, among others. The suggested calculations from the cost model can then be applied to the equipment, followed by the collection of raw data once again by the SPA/PPM tools. This process forms a continuous loop from analysis to action (Figure 2.9).

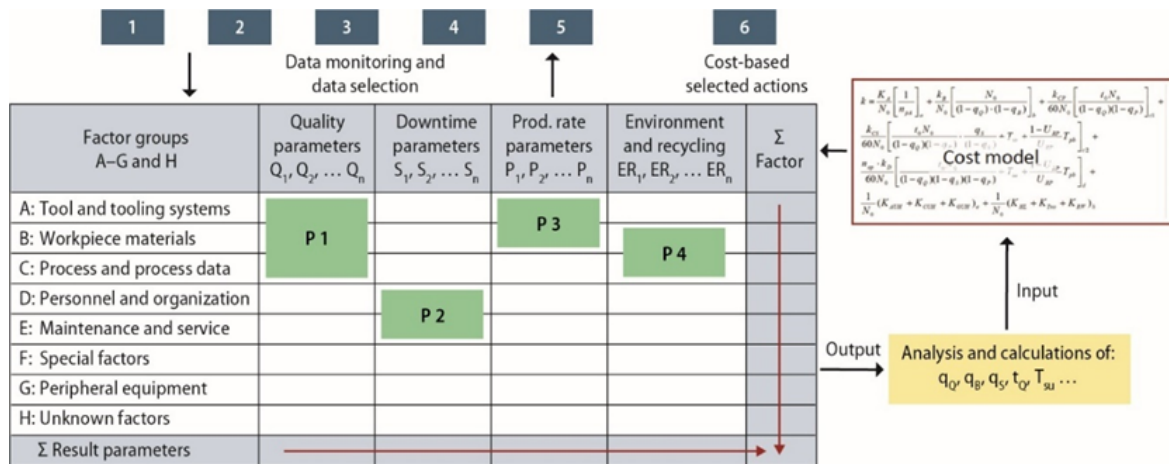


Figure 2.9: Example of SPA/PPM investigation tools complementing the cost model to create a continuous analysis to action loop [16].

In general, the loss parameters can be calculated as follows:

$$q_B = \frac{m_{tot} - m_{det}}{m_{tot}} \quad (2.12)$$

q_B represents the total mass of the raw material (m_{tot}) minus the determined mass after

processing (m_{det}) divided by the total mass.

$$q_S = \frac{t_p - t_0}{t_p} \quad (2.13)$$

q_S is expressed by the difference in actual production time (t_p) and nominal cycle time (t_0) over production time.

$$q_Q = \frac{N - N_0}{N} \quad (2.14)$$

q_Q is comprised of the incorrect parts ($N - N_0$) divided by the actual number of parts produced (N).

$$q_P = \frac{t_{0r} - t_0}{t_{0r}} \quad (2.15)$$

Finally, q_P is the time difference between cycle time adjustments (t_{0r}) and nominal cycle time (t_0) divided by the adjusted cycle time.

Both q_P and q_S involve time variables, which might initially appear confusing to differentiate between. However, the appropriate allocation of time delays in production can be executed within the SPA/PPM investigation tools, as previously discussed.

Aside from the loss parameters, most variables employed in the cost model are either self-explanatory or generally straightforward to observe. The remaining variables are detailed in Table 2.6. However, this does not imply that one cannot customize any of these variables upon closer examination. Each manufacturing system is unique, and the cost model provides a framework that can be customized and expanded upon to suit specific circumstances and requirements.

2.7.3 Explaining Equipment Costs

Examining equipment costs (k_{CP} and k_{CS}) more closely is particularly intriguing, especially concerning the melting process of metals. Ståhl and Windmark point out that the following equipment cost equation cannot be regarded as entirely universal, as inconsistencies emerge when modifications are made to the production schedule (T_{plan}), fluctuations occur in annual production volume, and the initial investment value (K_0) is reassessed. These equations suggest that consolidating production within a few pieces of equipment and extending the planned production time on each machine will lead to a reduction in part cost. While this relationship follows simple logic, it is now numerically expressed, providing a clearer understanding of the cost dynamics involved concerning equipment [16]. Regarding the melting process of secondary low alloy aluminum, the equation serves as a solid starting point for calculating equipment costs. Fortunately, this equation also accommodates the inclusion of additional parameters and allows for subsequent adjustments to be taken into account. The equipment costs are as follows:

$$k_{CP} = \frac{a_f \cdot K_0(1 + k_{0ren} \cdot N_{ren}) + A \cdot k_{Area} + k_{CM}}{T_{plan}} \quad (2.16)$$

$$k_{CM} = T_{plan} \cdot \left(\frac{k_{MHh}}{h_{MH}} + k_{ph} \right) \quad (2.17)$$

Table 2.6: Variables found within Equation 2.11 and their meanings [16].

Variable	Designation	Unit
k	Cost per part	Currency
k _A	Tool cost	Currency
k _B	Material cost	Currency
k _{CP}	Equipment cost during production	Currency/hr
k _{CS}	Equipment cost at standstill	Currency/hr
k _D	Labor cost	Currency/hr
N ₀	Nominal batch size	-
n _b	Number of batches per year	-
n _{part}	Number of parts	-
n _{op}	Number of operators	-
q _Q	Rejection rate loss	-
q _S	Downtime rate loss	-
q _P	Production rate loss	-
t ₀	Cycle time	min
T _{su}	Charngover or equipment setup time	min
T _{plan}	Production planned time	hr
T _{pb}	Production time per batch	hr
U _{RP}	Utilization Rate	-

$$k_{CS} = \frac{a_f \cdot K_0(1 + k_{0ren} \cdot N_{ren}) + A \cdot k_{Area}}{T_{plan}} \quad (2.18)$$

$$N_{ren} = trunc \left(\frac{n \cdot \frac{T_{plan}}{h_{year}}}{n_{syren}} \right) \quad (2.19)$$

In calculating k_{CP} and k_{CS}, the cost items are resolved concerning the planned production hours (T_{plan}) for the fiscal year. While maintenance costs (k_{CM}) are typically placed within the production section, its placement within the idling section will depend on the process layout.

$$a_f = \frac{a}{K_0} \cdot \frac{p \cdot (1 + p)^n}{(1 + p)^n - 1} \quad (2.20)$$

$$K_0 = \frac{a \cdot ((1 + p)^n - 1)}{p \cdot (1 + p)^n} \quad (2.21)$$

The annuity method yields a consistent annual expense (a), evenly distributed over the projected number of years (n) of equipment usage. K₀ represents the initial investment, while p denotes the cost of capital or interest [79].

Table 2.7: Variables found within equipment cost parameters k_{CP} and k_{CS} and their meanings.

Variable	Designation	Unit
a_f	Annuity factor	-
A	Area the machine occupies	m^2
h_{MH}	Number of operating hours per maintenance hour	-
h_{year}	Number of hours in a shift per year	hr/year
k_{0ren}	Percent of starting renovation cost based K_0	%
k_{Area}	Building cost per square meter	Currency/ m^2
k_{CP}	Equipment cost during production	Currency/hr
k_{CS}	Equipment cost at standstill	Currency/hr
k_{MHh}	Maintenance cost per hour	Currency/hr
k_{ph}	Variable machine hourly costs	Currency/hr
K_0	Basic investment	Currency
n	Number of years	years
n_{syren}	Number of shift years between renovations	year
N_{ren}	Number of renovations	-
p	Interest factor	-
T_{plan}	Production planned time	hr

2.8 Sustainable Eye

Using various approaches to estimate costs and carbon emissions in manufacturing, BRYNE created its own model for assessing these factors in Sweden's aluminum industry. The tool enables companies to evaluate different suppliers and their aluminum materials for processing. Its output includes important factors like energy content, carbon footprint, and recycling metrics such as estimated material loss and direct energy consumption per ton delivered. The model facilitates a practical comparison of quality and emissions, drawing on a database of Swedish aluminum ingot producers. Through this software, users can easily compare key factors to choose a provider that fits their company's values, objectives, and budget. It is an important tool for decision making on what suppliers align better with companies values, which in turn, can help with monitoring carbon footprint and improve a company's Scope three of the Scientific Base Targets [21].

3 Methodology

In collaboration with BRYNE, the practical experiments performed in this thesis utilize the LOOP technology and other experimental procedures used to observed the quality of low alloy aluminum, such as density index and first bubble technique. The following sections and subsections outline the melting and cleaning process of the melt.

3.1 Material Preparation

In this thesis experiment, secondary low alloy aluminum served as the test material. This alloy blend comprises 50% primary aluminum and 50% secondary aluminum, which is obtained from decommissioned car chillers. The addition of primary aluminum in the mixture was necessary to ensure the resulting alloy composition met the standards for classification as low alloy. This addition compensates for the observed weight loss of approximately 40% during the melting process of the heavily oxidized car chillers. The detailed composition resulting from this process is provided in Table A.1. Of the available material, priority was given to alloy types with sufficient weight to fill the crucible to approximately 60%. This ensured there was adequate molten metal to reach into with our ladle and take samples from. Occasionally, more than one alloy type had to be mixed in so there was enough material to conduct tests. When this took place, the resulting composition was determined by calculating the weight of alloying elements expressed in Table A.1 and simply combining the results to make a new alloy.

3.2 Heating the Furnace

The furnace used for testing generated heat from three electrical resistor coils. The coils were connected to an analog timer system featuring three plugs, one designated for each coil. Each plug incorporated a timer function programmed to activate one after the other, with one-hour intervals between activations. This sequential activation method gradually elevated the temperature within the furnace, mitigating the risk of thermal shock and potentially cracking crucible. The timer sequence began at 1:30 AM, 2:30 AM, and 3:30 AM for each respective plug. Ideally, the temperature of the metal would surpass the melting temperature of 650°C to 700°C, climbing to the desired holding temperature of 850°C by roughly 9:00 AM.

The holding temperature had been determined based on the fluidity results from trail LOOP tests. Apart from adjusting the material composition, the best methods available to influence fluidity were either to increase the temperature of the melt or to use a LOOP with deeper channels.

3.3 Equipment Setup and Safety

Figure 3.1 shows the general layout of equipment used during the tests. To the left of the furnace is a cart that stations the empty LOOP cartridges. To the right of the furnace, a workbench holds the ladles, shovels, tongs, and other steel tools used to handle the molten metal. Above the furnace, the cart, and at the back of the room, a ventilation system evacu-

ates the air inside the room. Beneath the furnace in Figure 3.2c, a small pan lies on the floor. This pan collects any dross skimmed off the surface of the melt.



Figure 3.1: From left to right: testing cart, furnace, workbench. *Source: BRYNE AB.*

The LOOP cartridges were placed on a level mesh surface with a drop-catch platform underneath; in the event of a spill, the molten metal does not run off the edge of the cart (Figure 3.2b). Several thermometers are equipped to the cart and are positioned with a railing gantry to ensure proper placement and free up the hands of the operator (Figure 3.2a).

Operators must wear 100% cotton-based clothing rated to withstand high temperatures when operating inside the furnace room (Figure 3.2c). Proper safety shoes are also required. When handling molten metal, the operator must equip a heat shield visor to cover the face. Molten metal reacts suddenly when coming into contact with water, leading to small explosions that can splash the molten metal. To avoid the risk of operators coming into contact with temperatures over 800°C, all tools are preheated above the furnace, akin to roasting marshmallows over a campfire, to eliminate any moisture gathered on the tools.

3.4 Density Index and First Bubble Methods

The Density Index (DI) and First Bubble methods are similar procedures aimed at understanding the porosity of the alloy in question. These methods complement the LOOP results by integrating insights into fluidity and hydrogen content at specific stages of the melting process. A small steel cup is used to carefully scoop samples from the furnace once the melt has reached the desired holding temperature. In this thesis, to gain insight into the effects of salt flux treatment, samples are taken before and after treatment.



(a) Testing cart with LOOP cartridges placed on mesh shelf.



(b) Testing with LOOPS gone wrong.



(c) Alternate view of equipment and modeling of operator safety gear.

Figure 3.2: Complimentary pictures of setup, spillage, and safety. *Source: BRYNE AB.*

3.4.1 Operational Steps for Density Index

1. A small portion of molten aluminum is poured or scooped into a thin, steel cup. Subsequently, it is promptly transferred to the vacuum enclosure of a Reduced Pressure Tester (Figure 3.3).
2. The sample undergoes solidification within this apparatus, subjected to a vacuum of less than 80 mbar. Solidifying under vacuum conditions induces the volume of hydrogen gas to expand approximately tenfold in comparison to solidification under standard atmospheric conditions. At the same time another sample is taken and left to solidify under atmospheric pressure as seen above the operator's hand on a small shelf in Figure 3.3.



Figure 3.3: Density Index setup. *Source: BRYNE AB.*

3. After both samples have solidified, there will be an increase in hydrogen porosity within

them. By inspecting the samples for pores and measuring density using DI calculations, we can determine a numerical value for hydrogen content. This measurement aims to evaluate the different gas levels within the melt and to provide additional insights into the resulting alloy's porosity.

4. Label which sample solidified under room pressure and which one under vacuum.
5. Utilize a scale to weigh the specimens initially. Then, weigh the specimens again while they are submerged in water.
6. Calculation of the density index using Equation 2.5.



Figure 3.4: Weighing specimen submerged in water. *Source: BRYNE AB.*

3.4.2 Operational Steps for First Bubble

A second machine was provided to continue the measurements on porosity, being its principle the use of the first bubble method. This machine closely resembles the DI machine, yet it offers the added convenience of automatically calculating porosity. By utilizing the percent weight of Cu, Si, Mn, and Mg within the alloy, it approximates the alloy properties for calculation purposes. Moreover, it features a heating element within the loading bay of the vacuum chamber, where the specimen is placed. The First Bubble machine, as illustrated in Figure 3.5, was employed for six out of the eight alloys tested in this thesis.

1. To begin, first configure the machine to the chosen aluminum alloy. The graphical interface grants access to an internal database for recording data. Enter the percent weight of Cu, Si, Mn, and Mg found within the tested alloy.
2. Enter the temperature the loading bay will hold. Choose a temperature close to the working temperature of the alloy. In our case, a temperature of 820°C was used throughout our experiments.
3. A small portion of molten aluminum is poured or scooped into a thin, steel cup. Subsequently, it is promptly transferred to the vacuum enclosure.
4. The sample is left under a vacuum. According to the contents within the alloy, the bub-



(a) ALU COMPACT II.



(b) Top view with specimen loaded.

Figure 3.5: First Bubble Hydrogen Analysis Machine. *Source: BRYNE AB.*

bles appear around the 80 - 100 mbar mark. The operator manually records the hydrogen reading by pressing the “MEASURE” button once the first bubble appears.

5. The procedure is repeated until three reliable data points have been recorded.

3.5 Optical Emission Spectroscopy

According to informal interviews and open discussions with BRYNE, Optical Emission Spectroscopy (OES) stands out as a popular technique within the industry. To maintain practicality, the thesis employed this technology to ascertain the composition of the secondary low alloy aluminum. The focus was on comprehending the effects of adding salt flux (ARSAL 2125) as a refining agent during the melting process, specifically by observing any notable alterations in chemical composition. In simpler terms, the aim is to identify which elements were being removed from the alloy.

For each alloy tested, two Optical Emission Spectroscopy (OES) samples were extracted: one before the addition of salt flux and one afterwards. The samples were later taken to a different site that housed BRYNE’s OES machine, depicted in Figure 2.5.

Initially, a small portion of the melt was cast into a cylindrical container. Next, the surface was machined flat to ensure a smooth, polished surface. Finally, three tests were conducted on both samples. The outcome provided an analysis of the chemical composition, which was later utilized to compare and contrast the effectiveness of the salt flux in removing ITEs from the alloy.

3.6 LOOP Procedure

The LOOP procedure serves as the method employed to assess the fluidity of the material. When used in conjunction with the DI and First Bubble methods, as well as OES, it provides valuable insights into the material properties of the alloy. To ensure its proper application, the LOOP can be used by following the steps outlined in the following subsection [80].

3.6.1 Operational Steps for the LOOP

1. The components of the LOOP are illustrated in Figure 3.6. The operator first places the plug (label A) in the bottom plate. Initially, the operator inserts the plug (labeled A) into the bottom plate (labeled B). The temperature should be determined beforehand to reference when to remove the plug. The operator must ensure that the cup (labeled C) is positioned in the center of the plate and that the plug is securely mounted to prevent material leakage into the spiral (see previous Figure 3.2b). Additionally, a thermometer (labeled D) should be placed inside the cup for temperature measurements, positioned adjacent to, but not on top of, the plug for accurate readings.

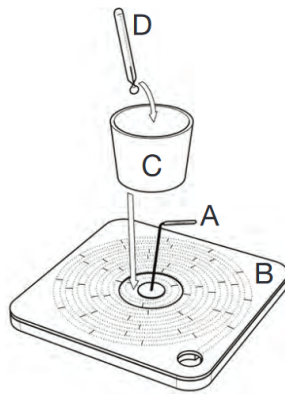


Figure 3.6: Step 1 of using the Loop.

2. The operator proceeds by filling the cup with the molten metal. It is important to pour the metal slowly at first, avoiding contact with the rim. Once the flow has been initiated, it's advisable to pour the remaining sample quickly and confidently to minimize its exposure to oxygen. However, caution should be exercised to prevent knocking the cup and causing a leak by pouring too rapidly. Handling molten metal, especially at temperatures near 800°C, requires adjustment due to its unique viscosity. The cup is conveniently marked to indicate the appropriate amount of material required for testing.



Figure 3.7: Step 2 of using the Loop.

3. Once the reference temperature determined by the thermometer in Step 1 (Figure 3.6) has been reached, the plug can be removed, allowing the molten metal to flow into the

spiral. Within seconds, the metal will solidify. Remember to remove the thermometer from the cup before the material solidifies inside to prevent any damage.



Figure 3.8: Step 3 of using the Loop.

4. Observing the indicators printed on the plate, the distance the metal has flowed into the spiral is determined by the operator. The plate material is intended to burn away as the molten metal passes through. After cooling, the metal contained within the LOOP can be recovered and remelted for further use. Breaking apart the fibrous material constituting the LOOP is easily achievable while wearing gloves and a respirator. Although the fibrous material poses no serious harm to the body, excessive handling or inhalation may cause irritation.

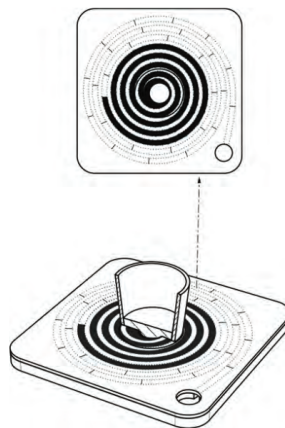


Figure 3.9: Step 4 of using the Loop.

3.7 Adding Salt Flux as a Refining Agent

In this stage, salt flux serves as a refining agent for the aluminum melt. When added, it is quickly submerged, gently mixed, and then left enclosed within the furnace until the reaction has finished. The salt flux employed consistently throughout the experiments is ARSAL 2125, as detailed in Section 2.4.2.1. According to the specification sheet for ARSAL 2125 (Figure A.1), the dross needs to fully form before removal. Based on the size of the furnace and instruction from BRYNE, the salt flux will take 15 minutes to fully react. The procedure for adding the salt flux is quite straightforward and is described below:

1. To determine the amount of salt flux required, we calculated it as 0.5% of the total weight of the alloy. This percentage is established based on the manufacturer's recommendation in Figure A.1.



(a) Preparation of ARSAL 2125.



(b) Salt flux being deposited into the melt.

Figure 3.10: Addition of salt flux as a refining agent *Source: BRYNE AB.*

2. The salt flux is deposited into the molten material using a porous ladle, as depicted in Figure 3.10b. It is then submerged and gently mixed with the molten material for approximately 1 - 3 minutes, continuing until all the pellets cease to appear blue.
3. The process is finished by removing the dross that forms on the surface.

3.8 Documentation

For the tests, a form was fashioned solely through creativity. Figure 3.11 illustrates the form we devised and offers further insight into how the data was recorded throughout the tests.

3.9 Constructing the Models

In this thesis, a theoretical model for both cost and carbon emissions will be presented, drawing from Ståhl's manufacturing cost equation (see Equation 2.11). This model will be adapted to focus specifically on the melting process. The aim is to develop a versatile model suitable for adoption within the foundry industry, allowing for the inclusion of custom variables to accurately quantify both costs and carbon emissions, tailored to individual user needs.

Preparations were made to develop both models. Visits to various companies provided insights into different production methods. Informal interviews and open discussions with industry professionals were crucial for understanding companies' processes and the theoretical background behind their designs. Practical workshops with academics and supervisors offered a better understanding of the melting process stages covered in the thesis. These workshops also involved brainstorming sessions and ongoing discussions about assumptions to be made in the models, as well as different perspectives on experiments conducted during the thesis and foundry processes in Sweden. By combining these discussions with

Loop Test					ALLOY	Kg	DATE
HOLD TEMP	LOAD TEMP	PULL TEMP	POUR TEMP	PLUG TEMP			
°C	°C	°C	°C	°C			
1L1		°C	°C	°C			
1L2		°C	°C	°C			
1L3		°C	°C	°C			
Salt:					GRAMS		
Density:					CCM/100g H	CCM/100g H	CCM/100g H
°C	°C	°C	°C	°C			
2L1		°C	°C	°C			
2L2		°C	°C	°C			
2L3		°C	°C	°C			
Density:					CCM/100g H	CCM/100g H	CCM/100g H

(a) Example page 1.

Loop Test					K ₃	12.75 Kg	12/04
HOLD TEMP	LOAD TEMP	PULL TEMP	POUR TEMP	PLUG TEMP			
°C	°C	°C	°C	°C			
850	821	800	780	770			
1L1		-	+3	-			
1L2		-	+6	-			
1L3		-	+9	-			
Salt:					63.75		
Density:					0.28	0.27	0.21 0.18
859	826	800	780	770			
2L1		-	+2	-			
2L2		-	+5	-			
2L3		-	+7	-			
Density:					0.22	0.40 0.30	0.30 0.26

(b) Test page 1.

Previous Results			DATE
ALLOY	Loop Distance	Loop Weight	
1L1	_____	GRAMS	
1L2	_____	GRAMS	
1L3	_____	GRAMS	
2L1	_____	GRAMS	
2L2	_____	GRAMS	
2L3	_____	GRAMS	
DROSS			
Pan:	_____	GRAMS	
Pre-Salt:	_____	GRAMS	
Post-Salt:	_____	GRAMS	

(c) Example page 2.

Previous Results			12/04
K _{2L2}	Loop Distance	Loop Weight	
1L1	24.7	340.06	
1L2	23.7	341.74	
1L3	23.6	331.59	
2L1	25.4	346.67	
2L2	24.7	347.42	
2L3	24.2	357.55	
DROSS			
Pan:	596		
Pre-Salt:	823.86		
Post-Salt:	798.86		

(d) Test page 2.

Figure 3.11: Form created to document tests.

research on cost modeling and carbon emission models in various manufacturing settings, equations were developed incorporating ideas from these sources.

4 Experimental Results

This section addresses the results obtained from the experiments performed during the thesis. The first section refers to the results obtained from the optical electron spectroscopy testing to verify the composition of the material samples before and after ARSAL 2125 treatment, determining the effects of the treatment in the low alloy aluminum. The second section refers to the results of density index calculations for the material samples before and after cleaning treatment. Section three refers to the results of LOOP measurements for all material samples used for experimentation. The combination of density index and LOOP is meant to provide a comprehensive understanding of the material quality through gas content in the samples and fluidity of the aluminum melt. Section four and five are dedicated to the proposal and calculation of cost and CO₂ emissions for the setup used for experiments using tailored equations for the process of melting, cleaning, and holding aluminum melt.

4.1 Optical Electron Spectroscopy

4.1.1 K1 Sample

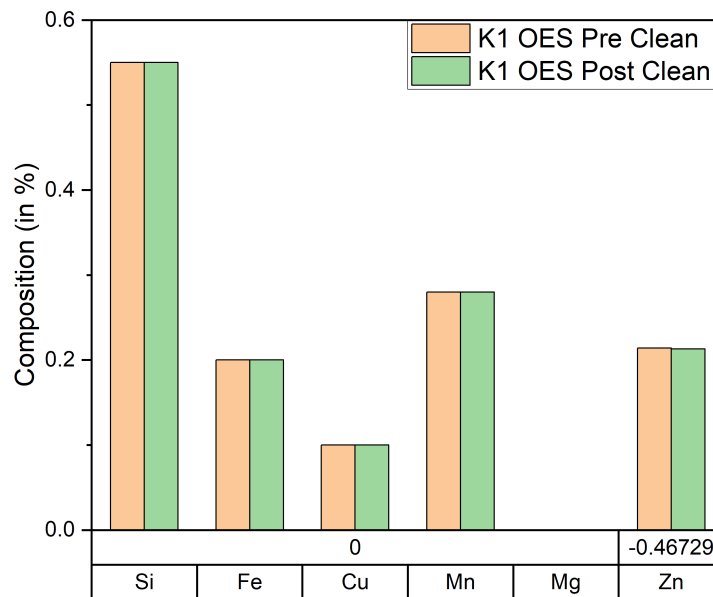


Figure 4.1: OES results for alloying elements for K1 sample before and after cleaning using ARSAL 2125.

For the alloying elements found in the K1 sample, after applying ARSAL 2125 for the cleaning treatment, zinc (Zn) was reduced by 0.46% in content while silicon (Si), iron (Fe), copper (Cu), manganese (Mn), and magnesium (Mg) remained unchanged after the process was finished.

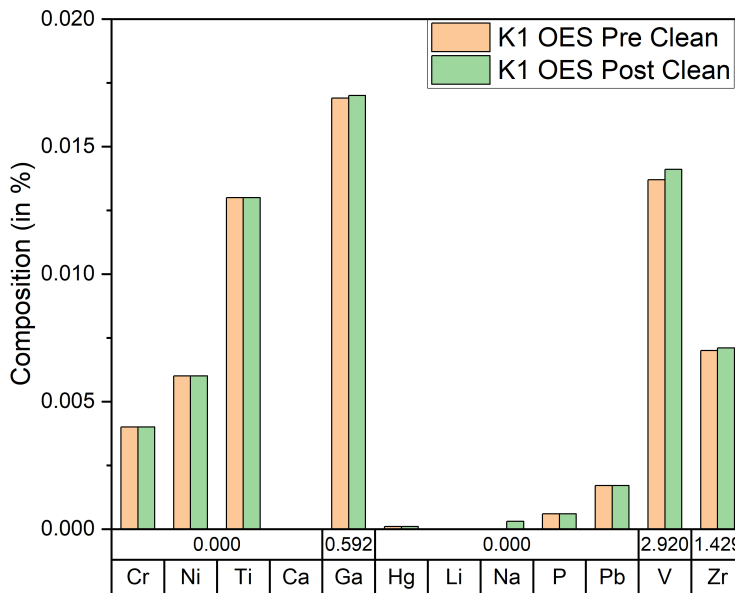


Figure 4.2: OES results for trace elements for K1 sample before and after cleaning using ARSAL 2125.

The trace elements found in the K1 sample, after applying ARSAL 2125 for cleaning treatment, the presence of vanadium (V), zirconium (Zr), and gallium (Ga) increased by 2.92%, 1.43%, and 0.59 % in content, respectively, while chromium (Cr), nickel (Ni), titanium (Ti), calcium (Ca), mercury (Hg), lithium (Li), sodium (Na), phosphorus (P), and lead (Pb) remained unchanged after the process was finished.

4.1.2 K2 & R2 Sample

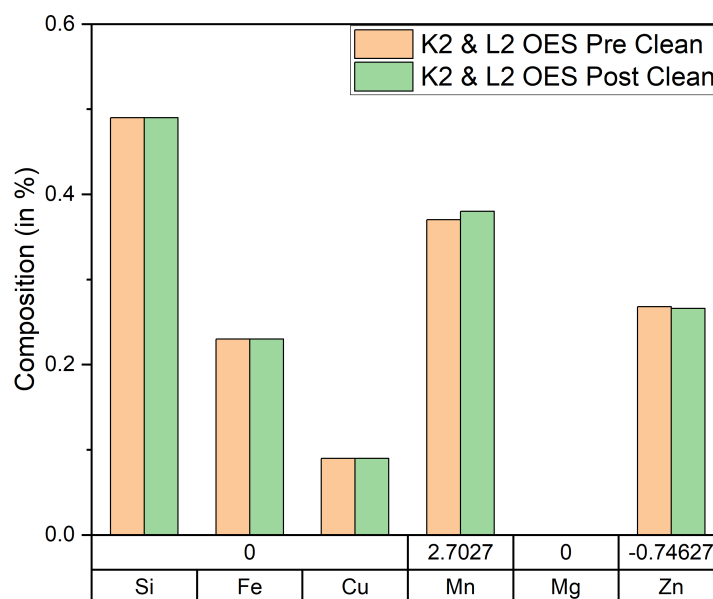


Figure 4.3: OES results for alloying elements for K2 & L2 sample before and after cleaning using ARSAL 2125.

For the alloying elements found in the K2 & L2 sample, after applying ARSAL 2125 for the cleaning treatment, zinc was reduced by 0.75% in content, manganese content increase by 2.72% while silicon, iron, copper, and magnesium remained unchanged after the process was finished.

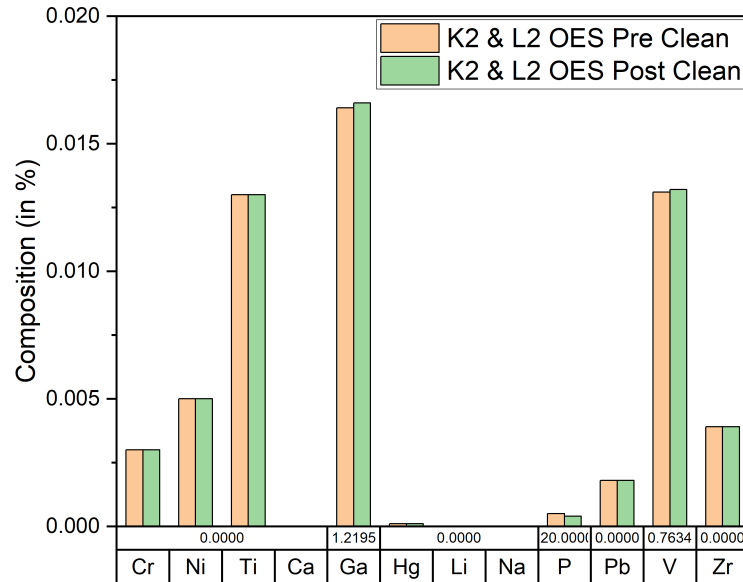


Figure 4.4: OES results for trace elements for K2 & L2 sample before and after cleaning using ARSAL 2125.

For the trace elements found in the K2 & L2 sample, after applying ARSAL 2125 for cleaning treatment, the presence of vanadium, phosphorus, and gallium increased by 0.7634%, 20%, and 1.22 % in content, respectively, while chromium, nickel, titanium, calcium, mercury, lithium, sodium, and lead remained unchanged after the process was finished.

4.1.3 K3 Sample

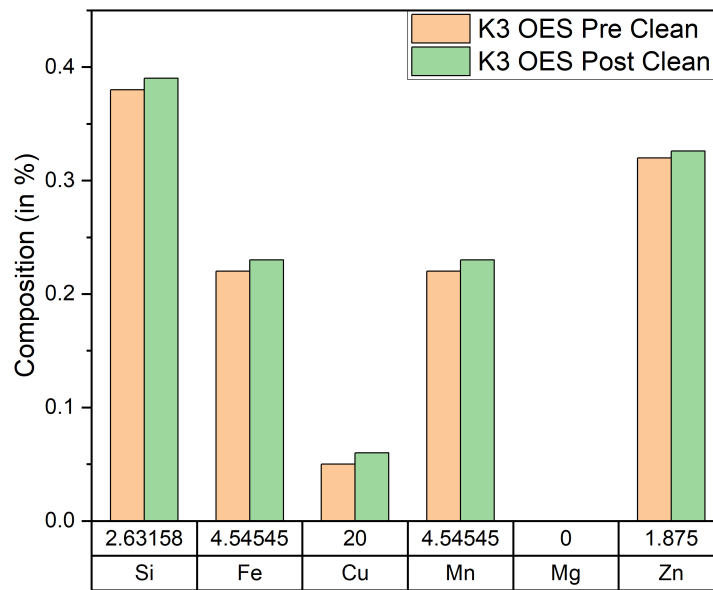


Figure 4.5: OES results for alloying elements for K3 sample before and after cleaning using ARSAL 2125.

For the alloying elements found in the K3 sample, after applying ARSAL 2125 for the cleaning treatment, silicon, iron, copper, manganese, and zinc increase by 2.63%, 4.55%, 20%, 4.55 %, and 1.88% respectively while magnesium remained unchanged after the process was finished.

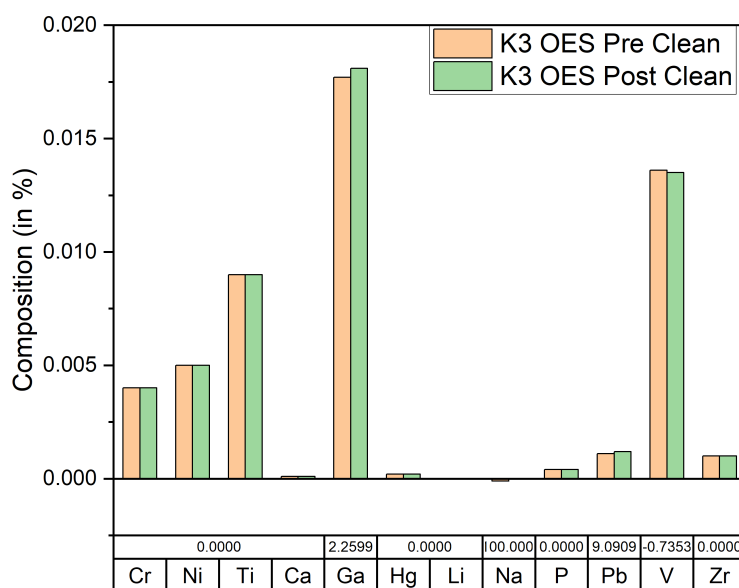


Figure 4.6: OES results for trace elements for K3 sample before and after cleaning using ARSAL 2125.

The trace elements found in the K3 sample, after applying ARSAL 2125 for cleaning treatment, the presence of gallium and lead increased by 2.60% and 9.09% in content, respectively, while chromium, nickel, titanium, calcium, mercury, lithium, phosphorus, and zirconium remained unchanged after the process was finished. Sodium did not appear after salt flux treatment.

4.1.4 L1 Sample

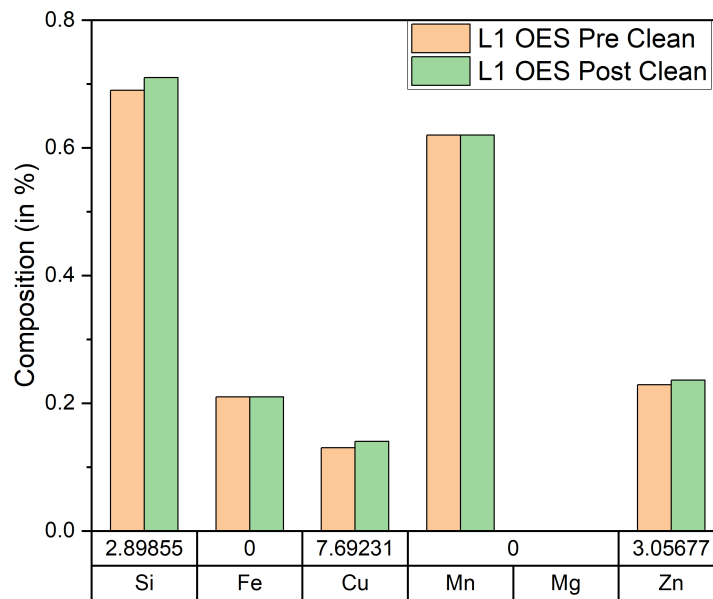


Figure 4.7: OES results for alloying elements for L1 sample before and after cleaning using ARSAL 2125.

For the alloying elements found in the L1 sample, after applying ARSAL 2125 for the cleaning treatment, silicon, zinc, and copper increased by 2.90%, 7.69%, and 3.06% in content respectively, while iron, manganese, and magnesium remained unchanged after the process was finished.

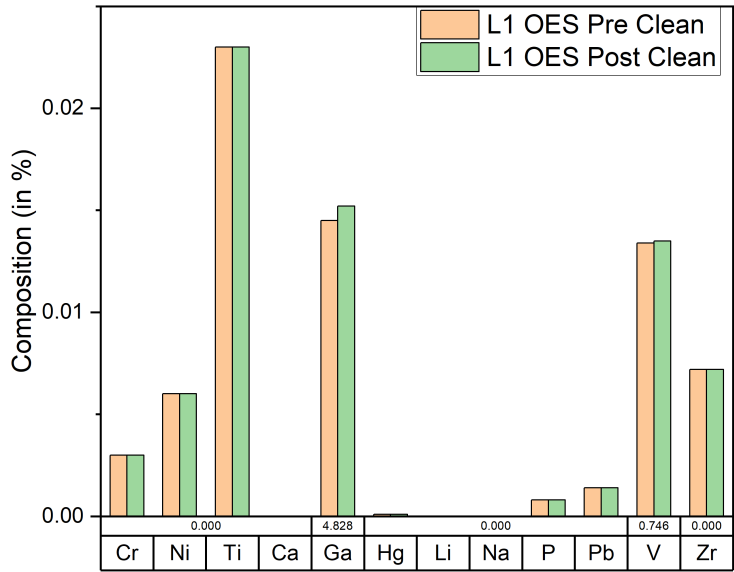


Figure 4.8: OES results for trace elements for L1 sample before and after cleaning using ARSAL 2125.

For the trace elements found in the L1 sample, after applying ARSAL 2125 for cleaning treatment, the presence of gallium, and vanadium increased by 4.83% and 0.75% in content, respectively, while chromium, nickel, titanium, calcium, mercury, lithium, sodium, lead, and zirconium remained unchanged after the process was finished.

4.1.5 L2 Sample

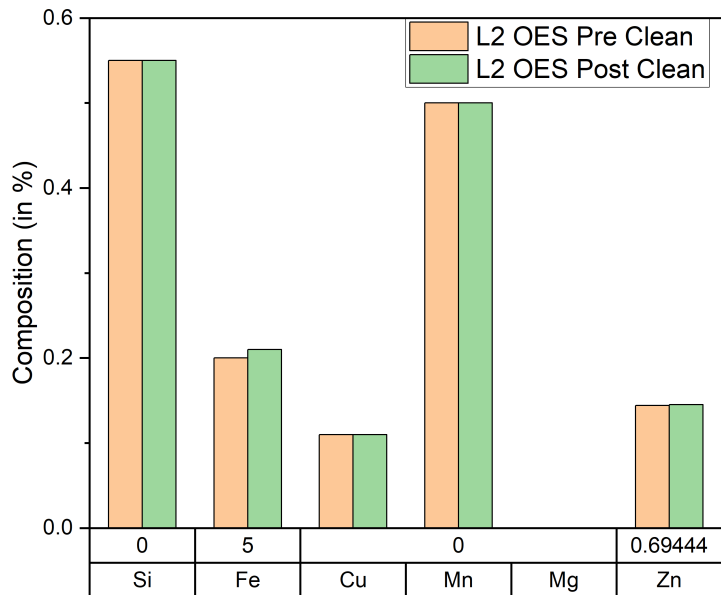


Figure 4.9: OES results for alloying elements for L2 sample before and after cleaning using ARSAL 2125.

For the alloying elements found in the L2 sample, after applying ARSAL 2125 for the cleaning treatment iron and zinc increased by 5% and 0.69% in content respectively,

while silicon, copper, manganese, and magnesium remained unchanged after the process was finished.

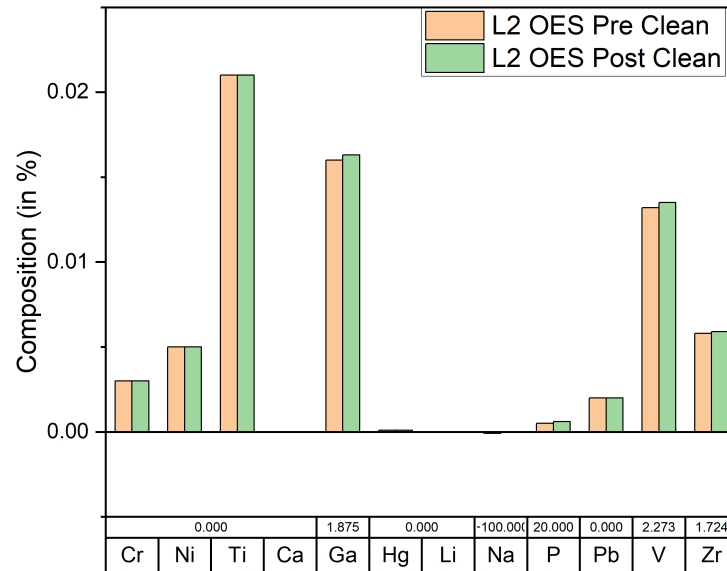


Figure 4.10: OES results for trace elements for L2 sample before and after cleaning using ARSAL 2125.

For the trace elements found in the L2 sample, after applying ARSAL 2125 for cleaning treatment, the presence of gallium, phosphorus, vanadium, and zirconium increased by 1.88%, 20%, 2.27%, and 1.72% in content, respectively, while chromium, nickel, titanium, calcium, mercury, lithium, and lead remained unchanged after the process was finished. sodium lectures state that during the experiment, the small percentage that was in prior to cleaning disappeared after the cleaning process.

4.1.6 R1 Sample

For the alloying elements found in the R1 sample, after applying ARSAL 2125 for the cleaning treatment, silicon, iron, and manganese increased by 1.85%, 4.55%, and 2.44% in content respectively, while Cooper and magnesium content remained unchanged after the process was finished. In the case of zinc, there was a decrease in content of 2.47% after the cleaning treatment.

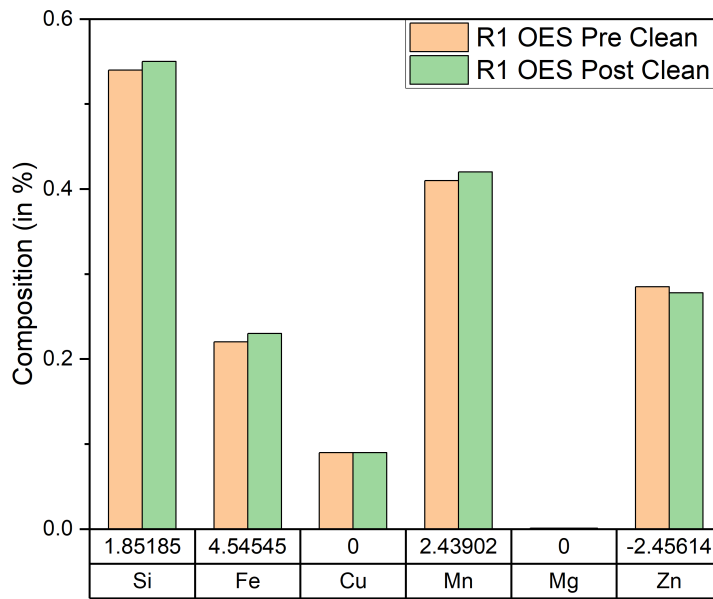


Figure 4.11: OES results for alloying elements for R1 sample before and after cleaning using ARSAL 2125.

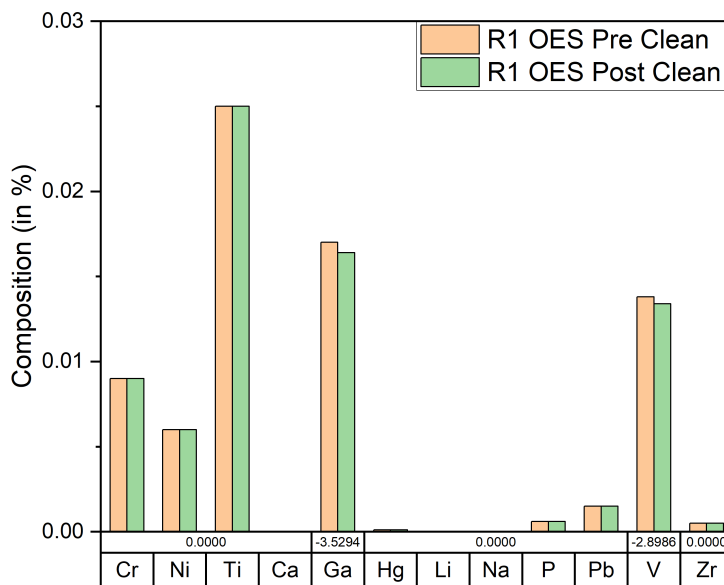


Figure 4.12: OES results for trace elements for R1 sample before and after cleaning using ARSAL 2125.

For the trace elements found in the R1 sample, after applying ARSAL 2125 for cleaning treatment, the presence of gallium and vanadium decreased by 3.53% and 2.90% in content, respectively, while chromium, nickel, titanium, calcium, mercury, lithium, sodium, phosphorus, lead, and zirconium remained unchanged after the process was finished.

4.1.7 R2 & R3 Sample

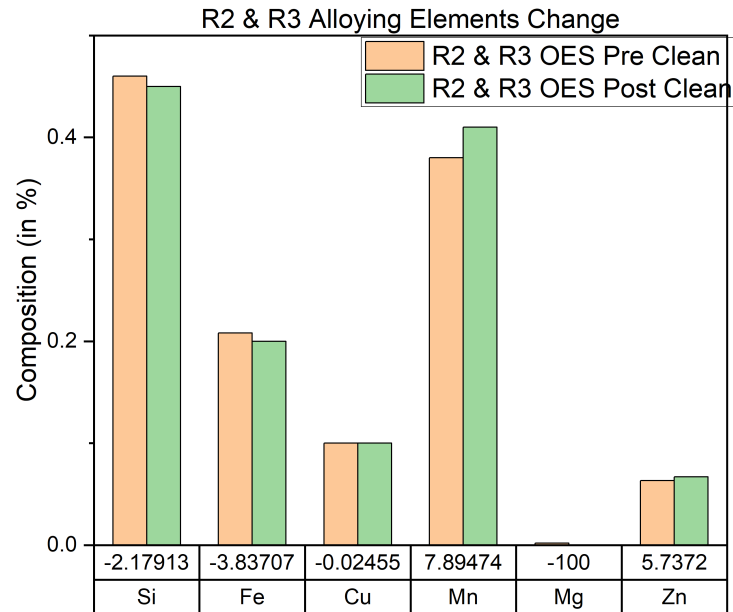


Figure 4.13: OES results for alloying elements for R2 & R3 sample before and after cleaning using ARSAL 2125.

For the alloying elements found in the R2 & R3 sample, after applying ARSAL 2125 for the cleaning treatment, zinc and manganese increased by 5.74% and 7.90% in content respectively, while silicon, iron, copper, and magnesium content decrease by 2.18%, 3.84%, 0.025%, and 100%.

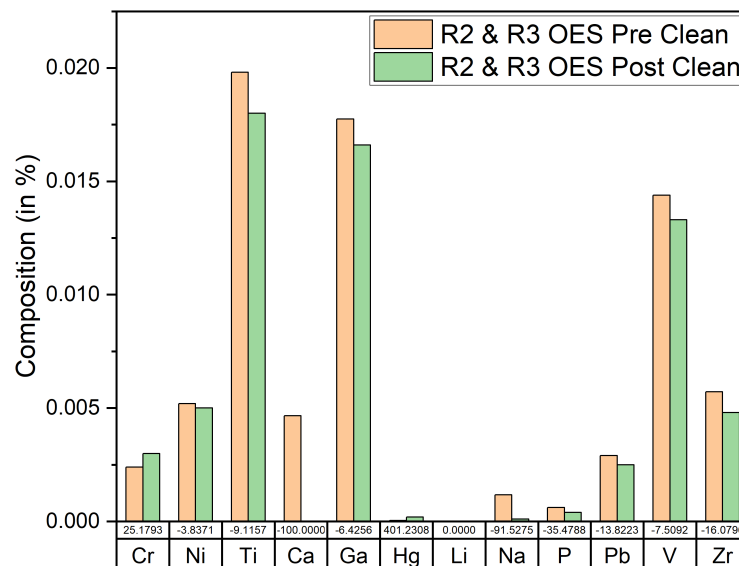


Figure 4.14: OES results for trace elements for R2 & R3 sample before and after cleaning using ARSAL 2125.

For the trace elements found in the R2 & R3 sample, after applying ARSAL 2125 for cleaning treatment, the presence of chromium and mercury increased by 25.18% and 401%

in content, respectively, while lithium remained unchanged after the process was finished. The lectures of composition show a decrease in content for nickel, titanium, calcium, gallium, sodium, phosphorus, lead, vanadium, and zirconium with changes of 3.84%, 9.12%, 100%, 6.43%, 92.53%, 35.48%, 13.82%, 8.51%, and 16.08% respectively.

4.1.8 R2 Sample

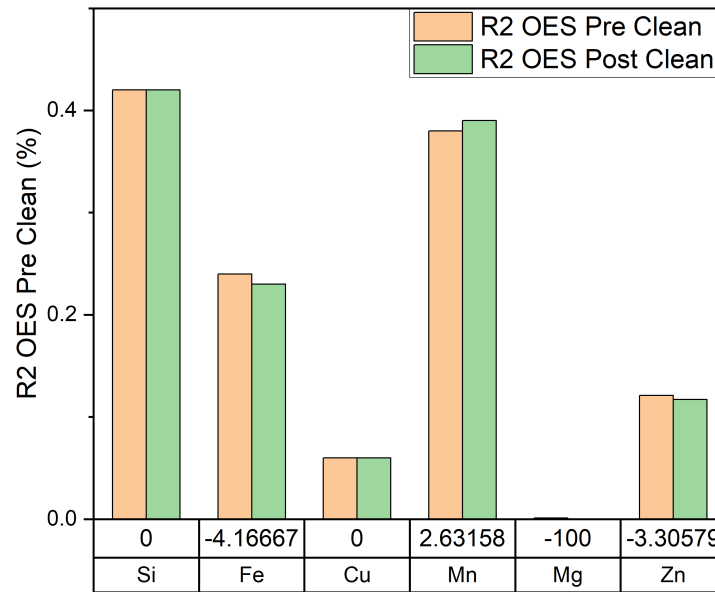


Figure 4.15: OES results for alloying elements for R2 sample before and after cleaning using ARSAL 2125.

For the alloying elements found in the R2 sample, after applying ARSAL 2125 for the cleaning treatment, manganese increased by 2.63% in content respectively, while silicon and copper content remained unchanged after the process was finished. The measurements of iron, magnesium, and zinc show a decrease in content of 4.17%, 100% and 3.31% after the cleaning treatment.

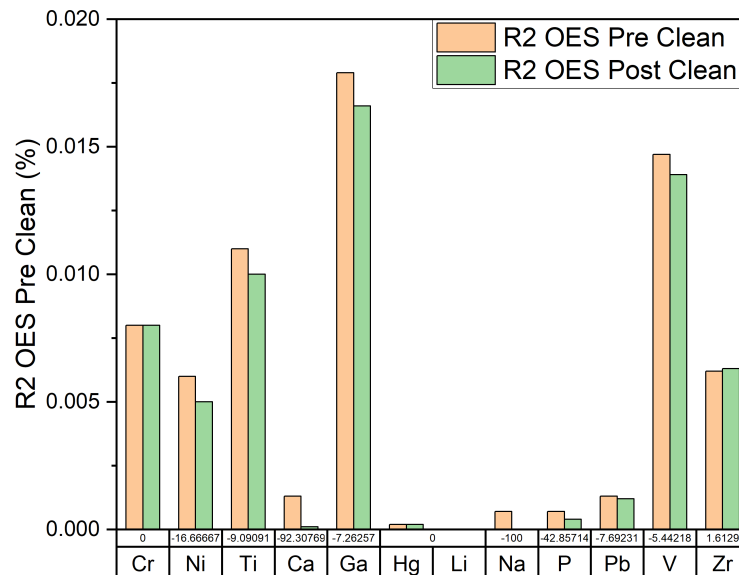


Figure 4.16: OES results for trace elements for R2 sample before and after cleaning using ARSAL 2125.

For the trace elements found in the R2 sample, after applying ARSAL 2125 for cleaning treatment, the presence of zirconium increased by 1.61% in content, respectively, while

chromium, mercury, and lithium remained unchanged after the process was finished. The lectures of composition show a decrease in content for nickel, titanium, calcium, gallium, sodium, phosphorus, lead, and vanadium with changes of 16.67%, 9.09%, 92.31%, 7.26%, 100%, 42.86%, 7.69%, and 5.44% respectively.

4.2 Density Index Estimation and First Bubble Experimentation

For density index estimation, the use of 2.5 establish in Chapter 3 was employed, using the density of the material hardening at atmospheric pressure and another at 80 mbar. The following graphs show the results prepare for two out of the eight samples. The first two graphs correspond to density index measurements and the remaining six graphs for "first bubble" measurements.

4.2.1 R2 Sample

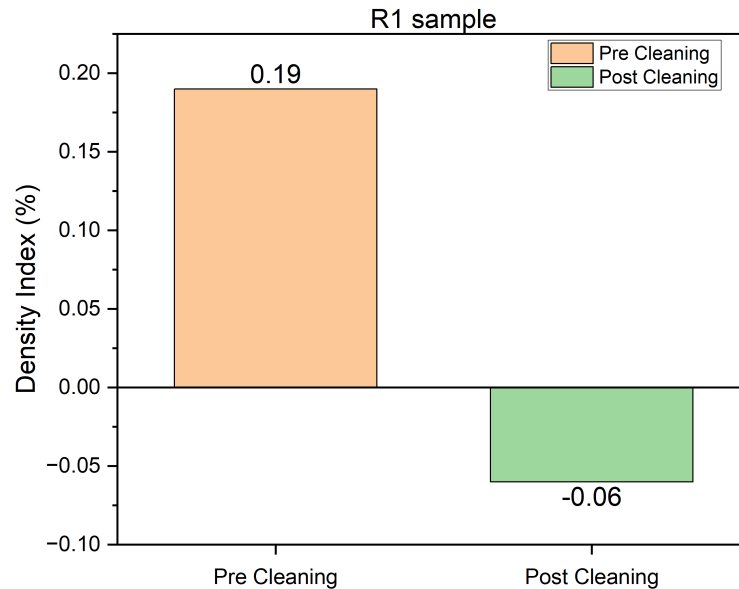


Figure 4.17: Density index results of R1 sample before and after cleaning using ARSAL 2125.

For sample R2, there is final value of -0.06% a considerable decrease from the original 0.19%. This final value is not mathematically logical and will be subject of discussion in the next chapter.

4.2.2 R2 & R3 Sample

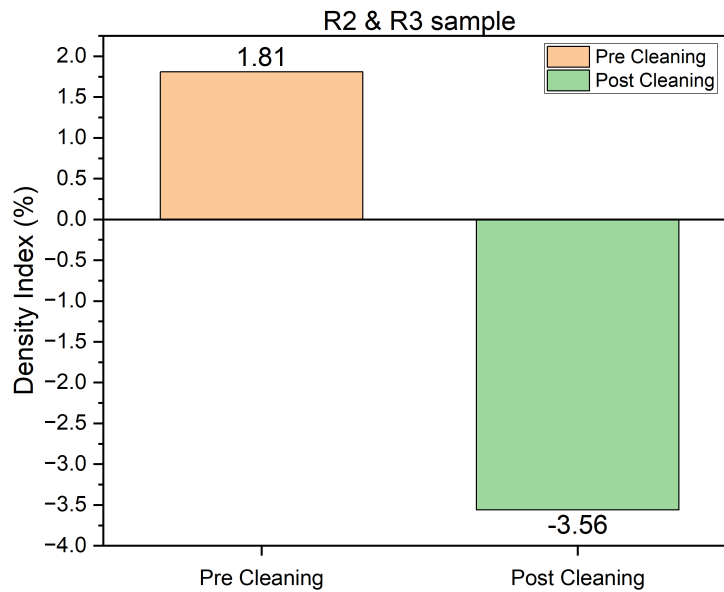


Figure 4.18: Density index results of R2 & R3 sample before and after cleaning using ARSAL 2125.

For sample R2 & R3, there is final value of -3.56% a considerable decrease from the original 1.81%. This final value is not mathematically logical and will be subject of discussion in the next chapter.

4.2.3 K1 Sample

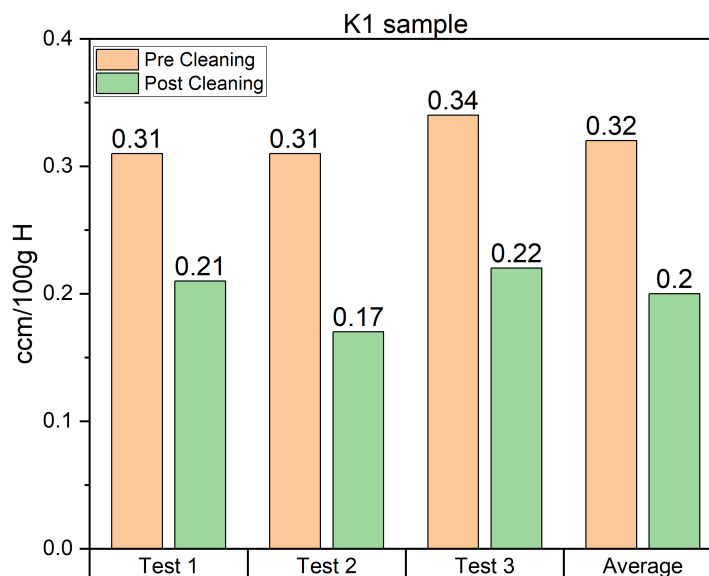


Figure 4.19: First bubble results of K1 sample before and after cleaning using ARSAL 2125.

For sample K1, using the nucleating technique, on average, a decrease of 37.50% is observed after the application of the cleaning treatment using ARSAL 2125 between different sets of experiments.

4.2.4 K2 & L2 Sample

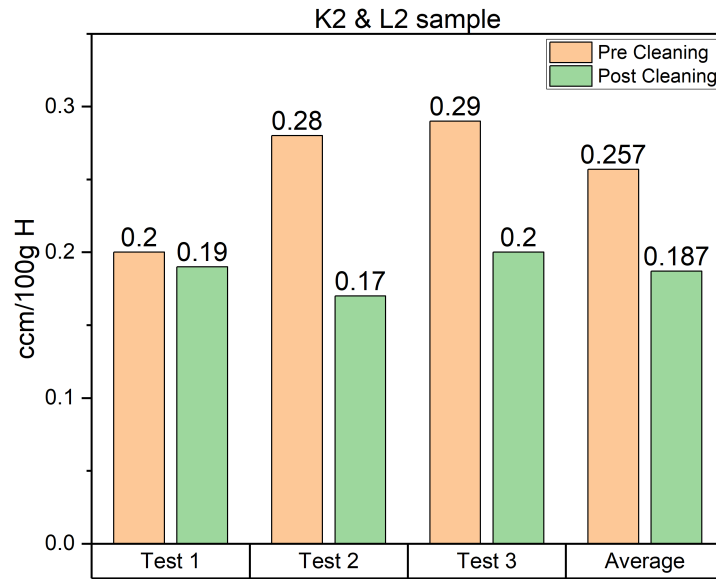


Figure 4.20: First bubble results of K2 & L2 sample before and after cleaning using ARSAL 2125.

For sample K2 & L2, using the nucleating technique, on average, a decrease of 27.24% is observed after the application of the cleaning treatment using ARSAL 2125 between different sets of experiments.

4.2.5 K3 Sample

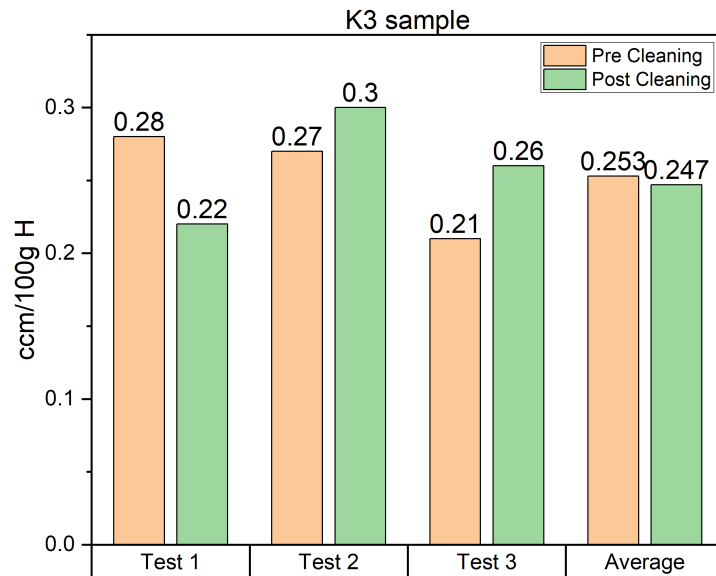


Figure 4.21: First bubble results of K3 sample before and after cleaning using ARSAL 2125.

For sample K3, using the nucleating technique, on average, a decrease of 2.37% is observed after the application of the cleaning treatment using ARSAL 2125 between the different sets of experiments.

4.2.6 L1 Sample

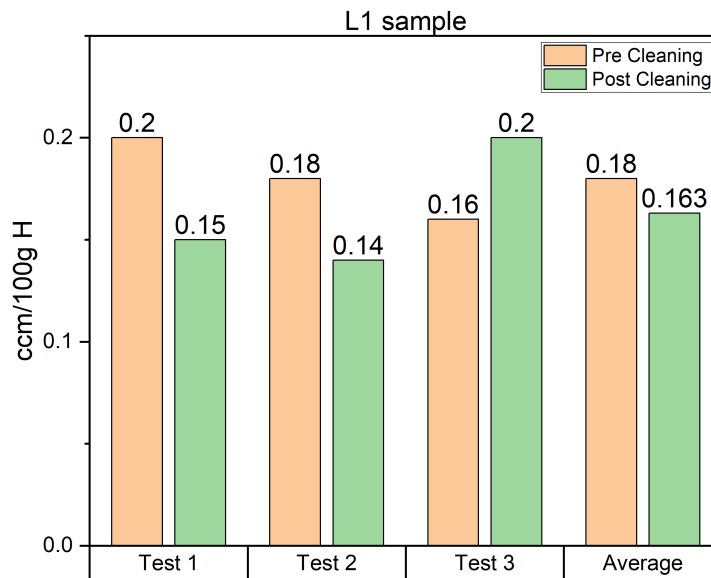


Figure 4.22: First bubble results of L1 sample before and after cleaning using ARSAL 2125.

For sample L1, using the nucleating technique, on average, a decrease of 2.80% is observed after the application of the cleaning treatment using ARSAL 2125 between the different sets of experiments.

4.2.7 L2 Sample

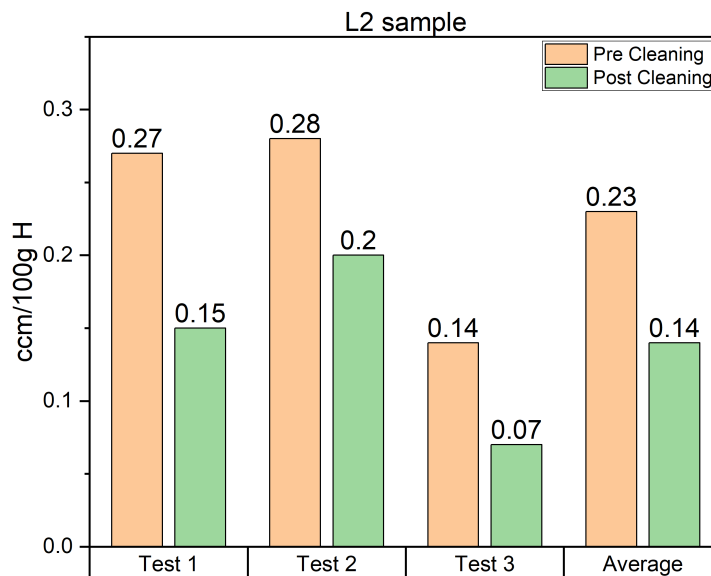


Figure 4.23: First bubble results of L2 sample before and after cleaning using ARSAL 2125.

For sample L2, using the nucleating technique, on average, a decrease of 9.44% is observed after the application of the cleaning treatment using ARSAL 2125 between the different sets of experiments.

4.2.8 R1 Sample

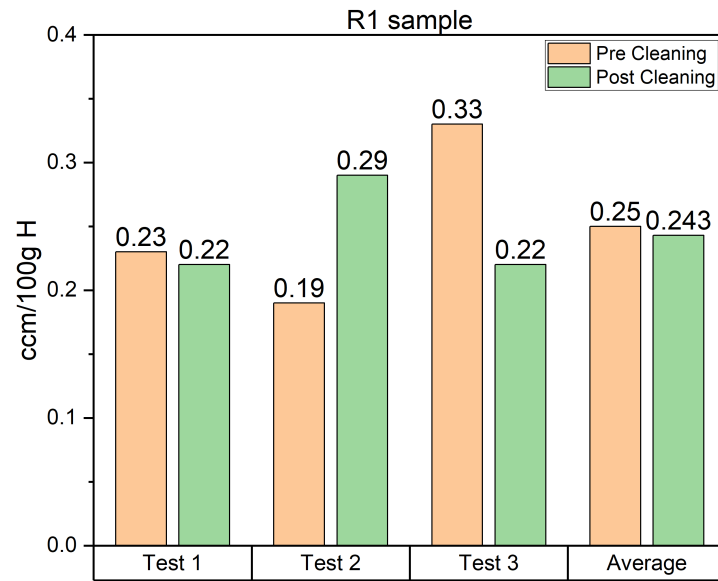


Figure 4.24: First bubble results of R1 sample before and after cleaning using ARSAL 2125.

For sample R1, using the nucleating technique, on average, a decrease of 29.13% is observed after the application of the cleaning treatment using ARSAL 2125 between the different sets of experiments.

4.3 Loop Measurements

4.3.1 K1 Sample

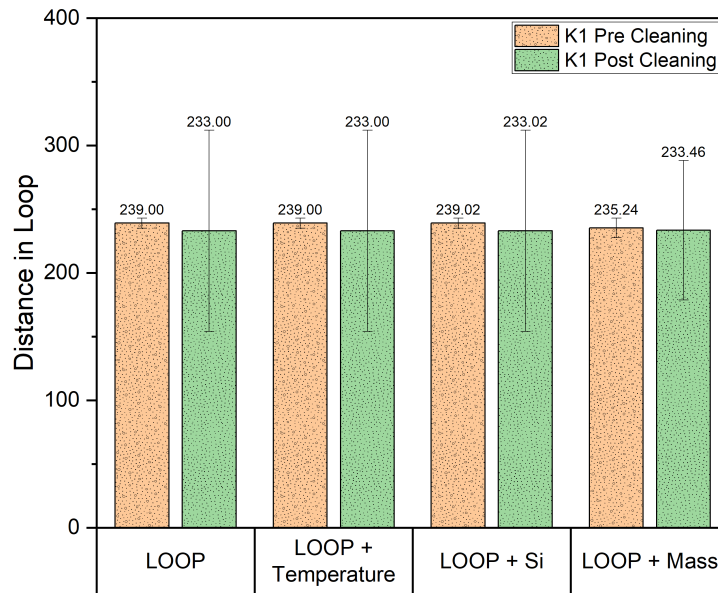


Figure 4.25: LOOP results for K1 sample before and after cleaning using ARSAL 2125.

For the K1 sample, LOOP measurements show a decrease for all the instances of the LOOP lectures before and after temperature, silicon content, and mass of aluminum melt adjustment. After the cleaning process and continuous preparation for second batch of LOOP measurements, the results indicate a decrease of 2.51%, 2.58%, 2.57%, and 0.76% respectively.

4.3.2 K2 & L2 Sample

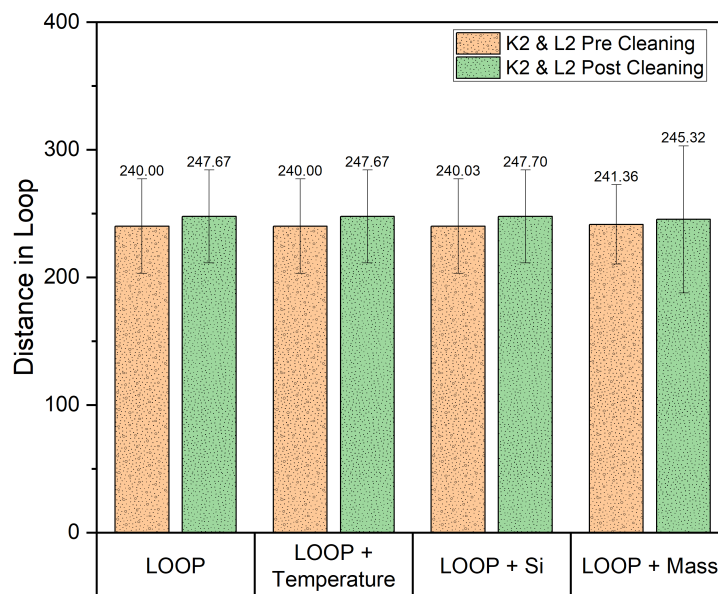


Figure 4.26: LOOP results for K2 & L2 sample before and after cleaning using ARSAL 2125.

For the K2 & L2 sample, LOOP measurements all the instances of the LOOP lectures before and after temperature, silicon content, and mass of aluminum melt adjustment with values corresponding to 3.19%, 3.10%, 3.10%, and in 1.61%.

4.3.3 K3 Sample

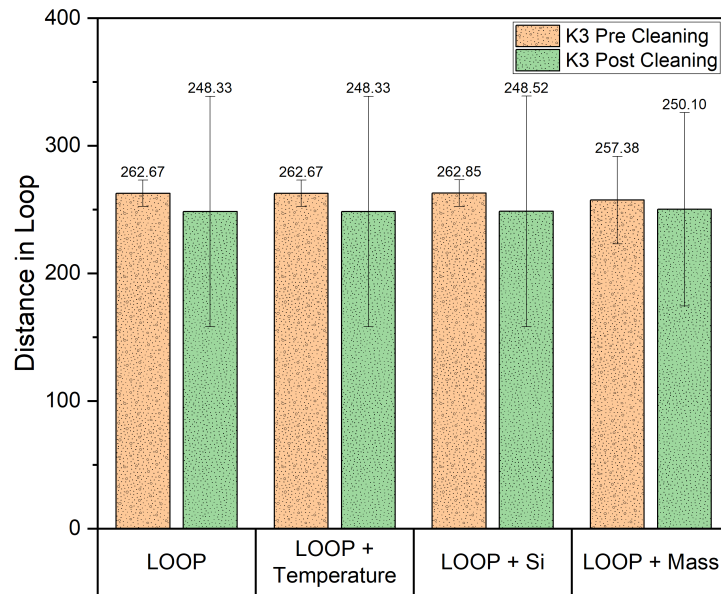


Figure 4.27: LOOP results for K3 sample before and after cleaning using ARSAL 2125.

For the K3 sample, LOOP measurements show a decrease for the all instances of the LOOP lectures before and after all variable adjustments with the corresponding being 5.46%, 5.77%, 5.77%, and 2.91% respectively.

4.3.4 L1 Sample

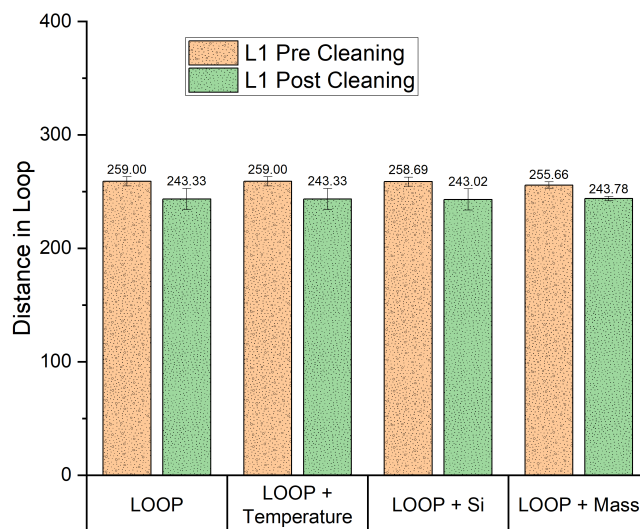


Figure 4.28: LOOP results for L1 sample before and after cleaning using ARSAL 2125.

For the L1 sample, LOOP measurements show a decrease for the all instances of the LOOP lectures before and after all variable adjustments with the corresponding being 6.05%, 6.44%, 6.45%, and 4.87% respectively.

4.3.5 L2 Sample

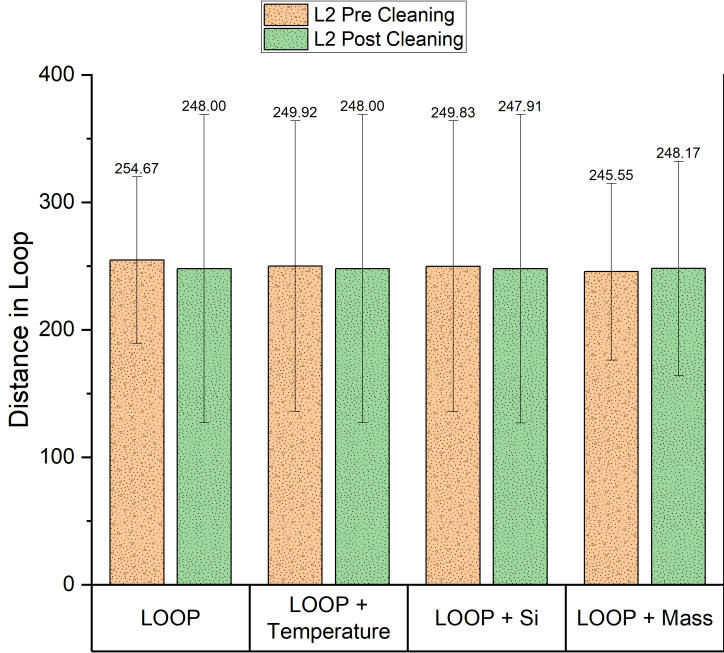


Figure 4.29: LOOP results for L2 sample before and after cleaning using ARSAL 2125.

For the L2 sample, LOOP measurements show an increase for the instance of the LOOP lectures after mass of aluminum melt adjustment with a corresponding value of 1.06%. The remaining values indicate a decrease in flow before adjustments and after temperature and silicon content adjustment with values corresponding to 2.62%, 0.77%, and 0.77% respectively.

4.3.6 R1 Sample

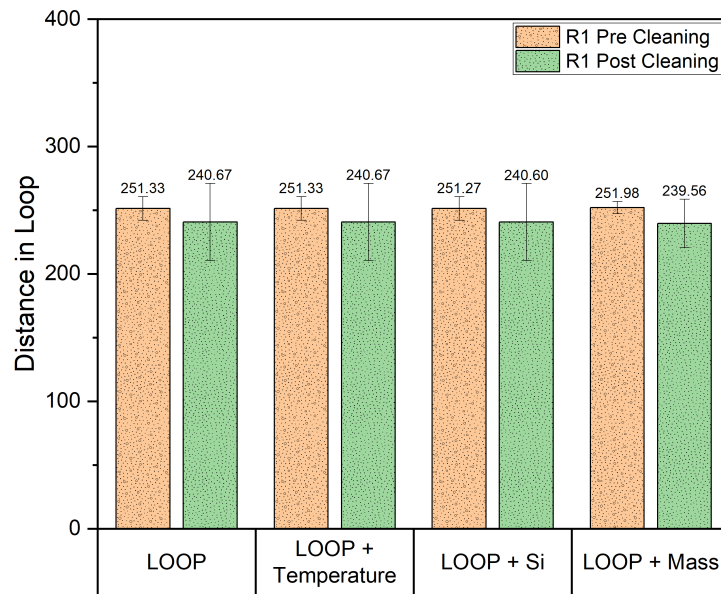


Figure 4.30: LOOP results for R1 sample before and after cleaning using ARSAL 2125.

For the R1 sample, LOOP measurements show a decrease for the all instances of the LOOP lectures before and after all variable adjustments with the corresponding being 4.24%, 4.43%, 4.43%, and 5.18% respectively.

4.3.7 R2 & R3 Sample

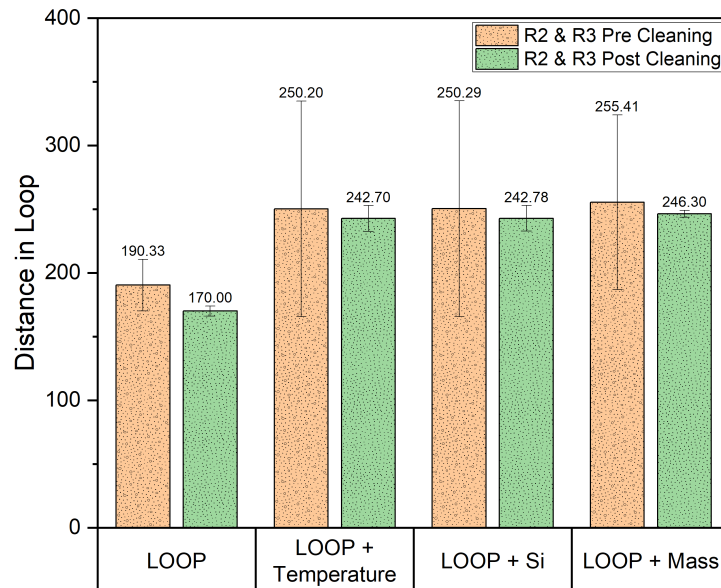


Figure 4.31: LOOP results for R2 & R3 sample before and after cleaning using ARSAL 2125.

For the R2 & R3 sample, LOOP measurements show a decrease for the all instances of the LOOP lectures before and after all variable adjustments with the corresponding being 10.68%, 3.09%, 3.09%, and 3.70% respectively.

4.3.8 R2 Sample

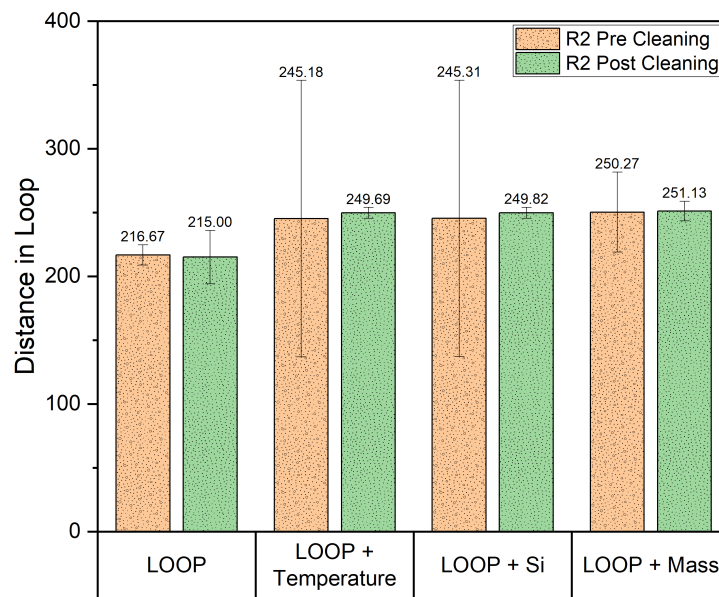


Figure 4.32: LOOP results for R2 sample before and after cleaning using ARSAL 2125.

For the R2 sample, LOOP measurements show a decrease for the instance of LOOP calculations before adjustments with a resulting decrease value of 0.77%. In comparison, the instances with adjustments in temperature, silicon, and mass variable adjustments have a percentual increase with corresponding values of 1.81%, 1.81%, and 0.34% respectively.

4.4 Production Cost Model Proposal

The core idea guiding the proposed production cost model is that all activities related to melting metal, from preparation to post-production, should be cost-conscious. The costs of pre-melting preparations need to be assessed based on their potential to reduce downtime or rejection rates. Similarly, expenses after melting, such as disposing of residuals like salt slag and reclaiming metallic aluminum from dross, should be economically assigned to the material being melted. To cover all cost aspects observed during the melting process in this thesis, various cost items can be outlined:

- Preparation Costs: K_{prep}
- Consumable Material Costs: K_A
- Material Costs: K_B
- Production Costs: K_{CP}
- Standstill Costs: K_{CS}
- Labor Costs: K_D
- Post-Production Costs: K_{post}

4.4.1 Proposed Equation

Equation 4.1 summarizes all cost items observed during the tests conducted in this thesis. $K_{process}$ represents the sum of all previously discussed cost items.

$$K_{process} = K_{prep} + K_A + K_B + K_{CP} + K_{CS} + K_D + K_{post} \quad (4.1)$$

K_{prep} and K_{post} are included in Equation 4.2 to highlight the importance of preparation and post-production steps in the melting process, which should definitely be accounted for in future versions of this proposed cost model. However, due to time constraints, K_{prep} and K_{post} are not elaborated on in the subsequent results, but are instead expanded upon within the discussion section. Meanwhile, other cost stages are explained based on test observations, interviews with industry, and calculations derived from Equation 2.11.

For convenience, the entire cost model is presented here and broken down into subsequent subsections:

$$\begin{aligned}
 K_{process} = & \frac{k_A}{n_{pB}} \Big|_a + \frac{k_B}{(1 - q_B)} \Big|_b + \frac{k_{CP} + (k_{CE} \cdot P_{CP})}{60} \left[\frac{t_0}{(1 - q_P)} \right]_{c1} \\
 & + \frac{k_{CS} + (k_{CE} \cdot P_{CS})}{60} \left[\frac{t_0}{(1 - q_P)} \cdot \frac{q_s}{(1 - q_S)} + T_{su} \right]_{c2} \\
 & + \frac{n_{op} \cdot k_D}{60} \left[\frac{t_0}{(1 - q_P)(1 - q_S)} + T_{su} \right]_d
 \end{aligned} \quad (4.2)$$

4.4.2 Consumable Material Costs — K_A

Given that Ståhl's previously defined batch size (N_0) is now measured in kilograms, several other variables must adjust accordingly. Consumables are now proportionate to the weight of N_0 . Therefore, to know the lifespan of a consumable product, we calculate the total weight of the consumable available and divide it by the percentage required based on the weight of N_0 . This yields the number of potential batches (n_{pB}) for which our consumable product will suffice. Upon determining n_{pB} , we integrate it into the cost of our purchased consumable (k_A), resulting in the cost per batch (K_A).

$$K_A = \frac{k_A}{n_{pB}} \Big|_a \quad (4.3)$$

$$n_{pB} = \text{trunc} \left(\frac{C_A}{N_0 \cdot C_Y} \right) \quad (4.4)$$

Variable	Designation	Unit
K_A	Consumable cost per batch	Currency
k_A	Purchase cost of consumable	Currency
N_0	Nominal weight of the batch	kg
n_{pB}	Number of possible batches	-
C_A	Weight of consumable available	kg
C_Y	Percent amount of consumable required based on the weight of N_0 as specified by the manufacturer	%

4.4.3 Material Costs — K_B

The melting process encompasses numerous stages (denoted as i). K_B captures all material costs incurred throughout each stage of the melting process. Depending on the amount of dross produced (m_{dross}) it might be necessary to introduce additional material (denoted as m_j). The addition of material could serve various purposes such as maintaining the value of N_i , diluting the batch using primary aluminum, or alloying the batch according to customer specifications.

$$K_B = \frac{k_{Bi}}{(1 - q_{Bi})} + \frac{k_{Bi+1}}{(1 - q_{Bi+1})} + \dots = \sum_{i=0} \frac{k_{Bi}}{(1 - q_{Bi})} \Big|_b \quad (4.5)$$

The cost of material added in a single stage (k_{Bi}) is the total of all materials added (m_j), with j counting the different material sources used. Each material has an assigned percent yield (Y_j) and a cost rate (R_j) expressed in currency/kg. This assignment is based on current procurement practices where buyers purchase secondary material from scrap yards, and suppliers specify a percent yield amount for the desired alloying element, which, in this case, is aluminum. For instance, suppose a buyer intends to acquire a decommissioned car chiller

composed of aluminum. The supplier assigns a percent yield based on their estimation of how much aluminum can be extracted from the alloys constituting the car chiller. And the cost rate is determined by the prevailing rate on the London Stock Exchange. If a deal is struck, the car chiller is weighed, and money passes hands.

$$k_{Bi} = (m_j \cdot Y_j \cdot R_j)_i + (m_{j+1} \cdot Y_{j+1} \cdot R_{j+1})_i + \dots = \sum_{j=0} (m_j \cdot Y_j \cdot R_j)_i \quad (4.6)$$

The term (q_{Bi}) refers to material losses during stage i . Calculating it is straightforward: first measure the weight of all the material added in the stage, including the resulting weight of the previous stage (N_{Ri}) if applicable. This gives the starting weight of material at stage i (N_i).

$$N_{Ri} = N_i - m_{dross,i} - m_{burn,i} \quad (4.7)$$

$$N_i = N_{Ri-1} + (m_j + m_{j+1} + \dots) = N_{Ri-1} + \sum_{j=0} (m_j)_i \quad (4.8)$$

Next, consider material losses. During the melting process of secondary material, losses depend on the ability to recover dross (m_{dross}), which means extracting any entrapped metallic aluminum, and/or filtering out the salt from salt slag.

$$q_{Bi} = \frac{m_{dross,i} - m_{trap,i} - m_{salt,i} + m_{burn,i}}{N_i} \quad (4.9)$$

Here, m_{trap} represents the mass of entrapped metal that can be recovered from dross, m_{salt} is the mass of salt filtered from the salt slag, and m_{burn} is the weight lost due to material burning away as gas or dust/ash escaping the furnace. In Equation 4.9 the mass of entrapped metal and salt are subtracted from the dross mass, but this would flip if these aspects of the dross were not recovered.

Determining the weight of each component in the dross while it is still in the furnace is complicated. Instead, a percent yield is applied to the dross as an approximation. This approach is commonly used in the industry, with the percent yield values based on experience with the process and knowledge of the material.

$$q_{Bi} = \frac{m_{dross,i} - m_{dross,i} \cdot Y_{trap,i} - m_{dross,i} \cdot Y_{salt,i} + m_{burn,i}}{N_i} \quad (4.10)$$

Variable	Designation	Unit
i	Term indexing the stage of the melting process	-
j	Term indexing the material(s) added within stage i	-
K_B	Material cost of entire melting process	Currency
k_{Bi}	Cost of material added at stage i	Currency
$m_{burn,i}$	Weight of the batch burned away at stage i	kg
$m_{dross,i}$	Weight of dross in stage i	kg
$m_{salt,i}$	Weight of salt filtered from the dross in stage i	kg
$m_{trap,i}$	Weight of entrapped metal within the dross in stage i	kg
m_j	Weight of added material j	kg
N_i	Starting weight of batch at beginning of stage i	kg
N_{Ri}	Resulting weight of batch at end of stage i	kg
q_{Bi}	Material loss term at stage i	-
R_j	Cost rate of added material j	Currency/kg
Y_j	Percent yield of added material j	%
Y_{trap}	Percent yield of entrapped metal	%
Y_{salt}	Percent yield of salt	%

4.4.4 Cost of Production — K_{CP}

The operations section of the model will cover all relevant stages performed in this thesis. It is important to note, that the stages are flexible and will depend on the type of furnace, allowing adjustments to suit specific operations. The term i is once again used to indicate the stage under investigation.

$$K_{CP} = \frac{k_{CP} + (k_{CE} \cdot P_{CP})}{60} \left[\frac{t_0}{(1 - q_P)} \right]_{c1} \quad (4.11)$$

Here, the equipment cost during production (k_{CP}) remains the same as explained in Ståhl's earlier equation (Equation 2.16). Added to this is the cost of energy (k_{CE}), expressed in currency per kilowatt-hour, and the power used in all production stages (P_{CP}), measured in kilowatts. Cycle time (t_0) represent the time it takes to complete the melting process. q_P is the production rate loss observed during the melting process.

$$P_{CP} = \sum_{i=0} \frac{P_i}{(1 - q_{Wi})} \quad (4.12)$$

$$P_i = \int_{m_{heel}}^{m_{full}} \frac{c_p \Delta T dm}{t_i} \quad (4.13)$$

P_{CP} is calculated by dividing the total power demand in all stages (P_i) by the power

losses (q_{wi}) within the system. Power, as commonly known, is mass multiplied by the specific heat multiplied by the change in temperature, all divided by the time taken to reach that temperature. This standard thermodynamic relationship faces a practical limitation: the furnace is never completely emptied between stages. A small amount of mass (m_{heel}) of molten metal always remains to completely submerge the new material for the next stage, which helps reduce oxidation and minimize burn losses.

Identifying the building components of cycle time can vary depending on factors such as the facility, furnace type, and material, among others. Equation 4.14 includes suggested terms that were identified as part of the cycle time.

$$t_0 = t_{sort} + t_{load} + t_{melt} + t_{skim} + t_{empty} \quad (4.14)$$

t_{sort} represents the time needed to gather material from storage and sort or organize it to align with the desired composition of the melt. t_{load} denotes the time spent loading the material and/or consumable material (such as salt flux) into the furnace. t_{melt} signifies the time taken for the input material to reach melting temperature or the desired temperature of the melt. t_{skim} stands for the time required by operators to remove the dross layer from the surface of the melt. Finally, t_{empty} represents the time needed to empty some or all of the melt.

Variable	Designation	Unit
ΔT	Change in temperature	$^{\circ}\text{C}$
c_p	Specific heat of material	$\text{kJ/kg}^{\circ}\text{C}$
i	Term indexing the stage of the melting process	-
K_{CP}	Cost of production	Currency
k_{CP}	Equipment cost during production	Currency/hr
k_{CE}	Cost of energy	Currency/ $\text{kW}\cdot\text{hr}$
m_{full}	Weight of a full furnace	kg
P_i	Power demand of stage i	kW
P_{CP}	Power demand of production processes	kW
q_{wi}	Power loss of stage i	-
q_p	Production loss term	-
t_0	Cycle time	min
t_i	Time spent within stage i	min

4.4.5 Cost of Standstill — K_{CS}

Similarly to production, equipment cost during standstill (k_{CS}) remains unchanged. It still includes energy costs but now covers the power demand from all standstill operations

(P_{CS}). Additionally, new time parameters for downtime losses (q_S) and setup time (T_{su}) are included as part of standstill. P_{CS} is calculated the same way as P_{CP} in Equation 4.12.

$$K_{CS} = \frac{k_{CS} + (k_{CE} \cdot P_{CS})}{60} \left[\frac{t_0}{(1 - q_P)} \cdot \frac{q_s}{(1 - q_S)} + T_{su} \right]_{c2} \quad (4.15)$$

4.4.6 Cost of Labor — K_D

With the exception of q_Q being removed, there are no changes to cost of labor (K_D) from Equation 2.11.

$$K_D = \frac{n_{op} \cdot k_D}{60} \left[\frac{t_0}{(1 - q_P)(1 - q_S)} + T_{su} \right]_d \quad (4.16)$$

4.4.7 Cost of Post-Production — K_{post}

The cost of post-production (K_{post}) is referring to the material losses due to thermitting, the costs or fees from disposing dross or salt slag depending on what is recoverable by the company, and transportation costs of any dross or salt slag that is sent away.

4.5 Carbon Emission Model Proposal

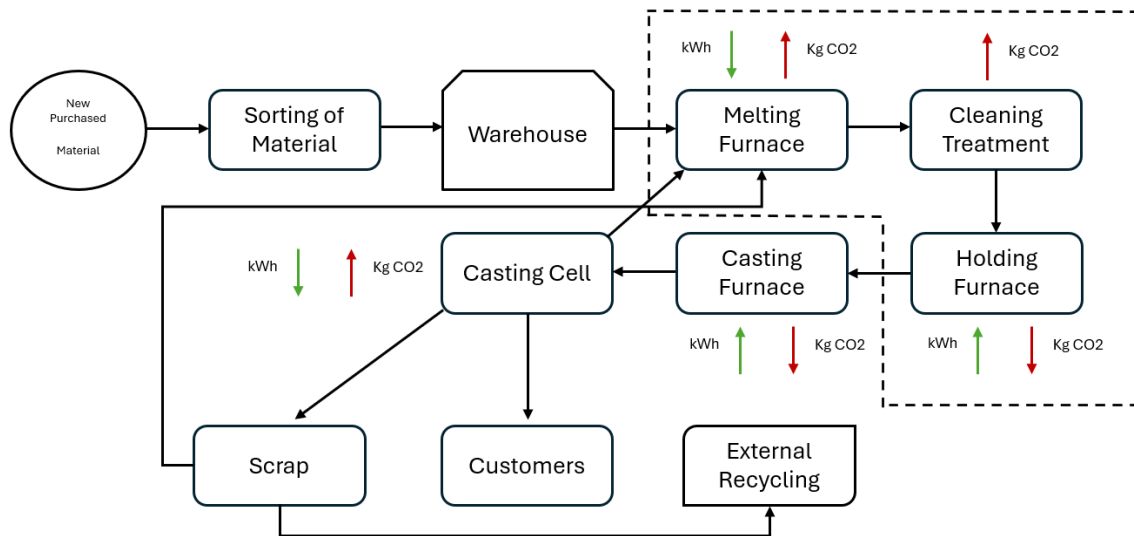


Figure 4.33: Conceptual framework of foundry workshop. [21]

In addition of the cost equation modeling proposal, a carbon emission model is another byproduct that can be generated for the current setup with the all the resources at hand. Observing a basic conceptual framework of how a foundry works, see Figure 4.33, the melting furnace, the addition of salt flux as refining agent, and the holding furnace is within the scope of the present thesis, representing a small of a rather bigger picture of foundry process. The cost model presented above was used as a reference for certain parameters of the carbon emission model. Major differences between the models is the replacement of all k_{values} with carbon emission factors or CEFs when applicable, which are standard coefficients

used to estimate carbon emission activities, and the removal of personnel data, to focus on operations within the three stages of the foundry. The calculations can be simple to very complex according to the operations, materials, and types of emissions. For simplification during calculations, carbon emissions (CE) are estimated using CEFs their purpose being estimating how much carbon dioxide emission is emitted on the operation and/or activity, or how much kg of material is used for one kg of carbon dioxide. Depending on the material, the CE might be already estimated or not. If the latter is the case, a very simple one to estimate it would be using the following equation:

$$CE_m = CEF_{material} \cdot (N_0 \cdot C_Y) \quad (4.17)$$

where $CEF_{material}$ stands for the carbon emission factor for the material component of the consumable and $(N_0 \cdot C_Y)$ is the mass of the consumable calculated through the number of batches use in production multiply with the percent amount of the consumable required based on the weight specified by the manufacturer. The use of these constants facilitates the creation of the carbon emission model that involves several aspects relevant to the foundry process encompassing the three stages pointed out in Figure 4.33. The general equation that describes the amount of carbon emissions produce by a stage in the process would be define as the following based on all the data gathered from all the sources pointed out in Section 3.9:

$$CE_{Total} = CE_A + CE_B + CE_{mach} \quad (4.18)$$

where

- CE_{Total} is the total carbon emissions generated in a stage of the process
- CE_A is the total carbon emissions generated by the use of consumables
- CE_B is the total carbon emissions generated by the materials used in a stage of the process
- CE_{mach} is the total carbon emissions generated by machinery and the energy consumption used for its operation

The following subsections refer to each component of the equation defined previously and its calculation method.

4.5.1 Consumables Carbon Emissions — CE_A

With the definition of consumable items being adapted to the lifespan of the product, using the CE that represents how much carbon dioxide is emitted for the entire use of the product divide by the number potential batches that the product will allow the estimation of to CE per use of the consumables, see Equation 4.17. With this methodology, an accurate perception of the emissions produced by the consumables can be monitor within the process using the same concept developed for the consumables section proposed in the cost model. The equations proposed for carbon emission of consumables are described below with the definitions of the variables used:

$$CE_A = \sum_{i=0} \frac{CE_{Total,A}}{n_{pB}} \Big|_a \quad (4.19)$$

In this equation:

- $CE_{Total,A}$ is the total carbon emissions generated by the materials used in a stage of the process
- n_{pB} is the number of possible batches in a stage process

$$n_{pB} = trunc \left(\frac{C_A}{N_0 \cdot C_Y} \right) \quad (4.20)$$

Variable	Designation	Unit
CE_A	Consumable carbon emission produced per batch	$\frac{kgCO_2}{kg}$
$CE_{Total,A}$	Total carbon emission of available consumable	$\frac{kgCO_2}{kg}$
N_0	Nominal weight of the batch	kg
n_{pB}	Number of possible batches	-
C_A	Weight of consumable available	kg
C_Y	Percent amount of consumable required based on the weight of N_0 as specified by the manufacturer	%

4.5.2 Material carbon emission — CE_B

The melting process encompasses numerous stages (denoted as i). CE_B is design to monitor material costs incurred throughout each stage of the melting process. As in a standard industrial setup, depending on the amount of dross produced (m_{dross}) it might be necessary to introduce additional material (denoted as m_j). The addition of material could serve various purposes such as maintaining the value of N_i , diluting the batch using primary aluminum, or alloying the batch according to customer specifications. Hence each new material added to the mixture will contribute to the emissions. Most materials have CEFs, so using such factors in to the formulas will help estimate the amount of the carbon emissions such materials can emit. The Formula 4.17 is very simple way to estimate the carbon emission of any material. A number of considerations are taking into account in the construction of the model, including the possible degradation of material, described through parameter q_{Bi} and the addition of CE of material added in a single stage (k_{Bi}), which is the cumulative sum of all materials' CE, with j tracking the count in case multiple sources of material are utilized. Each material is assigned a yield (Y_j) and a CEF (R_j) based on the carbon emission factor of the material used. The equations for material carbon emissions calculations are described in Equations 4.7 to 4.9.

$$CE_B = \frac{CE_{Bi}}{(1 - q_{Bi})} + \frac{CE_{Bi+1}}{(1 - q_{Bi+1})} + \dots = \sum_{i=0} \frac{CE_{Bi}}{(1 - q_{Bi})} \Big|_b \quad (4.21)$$

The estimation of q_{Bi} , referred to Equation 4.9 is kept the same as in the proposed cost model, as the coefficient provides a mathematical relation to the degradation of mass in each stage the material is going through, in the form of dross and evaporation into the air.

$$\begin{aligned}
 CE_{Bi} &= (m_j \cdot Y_j \cdot CEF_j)_i + (m_{j+1} \cdot Y_{j+1} \cdot CEF_{j+1})_i + \dots \\
 &= \sum_{j=0} (m_j \cdot Y_j \cdot CEF_j)_i
 \end{aligned} \tag{4.22}$$

Variable	Designation	Unit
i	Term indexing the stage of the melting process	-
j	Term indexing the material(s) added within stage i	-
CE_B	Carbon emissions of entire melting process	$\frac{kgCO_2}{kg}$
CE_{Bi}	Carbon emission for material added at stage i	$\frac{kgCO_2}{kg}$
$m_{burn,i}$	Weight of the batch burned away at stage i	kg
$m_{dross,i}$	Weight of dross in stage i	kg
m_j	Weight of added material j	kg
N_i	Starting weight of batch at beginning of stage i	kg
N_{Ri}	Resulting weight of batch at end of stage i	kg
q_{Bi}	Material loss term at stage i	-
CEF_j	Carbon Emission Factor of added material j	$\frac{kgCO_2}{kg}$
Y_j	Percent yield of added material j	%

4.5.3 Equipment & Machinery Carbon Emissions — CE_{mach}

For equipment and machinery, in this context the main machinery would be furnaces, the main source of carbon emissions are fossil fuels and electricity needed to power them up. Assuming for those cases that the equipment and machinery are running for a standard amount of shifts, an equation can be proposed:

$$CE_{mach} = \sum_{i=0} CE_{equip,e} + \sum_{i=0} CE_{equip,f} \tag{4.23}$$

In this equation, $CE_{equip,e}$ corresponds to carbon emissions the machinery running on electrical produces and $CE_{equip,f}$ correspond to the carbon emissions the equipment and machinery running on fuels. Such equations can be estimated using the following proposals:

$$CE_{equip,e} = CEF_{elec}(Power_{active} \cdot t_{active} + Power_{idle} \cdot t_{idle}) \tag{4.24}$$

$$CE_{equip,f} = CEF_{fuel}(Power_{active} \cdot t_{active} + Power_{idle} \cdot t_{idle}) \tag{4.25}$$

Here, CEF_{elec} stands for the carbon emission coefficient for electricity which depends on the electrical grid of the region or zone the facilities are located, P_{active} is the power require for the equipment and machinery to run at full power, t_{active} is equivalent to the running time, P_{idle} is the power require for the machine to remain one but no working, and t_{idle} is the define as the time that the equipment and machinery remains idle. The equation can broaden with the CEF of other energy sources and the same concept of active and idle power and time should be applicable.

5 Discussion

5.1 Production Cost Model

5.1.1 Adjustments Made from the Part Based Model

Throughout the proposed production cost model in Equation 4.2, several variables were adjusted, redefined, or omitted from the referenced part cost model (Equation 2.11). The following discussion will detail each variable, notable observations during testing, and the strengths and weaknesses of the variable changes.

5.1.1.1 Quality Loss and Handling Rejections — q_Q

The quality loss variable q_Q was completely excluded. During the melting process, no material is rejected due to quality issues. While mistakes do occur, material not meeting customer specifications is always reworked. Rejected material is diluted with cleaner aluminum until it meets the ITE limits. In this way, rejected material is recycled as new raw material with additional processing costs.

Quality loss in part production is based on the number of rejects in a batch. However, in the case of melting metal, the entire batch or melt is either good or bad. There may be instances where certain areas of the melt are not homogenized and could potentially be removed, but identifying these areas while the metal is still molten is not feasible, so it is assumed the entire melt is bad if an OES test indicates so.

In some practices, ITEs and oxides can be coaxed to the surface with salt flux and later machined off the cast. However, this thesis considers that material loss, even though it is deemed a bad part of the product. This is just one method of managing material quality. More research and industry interviews are needed to develop a more widely accepted definition of quality loss.

5.1.1.2 Batch size and Varying Furnace Weight — N

Further research is needed to accurately depict batch size, or in this case, batch weight. Tests and experiences have led to the formulation of the relationship shown in Equation 4.8. Adjusting batch size was tricky, and the choice of units affected almost all other cost parameters. Two scenarios for defining N were considered:

Batch size is based on incoming material: One approach is to link batch size with the incoming material supply. In industry, raw material is received in waves, often labeled to indicate that it was all cast from the same source and should be considered identical within the group. This naming system is widely used across manufacturing industries, not just in melting processes. Defining N this way could help the Enterprise Resource Planning (ERP) system align with production scheduling. Furthermore, factors linked to material properties would stay consistent as all materials in the group are considered identical. This approach would simplify computations regarding power and carbon emissions, as the differences due to material types would decrease. However, adopting this method requires a strong ERP

system and involves placing substantial trust in suppliers and their naming conventions, as well as adhering to quality norms and ensuring consistent delivery. While defining batch size based on internal processes should be effective, measures should be taken to lessen reliance on supplier-provided parameters.

Batch size is based on furnace capacity: This was the most straightforward approach as much of the sensors and operator presence was built around equipment. This unit declaration also fit well with the part based model and other parameters. Although changes needed to be made throughout the model to consider the material is lost during the melting process and this was difficult to accurately represent.

Optimal batch size (N_0) is effective in the part-based model because it accounts for quality loss, representing rejections. However, during melting, there are no rejections, only material loss. Thus, it was decided to utilize q_B to account for material losses based on weight, which would impact the subsequent stage in the process. This approach establishes both an initial and resulting batch size, represented by N_i and N_{Ri} , respectively, with ‘i’ indicating the stage within the melting process. Practical testing of the model is necessary to validate the proposition of representing batch sizes and stages in this manner.

5.1.1.3 Cycle Time and Segmenting into Stages — t_0

As mentioned before, stages were used to capture the different steps in the melting process. This method helped to distinguish parameters influenced by various input sources and alloying methods, but it also means that cycle time needs to be divided to fit these stages. There’s a worry that the time variables in the model might overlap or be too restricted in certain stages. Moreover, if the cycle time doesn’t accurately reflect the melting process, time-related losses might be unfairly distributed across cost items.

The testing setup at BRYNE was basic, lacking complex material handling or equipment setup procedures. A thorough examination of cycle time beyond the parameters suggested in Equation 4.14 is needed to accurately allocate time throughout the melting process and identify where losses occur.

5.1.2 Strengths and Weaknesses of Proposed Variables

In the suggested production cost model (Equation 4.2), several new variables were added to complement existing parameters or introduce entirely new cost factors, like including power costs.

5.1.2.1 Weighing Dross and Material Recovery — m_{dross}

Weighing dross presents practical challenges. While removing it at the end of a stage enables the measurement of material loss, its removal also promotes the generation of more dross. Therefore, the conventional practice does not involve measuring dross between stages; instead, the dross is collected at the final stage and analysed afterward. Another rationale for maintaining an uninterrupted melting process is when salt flux is utilized as a protective barrier over the melt’s surface.

The thickness of the dross layer can be estimated utilizing the theory outlined in Equa-

tion 2.4. However, as indicated in the literature review and observed in our experiments, factors such as oxidation growth rate, melting process operations, material input, among others, all play a role in the formation of dross in their respective ways. Additional research is necessary to improve the accuracy of determining dross accumulation without disturbing the surface of the melt.

In the industry, the aim is to operate in a manner that minimizes the production of dross as much as possible. The techniques outlined below to minimize dross are a fusion of recommendations from the literature review and insights gained from our own experiences:

- Material input should be as dry as possible.
- The melting temperature should be kept as low as possible.
- Avoid prolonged periods of holding the temperature at the melting point.
- Submerge loose material or salt additions and mix them within the melt to limit contact with air.
- Mixing should be gentle and ideally not disrupt the protective oxide layer formed on the surface of the melt.
- Crucible shape should be designed to minimize exposed surface area.
- Salt flux composition should be tailored to the alloy composition being melted and the desired alloy composition outcome.

Contributing to the challenge of assessing dross weight was figuring out how to allocate a cost for its recovery. The composition of dross can vary greatly depending on the secondary input, and there's no standard method to determine its value because reclaiming dross involves remelting it, subjecting it to the same loss factors like oxidation and burning, which isn't a consistent process. Labeling dross as a method to minimize material quality loss (q_B) assumes dross costs the same as the input material, which isn't accurate because the resulting alloy composition differs significantly from the initial material. Therefore, assigning this cost value to dross may not be suitable, and additional research is necessary to accurately reflect its realistic cost value.

Taking into account the identified shortcomings, it's worthwhile to explore the benefits of measuring dross and assessing its economic implications. According to interviews, investigations, and research, dross variables are typically overlooked in the stage 3 SBT calculations provided by companies. This omission might stem from the complexity involved in handling dross or the limited profitability recognized by the recycling system. Integrating the downstream impact of dross could significantly alter the reported values associated with "green" aluminum. This potential effect holds substantial implications for the sustainability of not only aluminum melting but also other metal production processes.

5.1.3 Cost of Power and Determining Demand per Stage — P_i

Measuring power consumption simplifies to understanding the cost rate charged by the energy company and the amount demanded by the process from the grid. Obtaining these values is straightforward and aligns with insights from industry interviews and public access of Stage 2 SBT reports.

An intriguing aspect, not uncovered in the literature search, is the fluctuation of power demand based on the weight of added material. Thermodynamics highlights that mass significantly influences the energy required to heat material. The material introduced into a furnace is represented by the batch size and impacts nearly all parameters within the proposed production cost model, including time parameters, power factors, and loss factors. No matter how straightforward thermodynamics explains heat transfer, the actual process in an industrial furnace is expected to yield a different outcome from the theoretical equation. This is mainly because some of the molten material remains in the furnace to aid in melting the next batch, known as m_{heel} . This technique brings advantages like lower burn losses, reduced oxidation, and quicker heat transfer. Utilizing the latent energy stored within the m_{heel} could also decrease power consumption from the grid. Understanding this phenomenon adds another dimension to consider, touching on factors like quality, cycle time, and dross accumulation.

5.2 Carbon Emissions Model

5.2.1 Scientific Base Targets

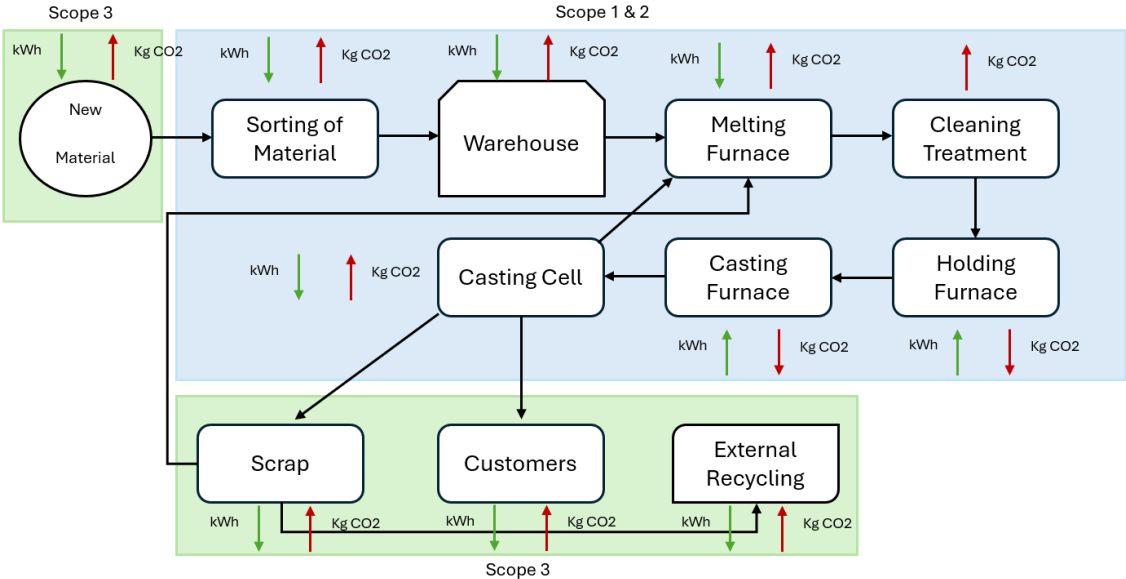


Figure 5.1: Conceptual framework of foundry workshop with three emission scopes.

Growing awareness of carbon emissions has led to new emission policies across Europe in recent years, like the Corporate Sustainability Reporting Directive. These policies require large companies to document their sources of carbon emissions and any other environmental hazards. Creating a model to monitor a company’s emissions and activities has now become a top priority.

The model in this thesis gives a clear picture of the activities carried out in the experiments. One of its main strengths is its adaptability. The emission model is designed to be modular, so new components that weren’t initially considered can be added, as long as they don’t overlap and overestimate values. This flexibility is important to prevent incorrect

data estimations and allows the model to expand to include multiple Scientific Base Target Emission Scopes.

Figure 5.1 illustrates the integration of all three emission scopes within the foundry process, as discussed in this thesis. Scope 3 encompasses processes that occur outside the company, including operations related to the purchasing of goods from suppliers, waste management, employee commuting, and the processing of sold products. In this context, the procurement of new material, scrap and recycle management, and selling to consumers all fall under Scope 3. Meanwhile, activities related to operations within the facilities and energy consumption are categorized under Scopes 1 and 2.

At this stage of the process, the proposed model mainly tackles Scope 1 with calculations of material processing, consumables and even combustion of emissions reflected through the use of CEF throughout the equations and Scope 2 with the usage of energy sources such as electricity and fossil fuels used for furnaces and experimental equipment such as the vacuum machine and first bubble apparatus. For the model to begin encompassing aspects of Scope 3, parameters regarding Preparation and Post-Production activities can be included.

Carbon emissions in the early stages of the supply chain for a foundry process include logistics emissions generated by suppliers' transportation methods, emissions from purchased goods and services, and emissions from business travel. These operations can be integrated into a larger framework of carbon emission calculations. Conversely, post-production emissions occur after the foundry has completed the products and distributed them to clients. These emissions encompass the transportation of goods to customers, waste management such as dross and slag disposal and recycling, and end-of-life treatment of the sold products (if applicable). These parameters, based on the resources used, can be converted into formulas and included within the overall carbon emission framework.

5.2.1.1 Strength and Weaknesses of the Carbon Emission Model

The current carbon emission model shows promise in carbon emission modeling, with its adaptable design catering to various needs within the foundry process, from melting to holding furnace operations. Considering material usage and potentially adding extra material to compensate for losses at these stages, the equations proposed in subsection 4.5.2 offer a solid understanding of material losses and compensation, often overlooked.

This model covers the main aspects of the three stages outlined in the thesis. Its flexibility allows many equations to apply to new components entering the process. For example, in the section on machinery and equipment carbon emissions, adding a new furnace or equipment only requires knowing its energy source and consumption, with minimal changes in calculations. Similarly, for materials, knowing the carbon emission factors (CEFs) per source and considering the amount of material added for compensation ensures adaptability to new circumstances.

A standout feature of the model is its ability to pinpoint stages with significant emission impact accurately. By breaking down the process into smaller components, the model can track new results if significant operational changes occur, enabling informed decision-

making. Furthermore, its flexibility makes it easy to comply with new European regulations like the CSRD, streamlining emission monitoring for companies and simplifying report generation.

Nevertheless, the model poses certain weaknesses that may limit its functionality and may imply fine tuning according to the situation that may present itself. First, the main obstacle of the model is the gathering and organization of all the necessary data to use as input. For a model to be accurate, it relies on the data that is being fed with. The data must be consolidated and validated with manufacturers of materials, equipment, and machinery and analysis of a foundry's process must be performed to comprehend the scale of the operation and determine parameters that reflect the reality of the operations. Second, this consolidation of information imposes time investment and knowledge regarding placing every piece of the model in place, which is why assumptions is common practice in parametrization of equations and may lead to uncertainties and overestimation of values that eventually end up with incorrect calculations. Lastly, as any relevant mathematical model, a validation is to ensure the reliability. This may incurred in performing multiple tests of operations and could proved difficult considering the set up of how foundries may work 24 hours per day, similar to a variety of manufacturing settings in the industry around the world.

As a final note, the model is limited to the three stages pointed in the framework at the beginning of the section, so it is certain, that if an implementation is desired, the need to include an analysis for all stages of the foundry process, which would be a major update and improvement for traceability of all carbon emissions found in a foundry system.

5.2.1.2 Improvements for the Carbon Emission Model

The carbon emission model proposed can be subject to improvements. Acknowledgement of that limitation is known hence an first easy improvement is an equation that includes operations outside the chosen scope. Inclusion of operations such as sorting, storage of raw materials, casting furnace, and cell will broaden capture of emissions produced during the entire of foundry process. Smaller but no less important activities including movement of conveyor belts, trajectories and energy expenditures of moving automated guided vehicles, and much more are all relevant toward the tally of carbon emissions generated in foundry, all within scope 1 and 2 of the Scientific Base Targets.

Moreover, recycling operations (regardless if they are executed within the facilities) and end of life treatment of products, in addition, to other downstream activities related to the supply chain can enhance the model to the point of covering all three scopes, which is the ideal scenario for any carbon emission model. As more components are added to the initial propose equation, the versatility will increase but so its complexity, thus a robust documentation system should go hand-by-hand with the implementation of the model and further expansions it might receive.

5.3 Remarks about Material Composition and OES Data

Upon completion of all tests, it became evident that incorporating ARSAL 2125 as a refining agent for secondary low alloy aluminum didn't notably alter its composition. De-

spite refining efforts, numerous impurities persisted within the aluminum post-melting. Our analysis underscores the pivotal role of salt flux selection, as no additional materials were introduced during the refining process. Optical Emission Spectroscopy (OES) results before and after refining remained relatively stable, except for tests K2L2 and R2R3. These tests involved blending two alloys due to insufficient quantities to fill the crucible to approximately 60%. This step was necessary to ensure a sufficient amount of molten metal for sampling. The compositional changes observed in these tests stemmed from alloying, as the two combined materials exhibited slight differences, resulting in higher weight percent changes in the resulting OES data compared to tests using a single alloy.

Regarding the oxidation of magnesium, it either remained unaffected or was too negligible for detection by OES. Our tests were conducted at temperatures significantly higher than the melting point. Literature suggests that alloying elements tend to oxidize at elevated temperatures exceeding 760°C. Thus, there's a possibility that magnesium, which readily reacts with atmospheric moisture, might have undergone reduction during the melting phase.

Further exploration of salt flux is recommended, as its composition or formulation can significantly influence impurity removal. Additionally, investigating different methods of introducing salt flux is advisable. These methods include adding salt flux before melting, incorporating it across multiple cleaning stages, varying weight percentages, and introducing it at various holding temperatures. These recommendations stem from insights gathered from informal interviews and open discussions at BRYNE and the literature review performed throughout the thesis. Two methods of particular interest were adding salt flux before melting and adding it at different holding temperatures. During our experimentation, we observed an above-normal amount of smoke production when salt flux was added at our holding temperature of 850°C. Subsequently, it was discovered that introducing ARSAL 2125 at elevated temperatures heightened the reaction rate between the salt flux and the melt.

Recognizing the potentially significant role of salt flux in reducing ITEs is essential. Even though it wasn't explored in the tests, employing a method or device to measure the composition of the dross could provide better insights into which elements were reacting with the salt flux. Measuring the dross during the tests proved challenging due to its mixed metal and slag nature. Given more time, this thesis could have delved deeper into the metallic components of the dross. However, understanding the composition of the slag is deemed more critical, especially considering the environmental risks associated with salt slag.

5.4 Material Degradation and Quality

The combination of the two methods help understand that a high concentration of oxides and gases within the melt, will produce inconsistent material properties even though the composition has not changed. The two instances where density index experiments were performed show negative values as results. Mathematically, that represents an error. From a practical perspective, it can be explained through the effects of shrinkage and pores resulting in the sample. The samples showed to have pores on the surface layer of the specimens. This phenomena in combination with shrinkage, expand the pores to form cracks on the

surface. The setup used in the thesis using the Archimedes principle for estimating density affects negatively as the possibility of water seeping inside the sample affect the density of the sample, altering the final results. Using the Archimedes principle is not suitable for samples when an even surface is present in the specimen.

The first bubble method, on the other hand, demonstrated the positive effects of the usage of in ARSAL 2125 usage in reducing hydrogen. As observed in Section 4.2, in all instances of hydrogen measurements, average wise, there is a decrease from as low as 2.37% up to 37.5% in all the cases. The effects of the salt granules effectively reduce hydrogen content in the aluminum melts for all samples. Reducing hydrogen content in aluminum melts is critical, as it diminishes the probability of hydrogen gas becoming trapped within the melt. Eventually, in a complete foundry process, the melt will continue on for further processing. If aluminum solidifies while containing hydrogen bubbles, the creation of pores becomes more likely and in turn leads to porosity. Porosity is a feature that is avoided as much as possible because it weakens the material structure and becomes subject for suffering structural integrity. Additionally, hydrogen content in aluminum melt is associated to originate embrittlement, in this case of aluminum, influencing its ductility properties. Not only reducing hydrogen content enhances the end product mechanical properties, it will also will improve the surface quality of the process product due to the decrease production of pores, hence increasing the quality of the aluminum melt. Knowing the porosity of the material can help determine whether or not the final product can be used for certain purposes, for example in high pressure die casting.

Bryne's LOOP technology is an original attempt to assess fluidity of an aluminum melt. The easy to learn procedure of setting up and performing measurements provides a convenient experimental process for execution. As seen in the result sections, the difference in flow distance before and after salt flux treatment remain consistent, while the spread or the variance between scenarios demonstrate more discernible differences. This leads to think that the chosen salt flux treatment for this type of alloy is not the adequate for reducing flow spread. Although there is little evidence to completely disregard the effect of the ARSAL 2125 in the flow, hydrogen content in the melt doesn't seem to be determining factor for flow distance measurement. Oxides continue to represent a major variable that limit the fluidity of aluminum, as aluminum reacts with air, especially with the high temperatures work (770°C to 850°C) during the experiments, forcing a constant manual removal of them from the aluminum melt's surface. Nevertheless, LOOP results contribute by telling us how the fluidity of an alloy behaves after each step in a foundry process. This in term can be used to determine performance on later stages in a foundry process, for example, during casting in case of casting process and extrusion and forming processes for wrought aluminum. Fluidity will play a role in these processes as it determines how well molten aluminum can flow through a die or a mould. With good fluidity, uniformity of flow is most probable to happen, asserting a correct distribution of the material for later processing and improve end product quality.

6 Conclusion

This thesis explores secondary low aluminum composition and quality after adding salt flux as a refining agent, aiming to propose two mathematical models addressing cost and emissions within the melting process. Evaluating secondary low aluminum quality utilized density index, first bubble method, optical electron spectroscopy, and LOOP technology. Gathering information involved researching theoretical background, interviewing professionals and academics, visiting industries, and attending workshops to devise cost and carbon emission models for the melting process under examination. This array of tools and techniques enabled addressing the following research questions:

RQ1: What costs and emissions might accompany the remelting process of heavily oxidized car chillers or other sources of secondary low alloy aluminum?

Several factors introduced in Ståhl's discrete part-based production cost model (Equation 2.11) were carried over to the proposed production cost model. These variables, including Power (P), batch size (N), and material loss related to dross (q_B), were of particular interest for further investigation within both the proposed production cost model (Equation 4.2) and the proposed carbon emissions model (Equation 4.18) as they heavily influenced the costs and emissions generated. By incorporating these parameters into the proposed models, SBT reports could encompass costs and emissions associated with all melting operations, particularly the production and handling of dross and the specifics of power generation. Heavily oxidized secondary low alloy aluminum products, like the car chillers melted during the tests, require salt flux for aluminum refinement which will produce hazardous dross. Considering disposal costs, fees, and the recoverability of dross is crucial for accurately evaluating final costs and emissions within the melting process.

RQ2: How does the oxide content, as identified by BRYNE's quality techniques, challenge the purification of secondary low alloy aluminum during remelting?

When remelting secondary low alloy aluminum, a major challenge will be its refinement through salt flux. The key lies in proper preparation and sorting of materials, alongside the identification of the composition of secondary low alloy aluminum. This enables more precise matching of the appropriate salt flux to refine the specific mix of elements in each batch of material. However, salt flux may not achieve all aspects of purification. Observations indicate that after salt flux refinement of the car chillers, no significant improvements in material quality, aside from reduced hydrogen content, were detected using the employed quality techniques. This suggests that while salt flux refinement can effectively remove ITEs and oxides during the remelting of heavily contaminated secondary high alloy aluminum, other refinement methods are necessary for refining secondary low alloy aluminum.

RQ3: What do the combined results of the LOOP, Density Index, and First Bubble Method indicate about the quality of the melt?

BRYNE's LOOP technology measures the fluidity of molten aluminum and provides insights into its oxide content. Oxides form due to aluminum's reactivity with oxygen, reducing production yield regardless of the method used, such as rolling or casting. LOOP test results indicate the distance traveled by the melt as it solidifies. By conducting multiple tests, the variance in the results quantifies the oxide content at a specific production stage. The LOOP technology is designed for easy integration into existing melting operations, enabling better control of material quality.

Porosity in low alloy aluminum occurs when air bubbles become trapped during the melting phase and manifest after solidification. This phenomenon is undesirable because it weakens the material structure, creating uneven surfaces and compromising structural integrity. Furthermore, high hydrogen content in the aluminum melt can cause embrittlement, negatively affecting its ductility. To mitigate these issues, salt flux refinement is incorporated into the melting process.

To monitor gas levels in the melt, both the Density Index and the First Bubble Method can be employed at various stages of the melting process. Using the Archimedes principle for Density Index measurements may lead to inaccuracies due to the various characteristics of secondary low alloy aluminum and the specifics of the experimental setup. On the other hand, the First Bubble method does reveal a trend in regards of hydrogen content when salt flux refinement is applied to the melt.

The combination of the LOOP and hydrogen quality techniques can help understand physical and chemical phenomena that affect oxide growth within molten aluminum and the resulting dross.

Moving forward, the next steps in this research line would involve testing various types of salt flux to gain deeper insights into which treatment methods can effectively purify secondary low aluminum to a greater extent. Additionally, it's essential to determine if alternative treatment approaches are necessary to achieve desired results, supplementing findings with the same quality techniques employed during this thesis and others found in literature and industrial visits that can add value to future studies.

Further exploration of the models is warranted if implementation is anticipated, particularly in larger-scale operations. This exploration would involve incorporating parameters that may have been overlooked or not covered due to the scope limitations of the current studies.

Bibliography

- [1] *United Nations Treaty Collection. Paris Agreement.* Dec. 2015.
- [2] European Commission. *EU's Waste Framework Directive.* URL: https://environment.ec.europa.eu/topics/waste-and-recycling/waste-framework-directive_en.
- [3] Rachel Carson. *Silent spring.* 40th anniversary ed., 1st Mariner Books ed. Boston: Houghton Mifflin, 2002. ISBN: 9780618249060.
- [4] Hannah Ritchie, Pablo Rosado, and Max Roser. *Breakdown of carbon dioxide, methane and nitrous oxide emissions by sector.* URL: <https://ourworldindata.org/emissions-by-sector>. Accessed: 20.04.2024.
- [5] Thomas Husson. *Nike Faces Lawsuit Over Greenwashing Claims. It Won't Be The Last.* May 2023. URL: <https://www.forrester.com/blogs/nike-faces-lawsuit-over-greenwashing-claims-it-wont-be-the-last/>. Accessed 10.05.2024.
- [6] Philosophy. *The Texas Sharpshooter Fallacy: Explanation and Examples.* June 2019. URL: <https://philosophyterms.com/the-texas-sharpshooter-fallacy/>. Accessed 10.05.2024.
- [7] Susan Galer. *SAP BrandVoice: Sustainability Trends 2023: Goodbye Greenwashing, Hello Business Results.* URL: <https://www.forbes.com/sites/sap/2023/01/31/sustainability-trends-2023-goodbye-greenwashing-hello-business-results/>. Accessed 10.05.2024.
- [8] Science Based Targets. *What are the emissions scopes which scopes do targets have to cover?* URL: <https://sciencebasedtargets.org/>. Accessed 10.05.2024.
- [9] The European Parliament and the Council of European Union. *Directive (EU) no 2022/2464.* 2022. URL: <https://eur-lex.europa.eu/legal-content/EN/TXT/PDF/?uri=CELEX:32022L2464>.
- [10] Subodh Das. "Designing Aluminium Alloys for a Recycling Friendly World". In: *Materials Science Forum* 519-521 (July 2006), pp. 1239–1244. DOI: 10.4028/www.scientific.net/MSF.519-521.1239.
- [11] Julian M. Allwood, Jonathan M. Cullen, and Rachel L. Milford. "Options for Achieving a 50% Cut in Industrial Carbon Emissions by 2050". In: *Environmental Science & Technology* 44.6 (2010). PMID: 20121181, pp. 1888–1894. DOI: 10.1021/es902909k. eprint: <https://doi.org/10.1021/es902909k>. URL: <https://doi.org/10.1021/es902909k>.

- [12] Timothy G. Gutowski, Sahil Sahni, Julian M. Allwood, Michael F. Ashby, and Ernst Worrell. “The energy required to produce materials: constraints on energy-intensity improvements, parameters of demand”. In: *Philosophical Transactions of the Royal Society A: Mathematical, Physical and Engineering Sciences* 371.1986 (2013). DOI: 10.1098/rsta.2012.0003. eprint: <https://royalsocietypublishing.org/doi/pdf/10.1098/rsta.2012.0003>. URL: <https://royalsocietypublishing.org/doi/abs/10.1098/rsta.2012.0003>.
- [13] Stefano Capuzzi and Giulio Timelli. “Preparation and Melting of Scrap in Aluminum Recycling: A Review”. In: *Metals - Open Access Metallurgy Journal* 8 (Apr. 2018), p. 249. DOI: 10.3390/met8040249.
- [14] Jerry Blomberg and Patrik Söderholm. “The economics of secondary aluminium supply: An econometric analysis based on European data”. In: *Resources, Conservation and Recycling* 53.8 (2009), pp. 455–463. ISSN: 0921-3449. DOI: <https://doi.org/10.1016/j.resconrec.2009.03.001>. URL: <https://www.sciencedirect.com/science/article/pii/S0921344909000548>.
- [15] Christina Windmark, Lucia Lattanzi, André Månberger, and Anders Jarfors. “Investigation on Resource-Efficient Aluminium Recycling – A State of the Art Review”. In: Apr. 2022. ISBN: 9781643682686. DOI: 10.3233/ATDE220122.
- [16] Jan-Eric Ståhl and Christina Windmark. *Sustainable Production Systems. The link between technology and economy with a global perspective*. Lund University, 2022.
- [17] Jirang CUI and Hans J. ROVEN. “Recycling of automotive aluminum”. In: *Transactions of Nonferrous Metals Society of China* 20.11 (2010), pp. 2057–2063. ISSN: 1003-6326. DOI: [https://doi.org/10.1016/S1003-6326\(09\)60417-9](https://doi.org/10.1016/S1003-6326(09)60417-9). URL: <https://www.sciencedirect.com/science/article/pii/S1003632609604179>.
- [18] European Aluminium. *VISION 2050 EUROPEAN ALUMINIUM’S CONTRIBUTION TO THE EU’S MID-CENTURY LOW-CARBON ROADMAP A vision for strategic, low carbon and competitive aluminium*. 2019.
- [19] Jaclyn L. Cann, Anthony De Luca, David C. Dunand, David Dye, Daniel B. Miracle, Hyun Seok Oh, Elsa A. Olivetti, Tresa M. Pollock, Warren J. Poole, Rui Yang, and C. Cem Tasan. “Sustainability through alloy design: Challenges and opportunities”. In: *Progress in Materials Science* 117 (2021), p. 100722. ISSN: 0079-6425. DOI: <https://doi.org/10.1016/j.pmatsci.2020.100722>. URL: <https://www.sciencedirect.com/science/article/pii/S0079642520300864>.
- [20] The White House. *USA’s CHIPS Act*. URL: <https://www.nist.gov/chips>.
- [21] BRYNE AB. *Loop*. URL: <https://bryne.se/home/bryne%20casting/LOOP.html>. Accessed: 05.04.2024.
- [22] The Aluminum Association. *American National Standard Alloy and Temper Designation Systems for Aluminum. ANSI H35.1*. May 2017.

- [23] Gabrian International. *Aluminum Alloy Nomenclatures*. Nov. 2021. URL: <https://www.gabrian.com/aluminum-alloy-nomenclatures/>.
- [24] Dierk Raabe, Dirk Ponge, Peter J. Uggowitzer, Moritz Roscher, Mario Paolantonio, Chuanlai Liu, Helmut Antrekowitsch, Ernst Kozeschnik, David Seidmann, Baptiste Gault, Frédéric De Geuser, Alexis Deschamps, Christopher Hutchinson, Chunhui Liu, Zhiming Li, Philip Prangnell, Joseph Robson, Pratheek Shanthraj, Samad Vakili, Chad Sinclair, Laure Bourgeois, and Stefan Pogatscher. “Making sustainable aluminum by recycling scrap: The science of “dirty” alloys”. In: *Progress in Materials Science* 128 (2022), p. 100947. ISSN: 0079-6425. DOI: <https://doi.org/10.1016/j.pmatsci.2022.100947>. URL: <https://www.sciencedirect.com/science/article/pii/S0079642522000287>.
- [25] Christoph Schmitz. *Handbook of aluminium recycling: mechanical preparation, metallurgical processing, heat treatment*. eng. 2. ed. Edition heat processing. Essen: Vulkan-Verl, 2014. ISBN: 9783802729706.
- [26] Mostafa Mahinroosta and Ali Allahverdi. “Hazardous aluminum dross characterization and recycling strategies: A critical review”. In: *Journal of Environmental Management* 223 (2018), pp. 452–468. ISSN: 0301-4797. DOI: <https://doi.org/10.1016/j.jenvman.2018.06.068>. URL: <https://www.sciencedirect.com/science/article/pii/S0301479718307205>.
- [27] Daniel Brough and Hussam Jouhara. “The aluminium industry: A review on state-of-the-art technologies, environmental impacts and possibilities for waste heat recovery”. In: *International Journal of Thermofluids* 1-2 (2020), p. 100007. ISSN: 2666-2027. DOI: <https://doi.org/10.1016/j.ijft.2019.100007>. URL: <https://www.sciencedirect.com/science/article/pii/S2666202719300072>.
- [28] Environmental Protection Agency. *European waste catalogue and hazardous waste list: valid from 1 January 2002*. Johnstown Castle Estate, County Wexford, Ireland: E.P.A., 2002. ISBN: 9781840950830.
- [29] Irving P. Herman. “CHAPTER 6 - Optical Emission Spectroscopy”. In: *Optical Diagnostics for Thin Film Processing*. Ed. by Irving P. Herman. San Diego: Academic Press, 1996, pp. 157–213. ISBN: 978-0-12-342070-1. DOI: <https://doi.org/10.1016/B978-012342070-1/50007-3>. URL: <https://www.sciencedirect.com/science/article/pii/B9780123420701500073>.
- [30] H.N. WILSON. “CHAPTER 14 - EMISSION SPECTROSCOPY”. In: *An Approach to Chemical Analysis*. Ed. by H.N. WILSON. Pergamon, 1966, pp. 260–279. ISBN: 978-0-08-011543-6. DOI: <https://doi.org/10.1016/B978-0-08-011543-6.50017-5>. URL: <https://www.sciencedirect.com/science/article/pii/B9780080115436500175>.

- [31] Somsubhra Ghosh, V Laxmi Prasanna, B Sowjanya, P Srivani, M Alagaraja, and David Banji. “Inductively coupled plasma–optical emission spectroscopy: a review”. In: *Asian Journal of Pharmaceutical Analysis* 3.1 (2013), pp. 24–33.
- [32] Thermo Fischer Scientific. URL: <https://assets.thermofisher.com/TFS-Assets/MSD/Application-Notes/analysis-iron-steel-ar1-ispark-8820-optical-emission-spectrometer-an41259-en.pdf>. Accessed: 01.05.2024.
- [33] D. E. J. Talbot. “Effects of Hydrogen in Aluminium, Magnesium, Copper, and Their Alloys”. In: *International Metallurgical Reviews* 20.1 (1975), pp. 166–184. DOI: 10.1179/imt1r.1975.20.1.166. eprint: <https://doi.org/10.1179/imt1r.1975.20.1.166>. URL: <https://doi.org/10.1179/imt1r.1975.20.1.166>.
- [34] H Iwahori, K Yonekura, Y Yamamoto, and M Nakamura. “Occurring behavior of porosity and feeding capabilities of sodium-and strontium-modified al-si alloys”. In: *AFS Transactions* 98 (1990), pp. 167–173.
- [35] Martin Riestra, Anton Bjurenstedt, Toni Bogdanoff, Ehsan Ghassemali, and Salem Seifeddine. “Complexities in the assessment of Melt Quality”. In: *International Journal of Metalcasting* 12.3 (Oct. 2017), 441–448. DOI: 10.1007/s40962-017-0179-y.
- [36] W Rasmussen and C Edward Eckert. “RPT gauges aluminium porosity”. In: *Modern casting* 82.3 (1992), pp. 29–31.
- [37] Mar. 2020. URL: <https://www.foundrymag.com/testing-qc/article/21123471/fundamentals-of-reduced-pressure-testing-porosity-solutions-llc>. Accessed: 02.05.2024.
- [38] Mile Djurdjevic, Zoran Odanović, and Jelena Pavlović-Krstić. “MELT QUALITY CONTROL AT ALUMINUM CASTING PLANTS”. In: (), p. 14.
- [39] BRYNE AB. URL: https://bryne.se/onewebmedia/FMA_Al_u_Test_Units.pdf. Accessed: 01.05.2024.
- [40] DY-Kast. *Compact Hydrogen Tester*. URL: <https://www.dykast.com/products/compact-hydrogen-tester/30168>. Accessed: 02.05.2024.
- [41] Prince Anyalebechi. “Techniques for Determination of the Hydrogen Content in Aluminium and its Alloys - A Review”. In: *Cast Metals* 3 (Jan. 1991), pp. 182–201.
- [42] J. Tiwari S. N.; Beech. “Origin of gas bubbles in aluminium”. In: *Metal Science 1978-aug vol. 12 iss. 8* 12 (8 Aug. 1978). DOI: 10.1179/msc.1978.12.8.356.
- [43] C Badini, Franco Bonollo, MP Cavatorta, GM La Vacchia, Andrea Panvini, Annalisa Pola, W Nicodemi, and M Verdani. “Process simulation of microstructure and relationship with mechanical properties in diecastings”. In: *Metallurgical Science and Technology* 20.2 (2002).

- [44] M. Di Sabatino. “On fluidity of aluminium alloys”. In: *La Metallurgia Italiana* 100 (Mar. 2008), pp. 17–22.
- [45] Francois R. Mollard, Merton C. Flemings, and Eisuke F. Niyama. “Aluminum fluidity in casting”. In: *JOM* 39.11 (Nov. 1987), 34–34. DOI: 10.1007/bf03257537.
- [46] K.R. Ravi, R.M. Pillai, K.R. Amaranathan, B.C. Pai, and M. Chakraborty. “Fluidity of aluminum alloys and composites: A review”. In: *Journal of Alloys and Compounds* 456.1 (2008), pp. 201–210. ISSN: 0925-8388. DOI: <https://doi.org/10.1016/j.jallcom.2007.02.038>. URL: <https://www.sciencedirect.com/science/article/pii/S0925838807004124>.
- [47] Robert D. Klassen and D. Clay Whybark. “The Impact of Environmental Technologies on Manufacturing Performance”. In: *Academy of Management Journal* 42 (1999), pp. 599–615. URL: <https://api.semanticscholar.org/CorpusID:167491958>.
- [48] Joseph Sarkis. “Manufacturing’s role in corporate environmental sustainability - Concerns for the new millennium”. In: *International Journal of Operations & Production Management* 21 (2001), pp. 666–686. URL: <https://api.semanticscholar.org/CorpusID:153678983>.
- [49] Timothy G. Gutowski, Julian M. Allwood, Christoph Herrmann, and Sahil Sahni. “A Global Assessment of Manufacturing: Economic Development, Energy Use, Carbon Emissions, and the Potential for Energy Efficiency and Materials Recycling”. In: *Annual Review of Environment and Resources* 38 (2013), pp. 81–106. URL: <https://api.semanticscholar.org/CorpusID:154397728>.
- [50] Michael Greenstone, John A. List, and Chad Syverson. “Nber Working Paper Series the Effects of Environmental Regulation on the Competitiveness of U.s. Manufacturing”. In: URL: <https://api.semanticscholar.org/CorpusID:9593544>.
- [51] Siyu Ma, Hui Liu, Ni Wang, Lidong Huang, Jinshuo Su, and Teyang Zhao. “Incentive-based integrated demand response with multi-energy time-varying carbon emission factors”. In: *Applied Energy* 359 (2024), p. 122763. ISSN: 0306-2619. DOI: <https://doi.org/10.1016/j.apenergy.2024.122763>. URL: <https://www.sciencedirect.com/science/article/pii/S0306261924001466>.
- [52] Tomás Norton, Da-Wen Sun, Jim Grant, Richard Fallon, and Vincent Dodd. “Applications of computational fluid dynamics (CFD) in the modelling and design of ventilation systems in the agricultural industry: A review”. In: *Bioresource Technology* 98.12 (2007), pp. 2386–2414. ISSN: 0960-8524. DOI: <https://doi.org/10.1016/j.biortech.2006.11.025>. URL: <https://www.sciencedirect.com/science/article/pii/S0960852406006092>.
- [53] Philip J Stopford. “Recent applications of CFD modelling in the power generation and combustion industries”. In: *Applied Mathematical Modelling* 26 (2002), pp. 351–374. URL: <https://api.semanticscholar.org/CorpusID:110857691>.

- [54] Chris T. Hendrickson, Arpad Horvath, Satish Joshi, and Lester B. Lave. “Economic Input–Output Models for Environmental Life-Cycle Assessment”. In: *Environmental Science & Technology* 32 (1998). URL: <https://api.semanticscholar.org/CorpusID:128130940>.
- [55] Anmar I. Arif, Zhaoyu Wang, Jianhui Wang, Barry A. Mather, Hugo Bashualdo, and Dongbo Zhao. “Load Modeling—A Review”. In: *IEEE Transactions on Smart Grid* 9 (2018), pp. 5986–5999. URL: <https://api.semanticscholar.org/CorpusID:53045113>.
- [56] Bin He, Shusheng Qian, and Tengyu Li. “Modeling product carbon footprint for manufacturing process”. In: *Journal of Cleaner Production* 402 (2023), p. 136805. ISSN: 0959-6526. DOI: <https://doi.org/10.1016/j.jclepro.2023.136805>. URL: <https://www.sciencedirect.com/science/article/pii/S0959652623009630>.
- [57] Luohe Hu, Chen Peng, Steve Evans, Tao Peng, Ying Liu, Renzhong Tang, and Ashutosh Tiwari. “Minimising the machining energy consumption of a machine tool by sequencing the features of a part”. In: *Energy* 121 (2017), pp. 292–305. ISSN: 0360-5442. DOI: <https://doi.org/10.1016/j.energy.2017.01.039>. URL: <https://www.sciencedirect.com/science/article/pii/S0360544217300373>.
- [58] Bin He, Jiachi Wu, Xuanren Zhu, Dong Zhang, and Jintao Cao. “Product Multibody Dynamics Analysis for Low-Carbon Footprint”. In: *Journal of Computing and Information Science in Engineering* 23.2 (2023). Cited by: 9. DOI: 10.1115/1.4054486. URL: <https://www.scopus.com/inward/record.uri?eid=2-s2.0-85143977258&doi=10.1115%2f1.4054486&partnerID=40&md5=100d90ff906777fa846027866fe82ff9>.
- [59] Resul Sercan Altıntaş, Müge Kahya, and Hakkı Özgür Ünver. “Modelling and optimization of energy consumption for feature based milling”. In: *The International Journal of Advanced Manufacturing Technology* 86.9–12 (Feb. 2016), 3345–3363. DOI: 10.1007/s00170-016-8441-7.
- [60] Shailendra Pawanr, Girish Kant Garg, and Srikanta Routroy. “Development of an empirical model to quantify carbon emissions for machining of cylindrical parts”. In: *Environmental Science and Pollution Research* 30.8 (2023), pp. 21565–21587.
- [61] Jun Zheng, Yunge Yu, Xingjian Zhou, Wei Ling, and Wei Wang. “Promoting sustainable level of resources and efficiency from traditional manufacturing industry via quantification of carbon benefit: A model considering product feature design and case”. In: *Sustainable Energy Technologies and Assessments* 43 (2021), p. 100893. ISSN: 2213-1388. DOI: <https://doi.org/10.1016/j.seta.2020.100893>. URL: <https://www.sciencedirect.com/science/article/pii/S2213138820313205>.

- [62] Guanghui Zhou, Ce Zhou, Qi Lu, Changle Tian, and Zhongdong Xiao. “Feature-based carbon emission quantitation strategy for the part machining process”. In: *International Journal of Computer Integrated Manufacturing* 31.4-5 (2018), pp. 406–425.
- [63] Chetan Agrawal, Jwalant Wadhwa, Anjali Pitroda, Catalin Iulian Pruncu, Murat Sarikaya, and Navneet Khanna. “Comprehensive analysis of tool wear, tool life, surface roughness, costing and carbon emissions in turning Ti–6Al–4V titanium alloy: Cryogenic versus wet machining”. In: *Tribology International* 153 (2021), p. 106597. ISSN: 0301-679X. DOI: <https://doi.org/10.1016/j.triboint.2020.106597>. URL: <https://www.sciencedirect.com/science/article/pii/S0301679X20304266>.
- [64] Bin Gao, Jun Xu, ke-wu He, Lei Shen, Hao Chen, Hui-jun Yang, Ai-hua Li, and Weihua Xiao. “Cellular uptake and intra-organ biodistribution of functionalized silica-coated gold nanorods”. In: *Molecular Imaging and Biology* 18.5 (Aug. 2016), 667–676. DOI: 10.1007/s11307-016-0938-9.
- [65] Manchen Hu, Yunxuan Wei, Hongjun Cai, and Yuchong Cai. “Polarization-insensitive and achromatic metalens at ultraviolet wavelengths”. In: *Journal of Nanophotonics* 13.3 (2019), p. 036015. DOI: 10.1117/1.JNP.13.036015.
- [66] Nikhil Kashyap, Rizwan Abdul Rahman Rashid, and Navneet Khanna. “Carbon emissions, techno-economic and machinability assessments to achieve sustainability in drilling Ti6Al4V ELI for medical industry applications”. In: *Sustainable Materials and Technologies* 33 (2022), e00458. ISSN: 2214-9937. DOI: <https://doi.org/10.1016/j.susmat.2022.e00458>. URL: <https://www.sciencedirect.com/science/article/pii/S2214993722000720>.
- [67] Zhuo Huang, Huajun Cao, Dan Zeng, Weiwei Ge, and Chengmao Duan. “A carbon efficiency approach for laser welding environmental performance assessment and the process parameters decision-making”. In: *The International Journal of Advanced Manufacturing Technology* 114.7–8 (Apr. 2021), 2433–2446. DOI: 10.1007/s00170-021-07011-8.
- [68] Congbo Li, Ying Tang, Longguo Cui, and Pengyu Li. “A quantitative approach to analyze carbon emissions of CNC-based Machining Systems”. In: *Journal of Intelligent Manufacturing* 26.5 (July 2013). DOI: 10.1007/s10845-013-0812-4.
- [69] Zhipeng Jiang, Gao Dong, Yong Lu, Linghao Kong, and Shang Zhendong. “Quantitative Analysis of Carbon Emissions in Precision Turning Processes and Industrial Case Study”. In: *International Journal of Precision Engineering and Manufacturing-Green Technology* 8 (Sept. 2019), pp. 1–12. DOI: 10.1007/s40684-019-00155-9.
- [70] Nitesh Sihag and Kuldip Singh Sangwan. “Development of a sustainability assessment index for machine tools”. In: *Procedia CIRP* 80 (2019). 26th CIRP Conference on Life Cycle Engineering (LCE) Purdue University, West Lafayette, IN, USA May 7-9, 2019, pp. 156–161. ISSN: 2212-8271. DOI: <https://doi.org/10.1016/>

- j.procir.2019.01.018. URL: <https://www.sciencedirect.com/science/article/pii/S2212827119300204>.
- [71] Shun Jia, Qinghe Yuan, Wei Cai, Meiyang Li, and Zhaojun Li. “Energy modeling method of machine-operator system for sustainable machining”. In: *Energy Conversion and Management* 172 (2018), pp. 265–276. ISSN: 0196-8904. DOI: <https://doi.org/10.1016/j.enconman.2018.07.030>. URL: <https://www.sciencedirect.com/science/article/pii/S0196890418307568>.
- [72] Raunak Bhinge, Jinkyoo Park, Kincho H. Law, David A. Dornfeld, Moneer Helu, and Sudarsan Rachuri. “Toward a Generalized Energy Prediction Model for Machine Tools”. In: *Journal of Manufacturing Science and Engineering* 139.4 (Nov. 2016), p. 041013. ISSN: 1087-1357. DOI: 10.1115/1.4034933. eprint: https://asmedigitalcollection.asme.org/manufacturingscience/article-pdf/139/4/041013/6405194/manu_139_04_041013.pdf. URL: <https://doi.org/10.1115/1.4034933>.
- [73] Lishu Lv, Zhaohui Deng, Tao Liu, Linlin Wan, Wenliang Huang, Hui Yin, and Tao Zhao. “A Composite Evaluation Model of Sustainable Manufacturing in Machining Process for Typical Machine Tools”. In: *Processes* 7.2 (2019). ISSN: 2227-9717. DOI: 10.3390/pr7020110. URL: <https://www.mdpi.com/2227-9717/7/2/110>.
- [74] C Herrman, Lars Bergmann, Sebastian Thiede, and André Zein. “Energy labels for production machines—an approach to facilitate energy efficiency in production systems”. In: *Proceedings of 40th CIRP International Seminar on Manufacturing Systems*. 2007.
- [75] Wei Cai and Kee hung Lai. “Sustainability assessment of mechanical manufacturing systems in the industrial sector”. In: *Renewable and Sustainable Energy Reviews* 135 (2021), p. 110169. ISSN: 1364-0321. DOI: <https://doi.org/10.1016/j.rser.2020.110169>. URL: <https://www.sciencedirect.com/science/article/pii/S1364032120304603>.
- [76] Freddy Olsson. *Systematisk konstruktion, doktorsavhandling vid Institutionen för Maskinkonstruktion*. LTH, Lund, 1976. (In Swedish).
- [77] Freddy Olsson. “Integrerad produktutveckling”. In: *Mekanförbundet, Stockholm, Sweden* (1985). (In Swedish).
- [78] Jan-Eric Ståhl, Carin Andersson, and Mathias Jönsson. “A basic economic model for judging production development”. In: *Swedish Production Symposium*. 2007.
- [79] Sven-Åke Nilsson. *Investeringskalkylering – Lönsamhetsbedömning av investeringar*. Liber Läromedel, Malmö, 1976. (In Swedish).
- [80] Pratheek Ullal. *Development of fluidity measurement technique and Automation of Measurement Station*. URL: <https://hj.diva-portal.org/smash/get/diva2:1335511/FULLTEXT01.pdf>.

A Appendix



	
<h3>ARSAL 2125</h3>	
Highly compacted cleansing and skimming granules for all hypoeutectic and eutectic aluminium, wrought and casting alloys such as e. g.: G-AlSi10Mg, G-AlSi7Mg, G-AlSi8Cu3, G-AlSi12 and G-AlZn10Si8	
01 Notes on Technology	<p>Aluminium and aluminium, wrought and casting alloys have the tendency to form oxides and to absorb hydrogen in the liquid state and, in addition, to an undesired dross and aluminium oxide foam formation which has an extremely high portion of metal.</p> <p>The granules ARSAL 2125 bind the oxides and transport them to the surface by a flotation process whereby a low-metal dross is obtained by the reduction of the surface tension. In addition to that during the treatment with an impeller the oxides are bound on the melt surface.</p> <p>ARSAL 2125 is a highly compacted preparation. Therefore, nearly no dust is released and it can also be used in the lower temperature range of the aluminium melt. The high degree of compaction permits an intensive reaction with the oxides which can easily be controlled thanks to the compactness of the granules (discoloration and dissolution).</p> <p>Types of compaction: ARSAL 2125 is produced as granules or flakes.</p> <ul style="list-style-type: none">• The granules consist of small cylinders of approximately 0.3 g / grain. They enable an important control of the operating staff as they remain their shape and colour if they are not thoroughly stirred in the melt and therefore did not reach the reaction time.• Flakes look like small crushed stones, weight approximately 0.05 g / grain and have a large distribution area. The reaction time is comparable with that of the granules. They reach the temperature of the metal faster and loose their colour before reacting. Thus, an effective control is very difficult.
02 Application Range	ARSAL 2125 stands out by good storage stability and is applicable within a wide reaction range, i. e. it can also be used in the lower temperature range of the aluminium melt. It is applicable for all aluminium, wrought and casting alloys which may contain small quantities of sodium.
03 Quality Characteristics	ARSAL 2125 <ul style="list-style-type: none">• removes oxides from the melt by flotation and reduces the hydrogen content• produces a fine, powdery and low-metal dross• works in all types of furnaces and crucibles• permits the easy removal of adherences• is of very low smoke and odour emission
04 Addition Rate	Depending on the level of impurities 0.05 – 0.25 % by weight or lower (rule of thumb: half the quantity compared with the powder addition).
05 Product Application	Add ARSAL 2125 in the pouring stream and stir it with a bell. When using it as cleansing preparation, submerge the required addition slowly and carefully into the melt. Gently stir the rising flotation products with a well pre-heated and coated tool until a fully reacted dross forms and then skim it off. ARSAL 2125 is highly suitable for the automatic addition with an impeller system (e. g. MBU of the company FUCO-HEG).
06 Typical Properties	Appearance: blue granules / flakes Odour: odourless Reaction temperature: from approximately 580°C (higher temperatures accelerate the reaction)
07 Packaging	1,000kg big bags. Special packaging units are available, e. g. 25 kg bags, 3-fold with plastics lining.
08 Advice on Special Types of Danger	Not applicable.
09 Storage and Shelf Life	Store in a cool place (below 32°C/90°F); keep container dry and tightly closed. The shelf life is at least 6 months if properly stored.
 <p>SCHÄFER Chemische Fabrik GmbH Bonner Str. 20, 53773 Hennef/Sieg (Germany) Phone: +49 (0) 22 42 / 91 33 90, Fax: +49 (0) 22 42 / 837 09 Email: kontakt@schaeferchem.de www.schaeferchem.de</p>	

Figure A.1: ARSAL 2125 Specification Sheet.

Table A.1: Composition of secondary alloys used in tests.

	Si	Fe	Cu	Mn	Mg	Cr	Ni	Zn	Ti	As	B	Be	Bi	Ca	Cd	Co	Ga	Hg	Li	Na	P	Pb	Sb	Sn	V	Zr	Al%
L11	0.0300	0.0900	0.0000	0.0000	0.0000	0.0010	0.0060	0.0020	0.0050	0.0000	0.0001	0.0000	0.0000	0.0003	0.0000	0.0002	0.0145	0.0000	0.0000	0.0005	0.0002	0.0009	0.0002	0.0003	0.0175	0.0003	99.8200
L12	0.6900	0.2000	0.1300	0.6100	0.0010	0.0030	0.0060	0.2300	0.0230	0.0008	0.0012	0.0000	0.0003	0.0001	0.0001	0.0003	0.0149	0.0002	0.0000	0.0001	0.0009	0.0014	0.0010	0.0009	0.0134	0.0071	98.0500
L21	0.0400	0.1100	0.0000	0.0000	0.0020	0.0000	0.0070	0.0040	0.0050	0.0004	0.0001	0.0000	0.0002	0.0034	0.0001	0.0001	0.0200	0.0001	0.0000	0.0034	0.0007	0.0010	0.0004	0.0004	0.0199	0.0003	99.7800
L22	0.5800	0.1900	0.1300	0.5600	0.0020	0.0040	0.0060	0.0680	0.0270	0.0010	0.0012	0.0000	0.0004	0.0020	0.0001	0.0002	0.0163	0.0002	0.0000	0.0016	0.0008	0.0021	0.0014	0.0027	0.0140	0.0072	98.3900
K11	0.0400	0.1000	0.0000	0.0000	0.0010	0.0000	0.0060	0.0020	0.0040	0.0000	0.0002	0.0000	0.0000	0.0006	0.0000	0.0002	0.0195	0.0001	0.0000	0.0015	0.0001	0.0010	0.0002	0.0003	0.0194	0.0003	98.8000
K12	0.3700	0.1800	0.0700	0.2700	0.0010	0.0040	0.0050	0.2090	0.0120	0.0004	0.0008	0.0000	0.0002	0.0003	0.0001	0.0002	0.0170	0.0001	0.0000	0.0004	0.0007	0.0012	0.0009	0.0006	0.0139	0.0071	98.8300
K21	0.0300	0.0900	0.0000	0.0000	0.0000	0.0000	0.0060	0.0020	0.0040	0.0000	0.0002	0.0000	0.0000	0.0001	0.0000	0.0002	0.0190	0.0001	0.0000	0.0003	0.0000	0.0009	0.0002	0.0003	0.0188	0.0003	99.8200
K22	0.4400	0.2300	0.0700	0.2800	0.0000	0.0030	0.0050	0.3450	0.0090	0.0006	0.0007	0.0000	0.0002	0.0000	0.0001	0.0002	0.0167	0.0001	0.0000	0.0000	0.0005	0.0016	0.0011	0.0008	0.0136	0.0025	98.5800
K31	0.0800	0.1100	0.0000	0.0000	0.0060	0.0000	0.0070	0.0050	0.0060	0.0005	0.0001	0.0000	0.0002	0.0118	0.0001	0.0001	0.0204	0.0002	0.0000	0.0068	0.0009	0.0010	0.0002	0.0004	0.0206	0.0003	99.7200
K32	0.3900	0.2300	0.0600	0.2200	0.0010	0.0040	0.0060	0.3160	0.0100	0.0010	0.0008	0.0000	0.0003	0.0048	0.0001	0.0002	0.0176	0.0002	0.0000	0.0012	0.0007	0.0013	0.0014	0.0007	0.0140	0.0011	98.7200
R11	N/A	N/A	N/A	N/A	N/A	N/A	N/A	N/A	N/A	N/A	N/A	N/A	N/A	N/A	N/A	N/A	N/A	N/A	N/A	N/A	N/A	N/A	N/A	N/A	N/A	N/A	N/A
R12	0.5400	0.2200	0.0900	0.4200	0.0040	0.0090	0.0050	0.2750	0.0250	0.0009	0.0009	0.0000	0.0003	0.0001	0.0001	0.0002	0.0163	0.0002	0.0000	0.0003	0.0006	0.0015	0.0009	0.0006	0.0134	0.0005	98.3800
R21	0.0400	0.1100	0.0000	0.0000	0.0020	0.0010	0.0070	0.0040	0.0050	0.0002	0.0002	0.0000	0.0001	0.0057	0.0001	0.0001	0.0201	0.0001	0.0000	0.0036	0.0005	0.0010	0.0002	0.0004	0.0202	0.0003	99.7700
R22	0.4200	0.2400	0.0600	0.3800	0.0010	0.0080	0.0060	0.1210	0.0110	0.0007	0.0009	0.0000	0.0003	0.0013	0.0001	0.0002	0.0179	0.0002	0.0000	0.0007	0.0007	0.0013	0.0016	0.0008	0.0147	0.0062	98.7000
R31	0.0400	0.1100	0.0000	0.0000	0.0030	0.0000	0.0070	0.0050	0.0050	0.0004	0.0001	0.0000	0.0002	0.0083	0.0001	0.0001	0.0204	0.0001	0.0000	0.0043	0.0007	0.0010	0.0003	0.0004	0.0204	0.0003	99.7700
R32	0.4700	0.2000	0.1100	0.3800	0.0020	0.0010	0.0050	0.0490	0.0220	0.0006	0.0010	0.0000	0.0002	0.0055	0.0001	0.0002	0.0177	0.0000	0.0000	0.0013	0.0006	0.0033	0.0011	0.0010	0.0143	0.0056	98.7100

How to read this data: ALLOY LETTER / ALLOY NUMBER / PRIMARY ADDED (1) RESULTING ALLOY (2)

L1 1 The 1 indicates that this alloy is relatively pure and will be used to dilute the car chiller.

L1 2 The 2 indicates this alloy is the resulting composition of the pure alloy above being melted together with car chiller.